

Extending cavity-mechanical cooling via a hot LC electrical circuit

& Framework for electromechanical coupling calculations

Emil Zeuthen



Supervisor
Anders S. Sørensen

A Thesis Presented for the
Degree of Cand. Scient. in Physics

The Niels Bohr Institute
University of Copenhagen

August 2012

Contents

0.1	Abstract	4
0.2	Resumé på dansk	5
0.3	Acknowledgments	5
1	Introduction	7
2	Survey of cavity mechanics	9
2.1	Objectives of the field	10
2.1.1	Component characteristics	11
2.2	Radiation pressure cooling	12
2.2.1	Parametric coupling of a mechanical oscillator to a driven electromagnetic cavity	13
2.2.2	Cavity-assisted resolved sideband cooling	15
2.2.3	Limiting mechanisms	17
2.3	Coupling schemes	19
2.3.1	Reflective coupling	19
2.3.2	Dispersive coupling	20
2.4	Transduction schemes	22
3	Electromechanical coupling calculations	24
3.1	Modeling	24
3.1.1	The electromechanical interface	25
3.1.2	The mechanical membrane	28
3.1.3	The electrical circuit	30
3.1.4	Evaluating the capacitive unit cell	40
3.2	Quantities of interest	42
3.2.1	Electromechanical coupling strength	43
3.2.2	Induced mechanical frequency shift	44
3.2.3	Static deflection of the mechanical element	46
3.3	Application to experiment	48
3.3.1	Description of the experiment	48
3.3.2	Experimental parameters and data	49
3.3.3	Numerical calculations	49
3.3.4	Numerical results and comparison	52

4	Quantum noise theory	55
4.1	Effective equations of motion for a system coupled to a Markovian reservoir	55
4.1.1	Physical systems and their environments	56
4.1.2	Classical Langevin equations: Brownian motion	57
4.1.3	Requirements for quantum noise theory	59
4.1.4	Derivation of the quantum Langevin equation	60
4.2	Steady state occupancies of coupled harmonic oscillators subjected to white noise	64
4.2.1	Time-domain solution via the Lyapunov equation	65
4.2.2	Frequency-domain solution	67
4.3	Effective description of weakly coupled subsystems	69
4.3.1	Structured reservoirs of bosonic harmonic oscillator degrees of freedom	70
5	Extending cavity-mechanical cooling	74
5.1	Main ideas and preliminaries	74
5.1.1	Single-component system	76
5.1.2	Direct cooling of an LC circuit	77
5.1.3	Cooling via a link	80
5.2	Structured reservoir description of the 'indirect' cooling system	82
5.2.1	Strong coupling regime of the cooling system	85
5.3	Harmonic oscillator analysis	86
5.3.1	Structured reservoir treatment	87
5.3.2	Exact solution	98
5.3.3	Comparison of reservoir result to exact solution	99
5.4	Implementations	102
5.4.1	Nuclear spin cooling	102
5.4.2	Indirect mechanical cooling	105
5.4.3	Indirect cooling of LC circuit with high Q-factor	105
6	Conclusions and perspectives	106
6.1	Electromechanical coupling calculations	106
6.1.1	Conclusions	106
6.1.2	Perspectives	106
6.2	Extending cavity-mechanical cooling	107
6.2.1	Conclusions	107
6.2.2	Perspectives	107
	Bibliography	108

A Mathematical derivations	112
A.1 Inversion of the kinetic energy matrix	112
A.2 Step-wise optimization	114
B Source code	116

0.1 Abstract

Recent experimental advances in the field of cavity mechanics have led to unprecedented control over macroscopic mechanical oscillators by means of coupling to an optical or electrical cavity. Specifically, efficient resolved-sideband cooling of the mechanical center-of-mass motion has been achieved, potentially allowing for quantum control of macroscopic objects. The idea of extending this efficient cooling mechanism by coupling additional objects to the mechanical oscillator is explored in this thesis.

As implied by its title, the thesis consists of two subprojects of rather different character: One project, “Framework for electromechanical coupling calculations”, aims to aid the design and implementation of experimental setups of electromechanical nature; thus, it is directly concerned with challenges faced by experimental researchers striving to realize the promises of the emerging new field of cavity mechanics. In contrast, the second project, “Extending cavity-mechanical cooling via a hot LC circuit”, seeks to add to the remarkable set of ideas of what might be achieved within the field; hence, the latter project is taking a visionary standpoint rather than a practical one.

In the chapter “Framework for electromechanical coupling calculations”, we establish a quantum description for the electromechanical interaction between a vibrating membrane and a capacitive element of an electric circuit. The approach presented here allows for manageable numerical calculation of the coupling parameters for given geometry and materials choice while capturing the essential features of the setup. Such a method may well be valuable in developing and engineering the electromechanical links that have been envisioned to participate in larger cavity-mechanical setups [27]. The method is demonstrated by application to a current experimental project.

In the other major chapter, “Extending cavity-mechanical cooling via a hot LC circuit”, we explore schemes for extending the successful technique of cavity-mechanical single-mode cooling by coupling to additional objects. We consider a new, indirect scheme involving a rapidly decaying link mode that mediates the cooling from the mechanical mode to a weakly coupled but long-lived target system. By optimizing this scheme we arrive at the surprising result that it is possible to cool the target system even under circumstances where it is impossible to cool the link mode significantly. This phenomenon may be understood in terms of interference and points toward new ways of thinking about and utilizing single-mode cooling. Possible implementations of the scheme are briefly discussed.

0.2 Resumé på dansk

Nylige eksperimentelle landvindinger inden for forskningsfeltet kavitetsmekanik har ført til hidtil uset kontrol over makroskopiske mekaniske oscillatorer ved kobling til en optisk eller elektrisk kavitet. Mere specifikt har man opnået effektiv *resolved-sideband* køling af bevægelsen af en mekanisk oscillators massemidt punkt, hvilket potentielt set muliggør kontrol over makroskopiske objekter på kvanteniveau. I denne afhandling undersøges det teoretisk, hvorvidt det er muligt at udnytte denne effektive køleteknik til at køle andre objekter ved at koble dem til den mekaniske frihedsgrad.

Som det antydes i afhandlingens titel, består den af to delprojekter af ganske forskellig karakter: Det ene projekt, med titlen “Procedure til elektromekaniske koblingsberegninger” har til hensigt at fremme udviklingen og implementeringen af elektromekaniske forsøgsopstillinger; det beskæftiger sig altså direkte med de udfordringer som eksperimentalfysikerne står over for i deres bestræbelser på at realisere de visioner, der er indenfor det kavitetsmekaniske forskningsfelt. Derimod forsøger det andet projekt, med titlen “Udbredelse af kavitetsmekanisk køling via et varmt LC-kredsløb”, at bidrage med nye idéer til hvad der kan være muligt inden for feltet kavitetsmekanik; altså anlægger sidstnævnte projekt en fremsynet snarere end en praktisk vinkel på feltet.

I kapitlet “Procedure til elektromekaniske koblingsberegninger” etableres en kvantemekanisk beskrivelse af den elektromekaniske vekselvirkning mellem en vibrerende membran og et kapacitørellement tilhørende et elektrisk kredsløb. Metoden der her præsenteres muliggør overkommelige numeriske beregninger af koblingsparametrene for en given geometri og materialevalg. En sådan beregningsmetode kan meget vel vise sig nyttig i udviklingen af de elektromekaniske bindeled der spås at ville kunne indgå i større kavitetsmekaniske apparater [27]. Proceduren demonstreres ved at anvende den i forbindelse med et igangværende eksperimentelt projekt.

I det andet store kapitel vedrørende delprojektet “Udbredelse af kavitetsmekanisk køling via et varmt LC-kredsløb” undersøges muligheden for at udnytte den effektive kavitetsmekaniske køleteknik ved at viderekoble til andre objekter der ønskes kølet. I den forbindelse analyseres en ny, indirekte kølemetode der benytter sig af et hastigt henfaldende system som bindeled mellem den mekaniske frihedsgrad og et svagt koblet system med lang henfaldstid, der ønskes kølet. Ved at optimere denne metode fremkommer det overraskende resultat, at det er muligt at foretage køling af det ønskede system, selv under omstændigheder hvor det ikke er muligt at køle bindeledet. Dette fænomen kan forstås som en interferenseffekt og peger på nye måder at forstå og udnytte den kavitetsmekaniske køleeffekt på. Afslutningsvist diskuteres mulige implementeringer af den nye kølemetode.

0.3 Acknowledgments

I wish to extend my thanks to the following people: Anders S. Sørensen and Jake Taylor for providing me with many of the ideas that appear in this thesis. My dear colleagues Eran Kot and Florentin Reiter for good company, input and valuable discussions at all hours. The QUANTOP membrane group for their

hard work which I am excited to take part in. Yeghishe Tsatsuryan for collaboration on some of the occupancy calculations. William Nielsen for figuring out FEM in MATLAB together with me. Klemens Hammerer for kindly pointing me to relevant and obscure references. My dear girlfriend Molly for supplying me with warm meals at the institute. My equally dear brother William for designing the front page that makes my thesis look like a textbook on computer programming. Jean-baptiste Béguin and Tom Bienaimé for patiently teaching me to speak French. Finally, Andreas Vollenweider for providing mild and soothing music for the somewhat agonizing process of writing everything down.

Chapter 1

Introduction

The fact that electromagnetic radiation can impart momentum to massive objects is well-established. However, an interesting new experimental regime has been reached in recent years offering unprecedented control over macroscopic objects by means of radiation pressure effects. This includes the ability to cool the Brownian center-of-mass motion of micromechanical oscillators to the ground state. Such quantum level control of objects of that length scale moves the boundary of the quantum regime significantly closer to the macroscopic world. This allows for fundamental tests of quantum mechanics by, for instance, attempting to realize Schrödinger’s cat in a micromechanical oscillator.

The cooling technique that has enabled this progress is that of cavity-assisted resolved-sideband cooling. Experiments of the kind mentioned above have been realized in both optical Fabry-Pérot type cavities and electrical microwave cavities. The fact that both of these setups are able to interact efficiently with a mechanical mode suggests fascinating prospects of hybrid systems involving vastly different frequencies with the mechanical mode acting as a transducer between the electromagnetic cavities [27].

A main aim of this thesis is to explore the possibilities of combining the efficiency of cavity-assisted cooling with the extendability provided by such hybrid systems. More specifically, we will analyse potential schemes for cooling a system by coupling it to a cavity cooled mechanical mode. In part, this can also be seen as an investigation of how the single-mode nature of the cooling manifests itself in such situations. We will see below that this kind of cooling does not comply with common intuition in all regards and that this may be used to our advantage.

The thesis also consists of another subproject, “Framework for electromechanical coupling calculations”, which considers the practical problem of achieving sufficient coupling strength in the electromechanical links imagined to participate in the hybrid cooling schemes mentioned above. This has resulted in a procedure for calculating the electromechanical coupling strength and related quantities which may serve as a tool in the design and optimization of electromechanical interfaces.

The thesis is structured as follows:

- Chapter 2 presents a survey of cavity mechanics with focus on the recent

experimental advances in cavity-assisted cooling and its limiting factors. Additionally, the physics of various different cavity-mechanical coupling mechanisms will be discussed.

- In Chapter 3, we develop the procedure for characterizing capacitive coupling scenarios in terms of coupling strength and induced frequency shifts. The steps of the derivation are motivated by the characteristics of a particular setup to which we eventually apply the procedure.
- Chapter 4 on quantum noise theory provides the theoretical and methodical basis for Chapter 5. In addition to a treatment of effective quantum Langevin equations in terms of Markovian reservoirs, it also provides mathematical methods for solving such equations.
- In Chapter 5, extensions of cavity-assisted cooling to other systems are explored. A new, 'indirect' scheme involving a rapidly decaying link is presented and fully optimized within an effective description. The chapter ends with a brief discussion of possible applications.
- In Chapter 6 we conclude on the results obtained in this thesis and future paths are indicated.

Chapter 2

Survey of cavity mechanics

This chapter will chart the theoretical ideas and experimental achievements that form the basis of the work presented in the rest of the thesis.

The related research disciplines of *opto-mechanics* and *electro-mechanics* have experienced rapid progress in recent years. Both are concerned with the coupling between a mechanical mode and electromagnetic radiation, within a specific frequency range, in a setting where the fundamental quantum nature of each may potentially manifest itself. While different technical challenges pertain to the two parts of the electromagnetic spectrum, optical and microwave domains respectively, the two disciplines are very similar from a theoretical point of view. This has led to the suggestion of considering these as specific instances within a broader field of *cavity mechanics* [22] and this is the perspective we will take in this thesis.

Given this conceptual parallelism, it does not require too much of a leap in abstraction to form hybrids of opto- and electromechanical systems, although naturally, there will be significant technical challenges in realizing such a quantum opto-electro-mechanical experiment. Thus, while it is in some sense straightforward to understand the combination of these three degrees of freedom theoretically, there is a challenge in devising realistic schemes exploiting it in a meaningful way. This hybrid approach is to a large extent uncharted territory, both experimentally and theoretically, and it is in this direction this thesis is intended to make a contribution.

Given the state of affairs sketched above, the present chapter will rather be a survey of *opto-mechanics* and *electro-mechanics* than their combination, although we will consider a few existing proposals regarding the latter in section 2.4. That said, the large extent of parallelism between opto- and electro-mechanics will be sought emphasized as this facilitates thinking about ways of integrating the two. Since a main focus of this thesis is the development of cooling schemes, we will in section 2.2 review the successful technique of cavity-assisted sideband cooling of a mechanical oscillator, which is one of the main achievements within the field of cavity mechanics. In section 2.3 we will consider different ways of realizing opto- and electro-mechanical coupling with the aim of indicating how these coupling schemes may enable the design of hybrid systems.

To begin with, however, we give in the following section a general characterization of the field [14, 19, 2, 22].

2.1 Objectives of the field

According to everyday experience, the radiation pressure of photons is negligible, but for sub-micrometer scale objects it becomes significant and, for instance, allows for a light beam to serve as an optical tweezer able to trap such particles. In fact, radiation pressure forces are exploited in many physical contexts. For instance, going to a smaller length scale, laser cooling of atomic motion is an indispensable technique with regard to obtaining Bose-Einstein condensates in atomic ensembles. For strongly confined ions it is possible to reach a regime where the vibrational states can be resolved. This allows for selectively driving transitions to lower-lying phonon number states resulting in efficient, *resolved-sideband* cooling [8].

A major breakthrough in the field of cavity mechanics is the achievement of an equivalent resolved-sideband regime for the interaction between a macroscopic mechanical mode and electromagnetic radiation. This recent development has led to the possibility of more sophisticated manipulation of mechanical objects than simply confinement: In recent experiments involving harmonically confined, micrometer scale mechanical objects, scenarios have been realized where cavity-enhanced radiation pressure has dominated the system dynamics. In this regime, where the lifetime of cavity photons is comparable to or larger than the harmonic period of the mechanical object, it is possible to achieve radiation pressure cooling of the center-of-mass motion of the mechanical component through the dynamical back-action of photons – potentially cooling to a low-lying quantum state in vicinity of the ground state. It is important to note that this cooling mechanism addresses a single mechanical mode, while the bulk temperature of the object is unaltered.

The potential of the resolved-sideband cooling technique is one of the main motivations behind the ideas presented in this thesis, and we shall consider it in some detail in section 2.2. The fact that this scheme does not require the assisting electromagnetic cavity to resonate at any specific absolute wavelength makes it applicable to both optical and electrical realizations and hence allows for the unified perspective of cavity mechanics.

The breakthroughs leading to the emergence of the field of quantum cavity mechanics have first and foremost been of technical nature: Micro- and nano-fabrication of high quality optical and mechanical elements. Theoretically, many of the ideas and tools of quantum optics can be transferred rather easily to cavity mechanics. Primarily, the analogy between the fields arises from the fact that, in the quantum realm, both electromagnetic field excitations and the motion of a harmonically confined object have the mathematical description of a bosonic harmonic oscillator. The interaction of two such modes is commonplace in both quantum optics and cavity mechanics. A notable difference between the two is the large gap between mechanical and optical or microwave frequencies.

Besides ground state cooling, there are several other interesting aims within the field of cavity mechanics; although outside the scope of this thesis, we will briefly mention some of them to give a sense of the breadth of the field:

Macroscopic quantum mechanics - Of fundamental interest is the prospect of probing the boundary between quantum and classical physics by bringing a macroscopic oscillator near its ground state. An intriguing question is whether it will be possible to prepare a macroscopic oscillator in a (non-classical) squeezed

state, a motional superposition state (à la Schrödinger’s cat) or generate entangled states between a pair of such oscillators. Hence, cavity mechanics may provide the setting for future fundamental tests of quantum mechanics for objects approaching human-scale.

Optical readout - The kind of single-mode cooling that concerns us here is closely related to sensing. Roughly speaking, if cooling is the process of removing excitations from a certain part of a system, then sensing can be achieved by examining those removed excitations. Regarding cooling of, for instance, a vibrating membrane, such analysis of the readout is required in order to establish to what extent the mechanical motion has been cooled. Current goals include quantum limited readout of mechanical motion and, by extension, excitations from an additional degree of freedom using the mechanical mode as an intermediary (the latter application will be discussed in section 2.4). Another technical asymmetry between opto- and electro-mechanics arises here, since the process of electrical readout of mechanical motion is not nearly as well-controlled.

Non-linear protocols - Driving of the electromagnetic cavity enhances the effective coupling strength, as is usually desirable, but it also necessarily entails linear interaction. Such circumstances allow for efficient cooling and sensing schemes, but preclude exploitation of the increased coupling for quantum protocols relying on non-linear effects. It is technically challenging to achieve the single-photon strong coupling to the mechanical mode required for such protocols to be realized cavity mechanically.

2.1.1 Component characteristics

Regarding the technical aspects of the development of the field, we will now comment on the component characteristics required for quantum operation. As far as the electromagnetic cavity is concerned, a high finesse is advantageous, meaning that excitations will perform many round trips before leaking out. This requirement is usually expressed in comparison to the mechanical frequency using the cavity decay rate as $\kappa \leq \omega_{\text{mech}}$. In incorporating the mechanical degree of freedom, typically in the MHz to low GHz frequency range, the following properties are beneficial:

High quality factor, $Q_{\text{mech}} = \omega_{\text{mech}}/\gamma_{\text{mech}} \gg 1$, implying a narrow level undergoing many oscillations per decay to the environment (membranes with $Q \sim 10^6$ are commercially available).

Low intrinsic heating rate, that is, the heating rate ascribed to the reservoirs coupled to the mechanical mode, e.g. clamping losses and friction (as opposed to other reservoirs that may influence the mechanical mode indirectly via an electromagnetic cavity). This requirement is often phrased in terms of the “ Q -frequency product” as

$$Q_{\text{mech}}\omega_{\text{mech}} \gg k_{\text{B}}T_{\text{bath}}/\hbar \quad (2.1.1)$$

in the high-temperature limit, which arises from rearranging the inequality

$$\omega_{\text{mech}} \gg \frac{k_{\text{B}}T_{\text{bath}}}{\hbar Q_{\text{mech}}} = \gamma_{\text{mech}}n_{\text{bath}}$$

stating that the mechanical frequency should be much larger than the heating rate. From either expression we see that we should seek to increase ω_{mech}

and Q_{mech} while keeping T_{bath} as low as possible. The latter factor can be influenced by means of conventional precooling of the experimental setup and choice of low-absorption materials as will be touched upon below, in section 2.2. Regarding the related quantities ω_{mech} and Q_{mech} , a promising approach is to use a high-stress tensioned mechanical oscillators, either a 1D string or a 2D membrane. The Q -frequency product of certain high-tension silicon nitride (SiN) membranes have been reported to surpass the threshold set by the right-hand side of Eq. (2.1.1) even at room temperature [30], $k_{\text{B}}T_{\text{room}}/\hbar \sim 2\pi \cdot 6\text{THz}$, potentially allowing for room temperature quantum operation of such opto-mechanical setups.

A *small mass* is desirable; however, in current experiments the mechanical masses range from picogram to gram-scale, the upper bound occurring for the vibrating mirrors used in the LIGO project for gravitational wave detection. In a quantized description, the motional mass m of the oscillator enters through the oscillator length $x_0 = \sqrt{\frac{\hbar}{2m\omega_{\text{mech}}}}$, whereby a linear coupling term in mechanical position will contain $x_0(\hat{a} + \hat{a}^\dagger)$, \hat{a} being the mechanical annihilation operator; hence, it is apparent that the mass m must be small for us to have significant coupling at the phonon level.

2.2 Radiation pressure cooling

In this section, we will give an account of the discipline of cavity-assisted cooling of a mechanical oscillator. But first, it is appropriate that we discuss what exactly we mean by cooling in this context. Cavity-assisted cooling has the effect of lowering the mean occupancy of a particular collective mode of the mechanical object, while all other degrees of freedom remain at the environmental temperature, i.e., the bulk temperature of the mechanical oscillator is unchanged. If we consider the cooled mode separately, its Brownian motion behaves as if the environment were at a lower temperature and, hence, we may speak of a reduced effective temperature for that mode. More specifically, the effective temperature can be defined from the amount of thermal energy in the membrane motion as found from integrating the mechanical peak appearing in the spectrum of reflected probe light. The width of the peak directly provides the total damping rate of the mechanical oscillator.

The cooling rate induced by the radiation pressure will be competing with heating rates from the thermal reservoirs that make up the environment that inevitably influence the various components of the setup. The mechanical oscillator, for instance, is mounted on a support of some sort with which phonons will be exchanged. From the point of view of the oscillator, this undesired coupling can be modelled as a thermal phonon bath, inducing a heating rate of $k_{\text{B}}T/\hbar Q$ (in the high temperature limit). Cryogenic precooling of the setup provides a way to lower the temperature of this bath and thus the heating rate. Even with such precooling, attention must be paid in materials choice to limit elevation of the bath temperature by optical absorption. The practical implementation of cryogenic precooling is substantially easier in the case of electrical microwave cavities than for optical cavities, a notable technical difference between the conceptually very similar opto- and electro-mechanical situations. Of course, a lower thermal bath temperature also means that the starting point

for the cavity-assisted cooling is a mechanical state of reduced phonon number compared to a scenario without precooling. Ground-state cooling of a high frequency piezo-electric mechanical oscillator has even been achieved by precooling alone [20].

An alternative approach to the passive scheme of resolved-sideband cooling, relying dynamic back-action, is *active feedback* cooling. The idea here is to continuously monitor the mechanical motion interferometrically and, based on this, exert an appropriate force on the mechanical oscillator. We will not consider such active schemes here.

2.2.1 Parametric coupling of a mechanical oscillator to a driven electromagnetic cavity

To provide some of the mathematical basis for cavity-assisted cooling, we will in this section derive the Hamiltonian for a cavity mechanical system. For definiteness we will consider a driven Fabry-Pérot cavity where one of the mirrors is performing harmonically confined motion (see figure 2.2.1).

First, let us consider intuitively why the circumstance that one mirror can move implies mutual coupling between the cavity mode and the mechanical degree of freedom. Movement of the mirror influences the occupancy of the cavity mode because the resonance frequency of the cavity is a function of the distance between the end mirrors. Changing the distance thus changes the detuning of the drive laser with respect to the cavity resonance frequency, which, in turn, alters the circulating power (assuming input power and laser frequency to be fixed quantities). Conversely, the radiation pressure force of the cavity field on the movable mirror depends on the circulating power; therefore a change in the cavity mode occupancy entails a change in the force on the mirror, thus influencing its motional state.

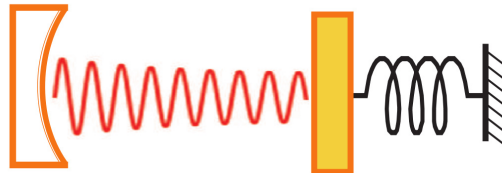


Figure 2.2.1: Simple illustration of a Fabry-Pérot type cavity with one moving mirror. The movement will modulate the resonance frequency of the cavity and thus the circulating power (for fixed drive laser frequency). In turn, this results in modulation of the radiation pressure impinging on the moving mirror.

As an alternative to the “reflective” setup in Fig. 2.2.1, cavity mechanical coupling – and cooling – may also be achieved using “dispersive” coupling schemes, as will be described in section 2.3. The form of the Hamiltonian derived below turns out to be valid for both approaches, at least in a certain limit. The derivation of the Fabry-Pérot/reflective type coupling has the advantage of being more straightforward as well as simpler to understand physically.

We will now show how to obtain the cavity mechanical Hamiltonian in the presence of a cavity drive. It has been argued recently that this drive need not be coherent [17]; although interesting, this is peripheral to our discussion and we shall assume a coherent cavity drive.

A rigorous derivation of the quantum Hamiltonian governing the interaction of radiation pressure and mechanics has been given in Ref. [15], starting from the classical equations of motion. The classical Hamiltonian (arrived at via a Lagrangian formulation) is then subjected to the canonical quantization prescription. This general quantum Hamiltonian can then, for our purposes, be linearized in small mechanical oscillation amplitudes relative to the equilibrium cavity length. By furthermore assuming that the mechanical frequency is small relative to the cavity mode spacing, we may retain just a single cavity mode. Rather than stating the resulting Hamiltonian straight away, we introduce it by a simple, more intuitive argument.

The free field Hamiltonian of an optical cavity mode in diagonal form may be written $\hat{H}_{\text{cav}} = \hbar\omega_{\text{cav}}\hat{b}^\dagger\hat{b}$ (neglecting its zero-point energy). The mode frequency ω_{cav} is one of the resonance frequencies of the cavity, the set of which depends on the cavity length (as well as the mirror geometry). Now, if we allow one mirror to move, the set of resonances will be altered; specifically, our chosen mode frequency will acquire a mirror position dependence $\omega_{\text{res}}(x)$. If the mirror is taken to perform small quantum oscillations \hat{x} around an equilibrium cavity length L (in absence of a drive), then we may Taylor expand around this to obtain a quantum description $\omega_{\text{res}}(x) \rightsquigarrow \omega_{\text{res},0} - \hat{x} \left. \frac{d\omega_{\text{res}}}{dx} \right|_{x=L}$, where $\omega_{\text{res},0} \equiv \omega_{\text{res}}(x=L)$ and we have defined the positive position axis of \hat{x} such that an increase corresponds to a decrease in cavity length. Substituting this into \hat{H}_{cav} above, the desired coupling term between cavity and mechanics appears,

$$\hat{H}_{\text{cav}} \rightsquigarrow \hat{H}_{\text{cav},0} + \hat{H}_{\text{int}} = \hbar\omega_{\text{cav},0}\hat{b}^\dagger\hat{b} - \hbar \left. \frac{d\omega_{\text{res}}}{dx} \right|_{x=L} \hat{b}^\dagger\hat{b}\hat{x}.$$

Considering the fundamental frequency, we have $\omega_{\text{res}}(x) = \frac{2\pi c}{x}$ and $\omega'_{\text{res}}(x=L) = -\frac{2\pi c}{L^2} = -\frac{\omega_{\text{cav},0}}{L}$, whereby we obtain the interaction term

$$\hat{H}_{\text{int}} = \frac{\hbar\omega_{\text{cav},0}}{L}\hat{b}^\dagger\hat{b}\hat{x} = \hbar g\hat{b}^\dagger\hat{b}(\hat{a} + \hat{a}^\dagger), \quad (2.2.1)$$

in agreement with the rigorous result in the limit of interest; in the second expression for the interaction we have introduced the usual creation and annihilation operators for the mechanical oscillator of characteristic length $x_0 = \sqrt{\frac{\hbar}{2m\omega_{\text{mech}}}}$ as well as the single-photon coupling $g \equiv \frac{\omega_{\text{cav},0}x_0}{L}$. Combining this radiation pressure interaction Hamiltonian with the free evolution terms and the coherent cavity drive term, we arrive at the full Hamiltonian accounting for the coherent part of the system evolution (in a rotating frame with respect to the drive frequency ω_{drive}) [31]

$$\hat{H} = \hbar\omega_{\text{mech}}\hat{a}^\dagger\hat{a} - \hbar\Delta'\hat{b}^\dagger\hat{b} + \hbar\frac{\Omega}{2}(\hat{b} + \hat{b}^\dagger) + \hbar g\hat{b}^\dagger\hat{b}(\hat{a} + \hat{a}^\dagger), \quad (2.2.2)$$

in terms of the drive detuning $\Delta' \equiv \omega_{\text{drive}} - \omega_{\text{cav},0}$ and the driving rate $\Omega \equiv 2\sqrt{P\kappa_{\text{ex}}/\hbar\omega_{\text{drive}}}$ accounting for the rate at which drive photons can enter the cavity, where P is the impinging power and κ_{ex} is the coupling rate to the

relevant free-space modes. In addition to the coherent dynamics, the inevitable coupling to the environment effectively results in incoherent dynamics, namely dissipation and the associated noise influx as will be discussed in more detail in section 4.1. Mathematically, the incoherent processes may be accounted for using either a master equation approach or by deriving Heisenberg-Langevin equations for \hat{a} , \hat{b} and their Hermitian conjugates.

A common next step is to perform a canonical shift of the operators $\hat{a} \rightarrow \alpha + \hat{a}$ and $\hat{b} \rightarrow \beta + \hat{b}$, where α, β are the classical equilibrium values of the dynamical variables given the applied drive [32, 7, 12]; in this way, the transformed operators \hat{a}, \hat{b} now represent the quantum fluctuations around the classical steady state of the driven cavity of mean photon number $|\beta|^2$. Under this canonical transformation the Hamiltonian (2.2.2) becomes

$$\hat{H}' = \hbar\omega_{\text{mech}}\hat{a}^\dagger\hat{a} - \hbar\Delta\hat{b}^\dagger\hat{b} + \hbar g(\hat{b}^\dagger\hat{b} + \beta^*\hat{b} + \beta\hat{b}^\dagger)(\hat{a} + \hat{a}^\dagger), \quad (2.2.3)$$

where the linear (drive) terms have disappeared and a frequency shift due to the interaction has been absorbed in the redefined detuning Δ . Given that the operators now describe relatively small quantum fluctuations, it is permissible in most cases of interest to neglect the cubic term $\propto \hat{b}^\dagger\hat{b}(\hat{a} + \hat{a}^\dagger)$ in Eq. (2.2.3), thereby obtaining a linear theory. From the remaining interaction term,

$$\hat{H}_{\text{lin-int}} = \hbar g(\beta^*\hat{b} + \beta\hat{b}^\dagger)(\hat{a} + \hat{a}^\dagger), \quad (2.2.4)$$

we reach two important conclusions about cavity opto-mechanical interactions: Firstly, the coupling between the mechanical degree of freedom and the cavity field is enhanced by the steady state cavity mode occupancy induced by the drive field. Thus, we are led to define the *many-photon coupling* strength $g' \equiv \beta g$. The vast majority of cavity opto-mechanical experiments rely on this effect to achieve appreciable coupling.

Secondly, the linearized interaction Hamiltonian, Eq. (2.2.4), allows for *beam-splitter type interaction* $\sim \hat{b}^\dagger\hat{a} + \hat{a}^\dagger\hat{b}$, suited for the process of cooling, but has two additional terms. It is possible, to some degree, to control which of the terms are dominant by adjusting the (effective) drive detuning Δ . By picking a drive frequency red-detuned by the mechanical frequency, $\Delta = -\omega_{\text{mech}}$, the beamsplitter terms become resonant (energy conserving) and thus dominate. Beamsplitter interaction can be understood as the coherent transfer of excitations between two modes conserving the total number of quanta. Conversely, a blue-detuned drive, $\Delta = +\omega_{\text{mech}}$, will favor the terms $\sim \hat{b}\hat{a} + \hat{a}^\dagger\hat{b}^\dagger$ resulting in two-mode squeezing by down-converting drive photons. In the weak coupling regime $g' < \sqrt{\kappa\gamma_{\text{mech}}}$, where no hybridization between the cavity and mechanical modes occurs, the suppression of the non-dominant pair of terms is mainly governed by the ratio $\kappa/\omega_{\text{mech}}$; this is, by definition, a small quantity in the resolved sideband regime. The neglect of the off-resonant terms amounts to the Rotating Wave Approximation (as will be discussed in a slightly different context in section 4.1.4.2).

2.2.2 Cavity-assisted resolved sideband cooling

We will now argue – physically and pictorially – why the resolved sideband regime, $\kappa < \omega_{\text{mech}}$, allows for efficient cavity-assisted cooling of the mechanical

degree of freedom when the drive is red-detuned from the cavity resonance by the mechanical frequency, $\Delta = -\omega_{\text{mech}}$. We do so by considering the Raman scattering of drive photons as visualized in a pair of energy and spectral density diagrams.

First, we consider a diagram of the spectral density of the cavity, Fig. 2.2.2, where two competing processes are indicated. An anti-Stokes scattering event has the cooling effect of carrying away a mechanical quantum of energy as the result of a drive photon being upconverted to the cavity resonance frequency. Conversely, a Stokes event has the heating effect of adding a mechanical phonon. Thus, corresponding upper and lower sidebands appear in the output spectrum of the cavity. It is the asymmetry in the density of states around the drive frequency that allows us to give priority to either the Stokes or anti-Stokes process. If, on the contrary, the width of the cavity resonance were broad compared to the mechanical frequency, $\kappa \gg \omega_{\text{mech}}$, then this asymmetry would essentially vanish. This is the intuitive reason why the resolved-sideband regime is desirable for cooling. Note that we are here assuming a narrow mechanical level, $Q_{\text{mech}} \gg 1$; if this were not fulfilled it would also destroy the desired asymmetry between the Stokes and anti-Stokes rates.

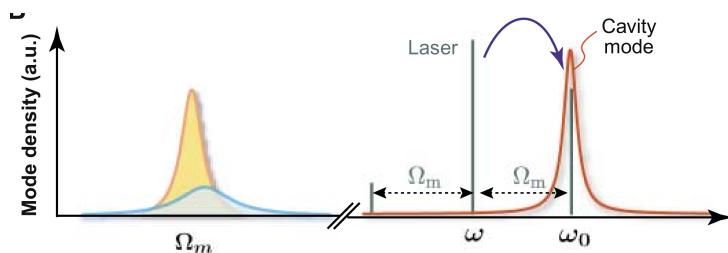


Figure 2.2.2: Cavity density of states with the competing processes indicated, cooling versus heating. The cavity drive is red-detuned from the narrow resonance by the mechanical frequency (here, $\Omega_m \equiv \omega_{\text{mech}}$); the mechanical mode may supply the remaining energy needed to reach the resonance by giving up a phonon. Reproduced from Ref. [14].

Fig. 2.2.2 is an illustration of the effective cooling rate formula as expressed in terms of the competing Stokes and anti-Stokes rates [18]:

$$\Gamma_{\text{cool}} = g^2 [S_{nn}(+\omega_{\text{mech}}) - S_{nn}(-\omega_{\text{mech}})], \quad (2.2.5)$$

here g is the single-photon coupling strength defined in section 2.2.1 above and $S_{nn}(\omega)$ is the power spectrum of the photon number autocorrelation function. The latter is defined as $S_{nn}(\omega) \equiv \int_{-\infty}^{\infty} dt e^{i\omega t} [\langle \hat{b}^\dagger(t) \hat{b}(t) \hat{b}^\dagger(0) \hat{b}(0) \rangle - \langle \hat{b}^\dagger(t) \hat{b}(t) \rangle^2] = \bar{n} \frac{\kappa}{(\omega + \Delta)^2 + (\kappa/2)^2}$, where the last expression (in terms of the mean occupancy \bar{n}) comes from evaluation for $g = 0$ as is appropriate for the purposes of the weak coupling result, Eq. (2.2.5); it is this Lorentzian distribution peaked at $\omega = -\Delta$ and of width κ that we considered in Fig. 2.2.2. The resulting steady state mechanical phonon occupancy is given by a weighted average of the competing influences from the cavity cooling and the thermal bath:

$$n_{\text{mech}}^{(\text{ss})} = \frac{\Gamma_{\text{cool}} n_{\text{RSB}} + \gamma_{\text{mech}} n_{\text{th}}}{\Gamma_{\text{cool}} + \gamma_{\text{mech}}},$$

where γ_{mech} is the intrinsic mechanical decay rate and the effective cavity occupancy is $n_{\text{RSB}} = (\kappa/4\omega_{\text{mech}})^2$ which goes to zero as we go further into the resolved-sideband regime.

The above picture may be supplemented with the energy level diagram seen in Fig. 2.2.3. Here we can think of the process of creating a phonon and a cavity photon from a red-detuned drive photon as being suppressed due to its detuning from the corresponding narrow level.

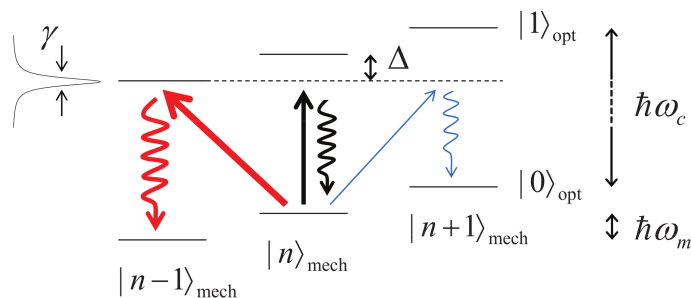


Figure 2.2.3: A partial product state level diagram for the system consisting of a mechanical and a cavity mode in the resolved sideband regime. The process of creating a cavity photon from a mechanical phonon and a drive photon is resonant while the creation of a phonon is suppressed due to the detuning. Reproduced from Ref. [22].

It must be noted that the above picture holds true in the weak cavity-mechanical coupling limit, $\Gamma_{\text{cool}} + \gamma_{\text{mech}} \ll \kappa$, as we will elaborate on in the next section. As hybridization between the cavity and mechanical modes sets in, the simple picture is no longer valid.

Finally, it should be mentioned that cooling in the resolved-sideband regime can also be understood as a consequence of so-called dynamical back-action. The long lifetime of the photons in the cavity, as compared to the mechanical period, implies that the mechanical oscillator will encounter each photon many times before it leaks out. This optical retardation allows the radiation pressure force to become anti-correlated with the mechanical motion and thus leads to damping.

2.2.3 Limiting mechanisms

To calculate the degree of cooling achievable, i.e., the minimal steady state occupancy of the mechanical degree of freedom, requires the combination of the Hamiltonian, Eq. (2.2.3), with a description of the dissipative dynamics arising from reservoir couplings, as also noted above. The latter is, of course, crucial because the resulting occupancy of the mechanical mode of interest, that is, its effective “temperature”, will be a weighted average of the occupancies of the reservoirs influencing it. (In fact, it can be argued that only in the presence of reservoirs is the notion of temperature meaningful.) The Hamiltonian, accounting for the coherent dynamics, can be regarded as dictating how the influences

of the environment (the various reservoirs) are distributed among the system degrees of freedom.

The calculation of the steady state occupancy can be approached using different approximation schemes depending (primarily) on whether the weak or strong coupling regime is considered; of these the weak coupling result was given in the previous section along with physical argument leading to it. An exact analytical solution of the linear theory is possible, but the resulting formulas are quite opaque [31]. Rather than delving into the technical derivations of various limits, we will in this section review the important mechanisms and influences limiting the achievable cooling of the mechanical mode at detuning $\Delta = -\omega_{\text{mech}}$ in the resolved sideband regime.

To the extent that we are in the weak coupling regime, $\Gamma_{\text{cool}} + \gamma_{\text{mech}} \ll \kappa$, where the interpretation embodied in Fig. 2.2.2 and Eq. (2.2.5) holds true, the achievable final mechanical occupancy depends on how deep into the resolved sideband regime we are. By detailed balance considerations applied to the Lorentzian spectrum we find this lower limit to be $n_{\text{RSB}} = (\kappa/4\omega_{\text{mech}})^2$, which approaches zero in the ultra resolved sideband limit. However, on physical grounds it is easy to realize that this picture has its limitations. For instance, if, contrary to our assumption, κ becomes comparable to γ_{mech} , then the intrinsic heating of the membrane is trapped due to the bottleneck imposed by the almost closed cavity.

As stated earlier in this section, the steady state mechanical occupancy will somehow be a compromise between the reservoir occupancies impinging on the system. The effective rates of excitation exchange with the reservoirs matter, of course, but in any case we cannot imagine to cool beyond the lowest-occupancy reservoir. An important environmental influence to consider is that of “intrinsic” mechanical heating, due to coupling to the vibrational modes of its support or internal friction. A remedy, outside simply improving the Q factor, is to subject the setup to cryogenic pre-cooling as previously mentioned, thereby decreasing n_{th} as a consequence of the lower temperature T . This may also counteract the heating of the membrane that follows from absorption of cavity photons.

For example, precooling to a temperature $T = 50\text{mK}$ and employing a 10MHz mechanical oscillator, the cavity-assisted cooling will be competing against a reservoir with an occupancy of about $n_{\text{th}} = [\exp(\hbar\omega_{\text{mech}}/k_{\text{B}}T) - 1]^{-1} \sim 100$. (It must be kept in mind, however, that in this competition, not only the various reservoir occupancies matter, but also the dissipation rates of the system into the respective reservoirs.) From this we see that increasing the mechanical frequency into the GHz domain makes it possible to reach the mechanical ground state by cryogenic means alone, as has indeed been achieved [20].

Due to the magnitude of optical frequencies (THz), the noise entering an optical cavity via the input port is essentially vacuum noise even at room temperature (disregarding technical laser noise). In the case of an electrical microwave resonator at a frequency of a few GHz, this is no longer the case.

Ultimately, the cooling process will be limited by quantum zero-point fluctuations. This is the so-called *quantum back-action* on the mechanical oscillator arising from the randomness of the momentum kicks from reflected photons; this effect sets a limit analogous to the Doppler limit in the cooling of atomic motion. Somewhat related to quantum back-action is detector shot noise due to the random arrival of photons; this is of interest because we most likely wish

to monitor the mechanical motion. The influence of the detector shot noise can be lessened by increasing the drive power, but this comes at the expense of increased quantum back-action.

2.3 Coupling schemes

In section 2.2.1, the parametric coupling Hamiltonian between a mechanical oscillator and a cavity mode was derived for the Fabry-Pérot type setup. The purpose of this section is to point to other cavity-mechanical coupling schemes that may give rise to essentially the same interaction. This opens up a range of possibilities for combining these into hybrid, multi-cavity systems, as we will consider later.

2.3.1 Reflective coupling

We have already considered in some detail the reflective coupling arising in the Fabry-Pérot cavity where one mirror is allowed to move. This can for instance be realized by attaching a micromirror to a cantilever of the sort used in Atomic Force Microscopy.

An electrical resonator may also participate in such reflective interaction. Analogously to the optical case above, this can be achieved by allowing one of the plates of a parallel plate capacitor to move, see Fig. 2.3.1. This could for instance be achieved by letting a conducting, vibrating membrane play the role of one of the capacitor plates. The coupling strength is proportional to the slope of the capacitance w.r.t. plate position relative to the total capacitance of the electrical resonator.

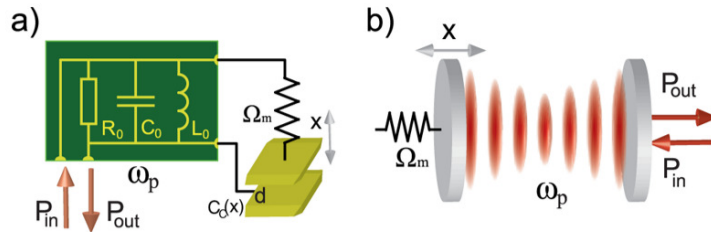


Figure 2.3.1: Reflective cavity mechanical coupling in electrical and optical settings, respectively. In the electrical case (a), the capacitive coupling strength is determined by the magnitude of the relative capacitance changes that result from the motion of one of the capacitor plates. Reproduced from Ref. [7].

To give an example of a more exotic geometry, it can be mentioned that one experiment [23] uses a microtoroidal optical cavity supporting whispering gallery modes (WGM) that are coupled to a mechanical radial breathing mode (RBM) (see Fig. 2.3.2).

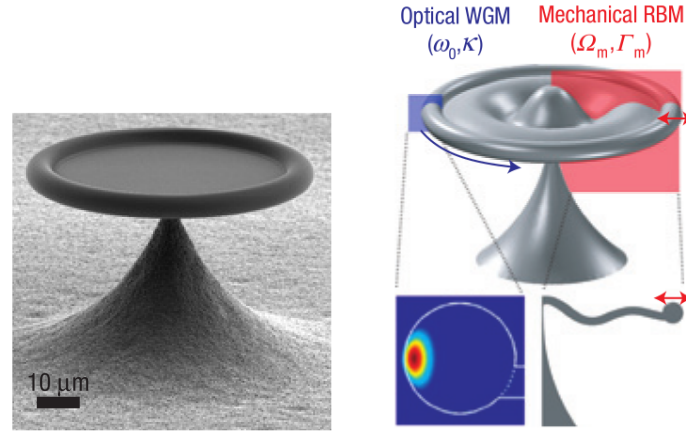


Figure 2.3.2: Microtoroidal optomechanical setup including a Whispering Gallery Mode interacting with a mechanical Radial Breathing Mode. Reproduced from [23].

2.3.2 Dispersive coupling

The reflective approaches mentioned above have the characteristic that the oscillating mechanical element forms an integral part of the cavity. This may lead to conflicting design requirements regarding implementations. For instance, the quality factor Q of a mechanical cantilever might suffer significant decrease when a micromirror is mounted to it for the purposes of building a Fabry-Pérot type setup.

Dispersive coupling schemes, on the other hand, offer the advantage of physically separating the cavity from the mechanical element. This may allow separate optimization of the two components. We consider opto-mechanical and electro-mechanical instances of dispersive coupling separately below.

2.3.2.1 Opto-mechanical link

In the opto-mechanical case, the dispersive coupling is also known as the “membrane-in-the-middle” approach, see Fig. 2.3.3 (left). Here, a dielectric, semitransparent membrane is placed inside a regular Fabry-Pérot cavity with fixed end mirrors. The fact that photons have to propagate through the dielectric will effectively change the resonance condition. Importantly, the modification of the resonance condition will have a dependence on the membrane position because its placement w.r.t. to the nodes and anti-nodes of the field matters; this can be seen from Fig. 2.3.3 (right) where the cavity detuning is plotted as a function of position for different membrane reflectivities. It follows that we may have mutual coupling between the cavity field and the mechanical mode, but it is perhaps not obvious that we can achieve cooling as in the reflective scenario. However, it can be shown in the limit of high reflectivity that optomechanical cooling is indeed possible with such a dispersive setup [12].

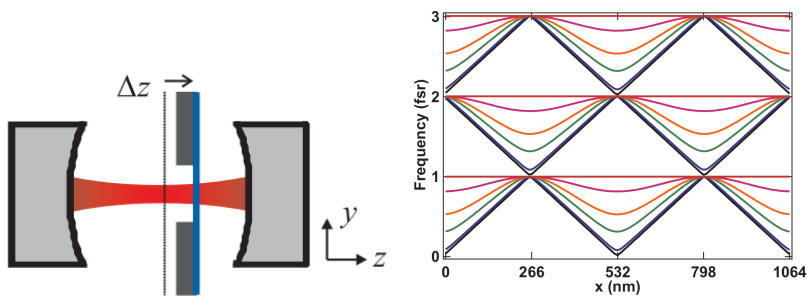


Figure 2.3.3: (Left) Dispersive opto-mechanical scenario with a membrane inside a regular Fabry-Pérot cavity. (Right) An example of a plot of cavity detuning as function of membrane position. The coupling strength is proportional to the slope evaluated at the equilibrium position. The curve follows the pattern of nodes and anti-nodes. By positioning the membrane between nodes \hat{x} coupling is achieved while if placed at a node \hat{x}^2 coupling takes place, potentially allowing for Quantum Non-Demolition measurements. Reproduced from Refs. [30, 12].

2.3.2.2 Electro-mechanical link

Dispersive coupling also occurs in the electro-mechanical setting when a polarizable mechanical oscillator is placed in the inhomogeneous electric field surrounding the capacitive element of an electrical circuit. This is an alternative to the reflective setup where the mechanical element serves as one of the capacitor plates.

The physics of the dispersive electromechanical coupling can be understood as follows: A dielectric object exposed to an electric \mathbf{E} field will attain a polarization, which is to say that the charges of the (typically overall neutral) object are redistributed in a non-uniform manner. Due to its polarized state, the dielectric object will experience a *Kelvin polarization force* if the electric field is inhomogeneous since then the total force on the positive and negative charges will no longer counterbalance (as compared to a spatially uniform field). In the case of a linear dielectric, the macroscopic polarization is given by the simple relation $\mathbf{P} = \epsilon_0(\epsilon_r - 1)\mathbf{E}$. Inserting this relation in the definition of the Kelvin polarization force density, we find [24]

$$\mathbf{f}_{\text{KP}} = (\mathbf{P} \cdot \nabla)\mathbf{E} = \epsilon_0(\epsilon_r - 1)(\mathbf{E} \cdot \nabla)\mathbf{E} = \frac{1}{2}\epsilon_0(\epsilon_r - 1)\nabla(\mathbf{E} \cdot \mathbf{E}), \quad (2.3.1)$$

pointing in the direction of higher field intensity. Consider for instance the dielectric beam mounted above a pair of electrodes depicted in Fig. 2.3.4; according to Eq. (2.3.1) it will be pulled into the inhomogeneous electric field of the electrodes, as will arise from applying a bias voltage. But since the capacitance of the configuration depends on the position of the mechanical element (and its dielectric properties), there will be mutual interaction between the vibrational mode of the beam and the mode of the electric circuit in which the electrodes enter. As for the reflective case, the coupling strength will depend on the relative capacitance change brought about by the movement of the mechanical element.

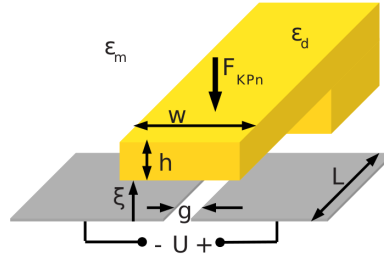


Figure 2.3.4: Dispersive electromechanical coupling between a capacitive circuit element and a dielectric beam placed in its fringing field. The vibrational mode of the beam acts back on the circuit through the capacitance fluctuations induced by its movement.

This particular type of coupling will receive special attention in this thesis: A calculation of the coupling strength and the mechanical frequency shift arising from dispersive electro-mechanical coupling is performed in Chapter 3.

2.4 Transduction schemes

In the greater perspective of quantum information science, cavity-assisted electromagnetic interaction with a mechanical oscillator is considered a promising candidate mechanism for wavelength conversion of quantum states [22], simply by letting a single mechanical oscillator interact simultaneously with two electromagnetic cavity modes.

In this direction it has been proposed that the mechanical mode of a cavity opto-mechanical setup may serve as an intermediary between two distinct optical modes of the same cavity, thus providing a mechanism for wavelength conversion of photonic quantum states in a quantum network [28]. However, wavelength conversion between two electromagnetic modes can be envisioned even when they do not live in the same cavity: By letting a mechanical oscillator be common to two electromagnetic cavities. It is in particular this kind of setup that is of interest for the purposes of this thesis. The partial catalogue of coupling schemes in section 2.3 was presented with the potential of such combinations in mind. A significant proposal along these lines lets cavity opto-mechanical systems function as conversion links between stationary qubits and an optical fiber, in turn, connecting the qubits in a quantum network [25]. In order to implement information protocols involving the transfer of quantum states, strong coupling must be attained; this is the regime where coherent interaction prevails over couplings to reservoirs. This usually requires many-photon enhancement of the coupling by means of a drive field applied to the cavity. The fact that this renders the coupling effectively linear is compatible with the beamsplitter interaction required for quantum state transfer. As discussed above, precooling may also be necessary for environmental heating not to overwhelm the coherent dynamics.

These ideas may also be exploited for cooling purposes. It has been proposed [27] to use the opto-mechanical cooling mechanism to cool additional objects via the

harmonically bound mechanical object, the latter acting as a transducer. More specifically, the following setup has been put forward: A vibrating microscale membrane, enclosed in an optical cavity and cooled by the above mechanism, is additionally capacitively coupled to an electrical LC circuit (with a radio frequency bias field bridging the frequency gap). In this way, cooling as well as sensitive readout of the electrical circuit can potentially be performed via upconverting microwave photons to optical frequencies.

As a further extension to this scheme, one can imagine coupling the LC circuit to yet another physical system with the aim of performing optical cooling or readout via the combined link of LC circuit and mechanical mode; chapter 5 is concerned with the exploration of the cooling aspect of this idea. There, in section 5.1.2, we will give a more thorough account of the aforementioned scheme to cool the LC circuit, the understanding of which is a preliminary to the further extensions we will consider later.

Chapter 3

Electromechanical coupling calculations

In this chapter, a procedure is developed for assessing capacitive coupling schemes. More specifically, it allows for the calculation of important quantities such as coupling strength and mechanical frequency shift based on the geometry of the setup and certain material properties. The procedure was developed with a specific experimental setup in mind and rely on certain geometrical circumstances to be present. Nevertheless, it seems likely to be applicable to most setups involving a vibrating membrane as its mechanical degree of freedom. It is a generalization of the derivation presented in Ref. [27] that takes into account the mode shapes of the interacting degrees of freedom of the circuit and the mechanical component.

In section 3.1 we present an approach to modeling a mechanical membrane and an electrical LC circuit as well as their interface at the capacitive element of the circuit. On this basis we obtain a Hamiltonian description of the capacitive interaction suited for quantization. The procedure relies on knowledge of the capacitance of the interface unit cell (to be defined below); this must be obtained numerically in most cases and therefore this aspect will also receive attention. The experimental setup that prompted the development of the procedure will be used to illustrate and motivate the derivation throughout; however, we will seek to emphasize to what extent the ideas presented here are applicable to other setups.

Based on our Hamiltonian description, we will in section 3.2 extract formulas for electromechanical coupling strength and the induced shifts of the mechanical frequency. These will be applied, in section 3.3, to the preliminary, ongoing experiments conducted by the membrane group at QUANTOP, NBI and compared to measurement data.

3.1 Modeling

The strategy employed here for obtaining a quantum description of the above system is the following: For each subsystem, circuit and mechanical mode, we

apply the canonical quantization procedure to their separate classical Hamiltonians. The interaction Hamiltonian H_{int} of the (parametric) capacitive coupling is obtained perturbatively by letting the capacitance depend on the membrane configuration $C \rightsquigarrow C[z(x, y)]$ and Taylor expanding in a suitable way. For the full system Hamiltonian this substitution translates into:

$$H = H_{\text{m},0} + H_{\text{c}} \rightsquigarrow H_{\text{m},0} + H_{\text{c},0} + H_{\text{int}}, \quad (3.1.1)$$

where $H_{\text{m},0}$ is the free mechanical oscillator term and $H_{\text{c},0}$ describes the non-interacting circuit evaluated at the classical equilibrium configuration of the membrane, $C^{(\text{eq})} = C[z^{(\text{eq})}(x, y)]$ (the coordinates of the membrane will be introduced below).

Admittedly, a fully rigorous quantization would have to start from the full set of coupled classical equations. This is in complete parallel to the distinction between the two alternative derivations of the cavity opto-mechanical coupling discussed in section 2.2.1. As in that case, it is reasonable to believe that the perturbative formalism developed here is valid for small quantum fluctuations around the classical equilibrium configuration.

In the sections to follow, the different components of the Hamiltonian (3.1.1) are worked out. But before considering any of the subsystems in particular, it is crucial to establish a model for their interface that is manageable yet sufficiently true to the physics. This is the topic of the following section.

3.1.1 The electromechanical interface

A capacitive element of an electrical circuit is, roughly speaking, a pair of sites where charges of opposite sign may pile up. The *capacitance* is a geometrical quantity in electrostatic theory signifying how much charge will pile up per unit voltage difference between the two opposing sites, $Q = C\Delta V$. The circuit diagram symbol for a capacitive element alludes to the parallel plate capacitor, but of course many other geometries can be envisaged, for instance, based on the “dispersive” physical interaction described in Section 2.3.2.2. Indeed, the particular setup from which this procedure arose and which will be used for illustration throughout relies on this is the of kind of interaction.

Capacitive coupling occurs if a segment of the capacitive arrangement is allowed to move and, additionally, the motion is affected by the rearrangement of charge in the circuit.¹ Given an instantaneous spatial configuration of the capacitive arrangement, we may in principle, analytically or numerically, calculate its capacitance. Analytical solutions are only available in special cases, while numerically, the task is certain to be demanding computationally in case of an arrangement with many minute features.

To circumvent this, we will model the system in a way that allows us to treat the capacitive arrangement in terms of a number of 3-dimensional spatial subdivisions, *capacitive unit cells*, for which we may calculate the capacitance independently of other cells by exploiting approximate symmetries. In general, the capacitance of the entire capacitor-mechanical configuration is a functional

¹If the latter is not the case, it will be formally equivalent to the capacitance being a given function of time, $C(t)$.

of the mechanical configuration, $C_{\text{tot}} = C_{\text{tot}}[z(x, y)]$ (expressed in some coordinate system). However, in our approximate description where the capacitive unit cells can be evaluated independently, it makes sense to define a capacitance C_i of cell i that only depends on the position, z_i , of the local patch of mechanical element contained in this cell. The unit cell segmentation must be chosen according to a periodic pattern in the structure of the capacitive circuit element; in this way it will conform to symmetries we will require below. Given this similarity of unit cells, the position z_i being the only geometrical variable, we may introduce the function $C_i \equiv C(z_i)$ providing the capacitance of a single cell.

To be clear, the unit cells are not treated as if they were alone in free space; rather, by assigning appropriate boundary conditions, we account for the fact that they are segments of a larger periodic structure. In that sense, the capacity C_i is not exclusively that of a single cell. Given a physical system for which the above approach is reasonable, the segmentation into unit cells may significantly reduce the computational burden.

These ideas will now be properly demonstrated in the context of the specific geometry shown in Fig. 3.1.1 (see also Fig. 3.3.1 on page 48). The capacitive circuit element is an InterDigitated Capacitor (IDC) comprised of two closely spaced sets of fingers; if a bias voltage V_b is applied across these two hands, they will become oppositely charged and an inhomogeneous electric field will arise. The membrane is imagined to be made of dielectric, conducting or semi-conducting material (or even a layered hybrid of these). Charges residing in it will be displaced in response to an electric field. If the field is inhomogeneous, the membrane will experience a net force which, in turn, is modulated by the position of the membrane. Hence, the capacitive interaction is realized by suspending the membrane in a region of appreciable field inhomogeneity.

The membrane and the IDM both lie in xy -planes, but their projections may not fully overlap. We map out the union of these two areas by a square grid as indicated in Fig. 3.1.1 (left). The grid increment $\Delta x = \Delta y$ is fixed by the center-to-center distance of neighboring fingers, with the intervals starting and terminating on such neighboring centers (see Fig. 3.1.1, (right)). Each square of the grid in the xy -plane is the projection of a rectangular box that also extends in the z -direction. The vertical z -distance between the top of the fingers and the membrane varies very little over the length scale Δx (in any (x, y) -direction) for small vibration amplitudes.² The latter observation along with the choice of (3-dimensional) grid allow for the following crucial approximations in calculating the capacitance of a unit cell: The assumptions of 1) reflection symmetry of the capacitive arrangement in the yz -planes bounding any unit cell, and 2) translational symmetry in the y -direction.

We now discuss the motivation for and validity of these related approximations: Regarding the first, '1)', it allows us to impose on the aforementioned yz -planes the boundary condition of no electric field component in the x -direction as follows from the (approximate) symmetry. If we imagine the IDC to have infinitely many fingers, then indeed this component of the arrangement has the

²Note that, ignoring the edges, the IDM has translational symmetry along the y -axis, hence no natural length scale offers itself here. However, since we require changes in the membrane displacement to be small over the entire xy -patch of any unit cell, it seems natural to treat the two directions equally by making the choice $\Delta y = \Delta x$.

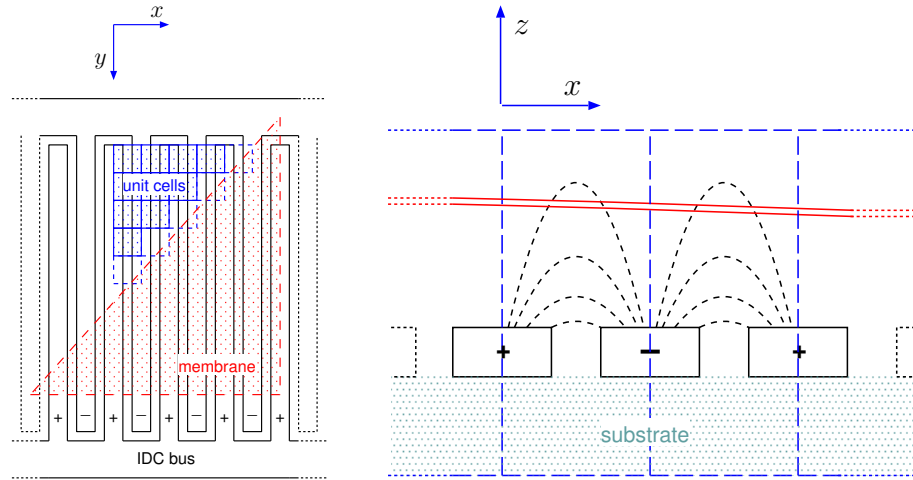


Figure 3.1.1: Capacitive coupling between a membrane and an InterDigitated Capacitor (IDC). (Left) Cross section in an xy -plane, parallel to that of the rectangular membrane (red, partly shown), which is suspended above the IDC (black). Only a few square projections of unit cells (blue) are shown, but the entire area of the IDC fingers is covered. (Right) Cross section in an xz -plane, view along the positive y -axis. Electric field lines between neighboring fingers are sketched (increasingly vertical towards the cell boundary). The distance between the fingers (black) and the membrane (red) is essentially constant over the length of a unit cell (blue). The IDC is mounted on a dielectric substrate (cadet blue).

stated symmetry. Even for a finite number of fingers, this is expected to be a good approximation for unit cells well within the interior of the IDC. But we must also consider the membrane, whose configuration does not obey this symmetry (except when it is in a globally flat state). However, given that the vertical distance is essentially constant on the length scale Δx of the unit cell, it is reasonable to consider the membrane flat (along x) in the vicinity of any unit cell. The deviations from flatness of more distant parts of the membrane is likely to have a small effect, and hence we take '1)' to be true for the membrane as well.

Regarding the second, '2)', it allows us to reduce the calculation of the unit cell capacitance to a 2-dimensional problem because of the (approximate) translational invariance in the y -direction. This relies on the fact that this is a continuous symmetry as opposed to the discrete symmetry of '1)'. First, we note that the IDC obeys this symmetry if we, again, ignore edge effects. Regarding the membrane, we argue as for '1)': It is essentially flat in the vicinity of any unit cell and distant membrane segments have negligible effect.

The validity of these two approximate symmetries determines to a large extent the validity of the procedure presented in this chapter. Without these symmetries it would make little sense to define a single-cell capacitance. How they explicitly enter the calculations will be demonstrated in Section 3.1.4, where we prepare the unit cell capacitance calculation for numerical evaluation. Additionally, the segmentation into unit cells will be decisive for how we model the

electrical circuit in Section 3.1.3.

3.1.2 The mechanical membrane

An ideal membrane is a very thin and flexible planar object, a film. It has no resistance to bending, that is, zero flexural rigidity. It will, however, react to (in-plane) tension and by applying such tension to the membrane it acquires a restoring force in response to out-of-plane displacements. This is the situation we will consider in the linear, small-deflection regime. The thinness criterion can be stated as the ratio of the thickness h and side length L obeying $h/L \lesssim 10^{-2}$, which is satisfied for the the experimental setup we are considering. [29]

The tensioned membrane is a 2-dimensional generalization of the well-known 1-dimensional vibrating string. As such, its (small) out-of-plane displacements from equilibrium obey the 2-dimensional wave equation

$$\nabla^2 z(x, y, t) = \frac{1}{v^2} \frac{\partial^2 z(x, y, t)}{\partial t^2}, \quad (3.1.2)$$

where the xy -plane is that of the membrane and v is the propagation velocity. To give a sense of how the theory is modified as we approach larger ratios h/L , we remark that in this transition the Laplacian ∇^2 appearing in the wave equation (3.1.2) is replaced by the biharmonic operator

$$\nabla^4 \equiv \frac{\partial^4}{\partial x^4} + 2 \frac{\partial^4}{\partial x^2 \partial y^2} + \frac{\partial^4}{\partial y^4}.$$

This is the transition from membrane theory to that of *thin plates*, for which the finite flexural rigidity must be taken into account.

3.1.2.1 Drum modes

It will prove useful to obtain a complete set of solutions to the equation of motion, Eq. (3.1.2), subject to boundary conditions. Especially so if these are modes of definite frequency, in which case we by expressing the motion of the membrane in terms of these obtain a diagonal Hamiltonian. For definiteness, we will consider a square membrane of side length L , but all geometries for which the spatial Helmholtz equation has a closed-form solution are compatible with the formalism employed in the following.

We approach the equation of motion by separation of variables, i.e., considering solutions in which the variable dependencies factorize, $z(\tilde{x}, \tilde{y}, t) = X(\tilde{x})Y(\tilde{y})f(t)$, where we have introduced dimensionless position variables $\tilde{x} \equiv (x/L)$, $\tilde{y} \equiv (y/L)$ in terms of the characteristic length L . Inserting this expression into Eq. (3.1.2) and dividing through by z we find

$$\frac{1}{X(\tilde{x})} \frac{\partial^2 X(\tilde{x})}{\partial \tilde{x}^2} + \frac{1}{Y(\tilde{y})} \frac{\partial^2 Y(\tilde{y})}{\partial \tilde{y}^2} = \frac{L^2}{v^2 f(t)} \frac{\partial^2 f(t)}{\partial t^2}. \quad (3.1.3)$$

Applying the usual argument that these three terms must be (dimensionless) constants, we are led to solve the separate differential equations

$$\frac{1}{X(\tilde{x})} \frac{\partial^2 X(\tilde{x})}{\partial \tilde{x}^2} = -k_m^2, \quad \frac{1}{Y(\tilde{y})} \frac{\partial^2 Y(\tilde{y})}{\partial \tilde{y}^2} = -k_n^2, \quad \frac{1}{f(t)} \frac{\partial^2 f(t)}{\partial t^2} = -\omega_{m,n}^2 \quad (3.1.4)$$

only connected by the dispersion relation implied by Eq. (3.1.3) in terms of the foresightedly labelled constants

$$k_m^2 + k_n^2 = \frac{\omega_{m,n}^2 L^2}{v^2}. \quad (3.1.5)$$

The former two differential equations of (3.1.4) constitute the spatial Helmholtz equation in cartesian coordinates. Solving these subject to the clamped boundary conditions of the square membrane, $X(0) = X(1) = 0 = Y(0) = Y(1)$, we find the orthonormal sets of spatial mode functions

$$\{X_m(\tilde{x}) = \sqrt{2} \sin(\pi m \tilde{x})\}, \{Y_n(\tilde{y}) = \sqrt{2} \sin(\pi n \tilde{y})\}, m, n \in \mathbb{Z}_+;$$

implying the relations $k_m = \pi m, k_n = \pi n$. Combining these by multiplication, as they appear in the assumed form of $z(\tilde{x}, \tilde{y}, t)$, we arrive at the complete set of drum modes

$$\{u_{m,n}(\tilde{x}, \tilde{y}) = 2 \sin(\pi m \tilde{x}) \sin(\pi n \tilde{y})\}_{(m,n) \in \mathbb{Z}_+^2},$$

orthonormal over the rescaled area of the membrane:

$$\int_0^1 \int_0^1 d\tilde{x} d\tilde{y} u_{m,n}(\tilde{x}, \tilde{y}) u_{m',n'}(\tilde{x}, \tilde{y}) = \delta_{m,m'} \delta_{n,n'}. \quad (3.1.6)$$

The dispersion relation (3.1.5) implies the frequencies $\omega_{m,n} = \frac{\pi v}{L} \sqrt{m^2 + n^2}$. Due to the completeness property, we can expand any reasonable configuration of the membrane on the set of drum modes as

$$z(\tilde{x}, \tilde{y}, t) = \sum_{m,n} \beta_{m,n}(t) u_{m,n}(\tilde{x}, \tilde{y}). \quad (3.1.7)$$

It follows from the above that the time-dependent coefficients $\beta_{m,n}(t)$ (which has units of length) must obey the differential equation of $f(t)$, (3.1.4).

3.1.2.2 Hamiltonian description

We will now show how the drum modes may be introduced into a Hamiltonian description of the vibrating membrane. Our starting point will be a classical Hamiltonian expressed as an area integral over the membrane, the integrand being a Hamiltonian density (see for instance Ch. 4 of Ref. [1])

$$H_{\text{mem}} = \int_0^L \int_0^L dx dy \left[\frac{\Pi^2(x, y)}{2\rho} + \frac{\rho v^2}{2} \left[\left(\frac{\partial z(x, y)}{\partial x} \right)^2 + \left(\frac{\partial z(x, y)}{\partial y} \right)^2 \right] \right];$$

here ρ is the uniform mass density (per area) and $\Pi = \rho \dot{z}$ is the momentum density conjugate to the displacement z . By shifting to the dimensionless position coordinates (\tilde{x}, \tilde{y}) defined above and performing partial integration on the potential energy term we may write

$$\begin{aligned} H_{\text{mem}} &= \int_0^1 \int_0^1 d\tilde{x} d\tilde{y} \left[\frac{L^2 \Pi^2(\tilde{x}, \tilde{y})}{2\rho} + \frac{\rho v^2}{2} \left[\left(\frac{\partial z(\tilde{x}, \tilde{y})}{\partial \tilde{x}} \right)^2 + \left(\frac{\partial z(\tilde{x}, \tilde{y})}{\partial \tilde{y}} \right)^2 \right] \right] \\ &= \int_0^1 \int_0^1 d\tilde{x} d\tilde{y} \left[\frac{L^2 \Pi^2(\tilde{x}, \tilde{y})}{2\rho} - \frac{\rho v^2}{2} z(\tilde{x}, \tilde{y}) \left[\frac{\partial^2 z(\tilde{x}, \tilde{y})}{\partial \tilde{x}^2} + \frac{\partial^2 z(\tilde{x}, \tilde{y})}{\partial \tilde{y}^2} \right] \right], \end{aligned}$$

noting that the boundary term vanishes due to the clamped condition. Inserting the drum mode expansion for $z = \sum_{m,n} \beta_{m,n} u_{m,n}(\tilde{x}, \tilde{y})$ and $\Pi = \rho \sum_{m,n} \dot{\beta}_{m,n} u_{m,n}(\tilde{x}, \tilde{y})$, acting with the differential operators and exploiting orthonormality of the mode set, Eq. (3.1.6), we find

$$\begin{aligned} H_{\text{mem}} &= \int_0^1 \int_0^1 d\tilde{x} d\tilde{y} \sum_{m,n} \sum_{m',n'} u_{m,n}(\tilde{x}, \tilde{y}) u_{m',n'}(\tilde{x}, \tilde{y}) \\ &\quad \left[\frac{1}{2\rho} L^2 \rho^2 \dot{\beta}_{m,n} \dot{\beta}_{m',n'} + \frac{\rho v^2}{2} (k_m^2 + k_n^2) \beta_{m,n} \beta_{m',n'} \right] \\ &= \sum_{m,n} \left[\frac{p_{m,n}^2}{2m} + \frac{1}{2} m \omega_{m,n}^2 \beta_{m,n}^2 \right]; \quad (3.1.8) \end{aligned}$$

where we have defined the momentum $p_{m,n} = m \dot{\beta}_{m,n}$, used the dispersion relation (3.1.5) and written the motional mass of the membrane as $m \equiv \rho L^2$. Eq. (3.1.8) is a sum of harmonic oscillator Hamiltonians in the position-momentum pairs $(\beta_{m,n}, p_{m,n})$. It is indeed a valid Hamiltonian for the drum modes as Hamilton's equations yield $p_{m,n}/m = \dot{\beta}_{m,n}$, showing that we have correctly identified the canonical momenta, and $\dot{p}_{m,n} = -m \omega_{m,n}^2 \beta_{m,n}$, which is equivalent to the equation of motion for $\beta_{m,n}$, the third of Eqs. (3.1.4). Moreover, since H_{mem} equals the total energy of membrane, Eq. (3.1.8) may serve as the connection to a quantum Hamiltonian by promoting the canonical variable pairs $(\beta_{m,n}, p_{m,n})$ to harmonic oscillator quantum operators in accordance with the canonical quantization prescription.

3.1.3 The electrical circuit

3.1.3.1 Kirchhoff circuit theory

The electrodynamics of electrical circuits are in general governed by Maxwell's equations, but under certain circumstances these equations reduce to two simple statements: Kirchhoff's circuit laws of charge and energy conservation, respectively. We will use these laws in Section 3.1.3.3 to obtain the classical equations of motion for the circuit participating in the capacitive interaction sketched in Fig. 3.1.1. For this reason, we briefly review some basic notions of circuit theory. Kirchhoff's laws are commonly applied in the context of diagrammatical representations such as Fig. 3.1.2.

The two loop equations (expressing energy conservation) and the junction equation (expressing charge conservation) read

$$L\dot{I} + L_1\dot{I}_1 + \frac{Q_1}{C_1} = V, \quad L\dot{I} + L_2\dot{I}_2 + \frac{Q_2}{C_2} = V, \quad I = I_1 + I_2, \quad (3.1.9)$$

where Q_i is the charge on capacitor C_i and $\dot{Q}_i = I_i$. Such a description is valid in the *lumped element limit*, where the transmission time of signals between different parts of the circuit is negligible compared to the rates of change of the Q_i . This amounts to the criterion that the wavelengths involved must be much larger than the dimensions of the circuit $\lambda \gg d$, where d is a characteristic length.

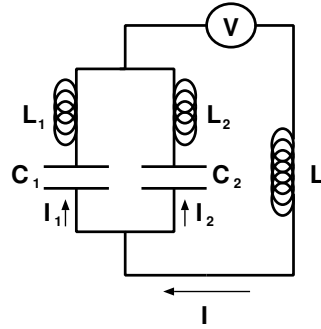


Figure 3.1.2: Simple circuit containing capacitive elements C_i , inductors L, L_i and a voltage source V . Currents I, I_i are indicated with arrows.

The constraint expressed by the 3rd of Eqs. (3.1.9) may be used to eliminate I from the set of equations leaving a pair of coupled differential equations in the (generalized) coordinates Q_1, Q_2 subject to no constraints. Such elimination of constraints is an important preliminary step to establishing Lagrangian and Hamiltonian descriptions of a system and, thus, to arrive at a quantum theory. There exists a systematic procedure for obtaining an independent set of coordinates for an arbitrary circuit [6], but given the simplicity of the circuit diagram we will end up considering, a more straightforward approach will suffice.

The normal modes of this system are formally equivalent to mechanical oscillators (as we shall see below) and we can therefore apply the successful quantization procedure known from that context.

3.1.3.2 Timescales of the interdigitated capacitor circuit

We may now start to think about how to determine an appropriate circuit diagram for the interdigitated capacitor (Fig. 3.1.1) and its accompanying (LC) circuit. We established in Section 3.1.1 that we may associate an individual capacitance $C_{i,j}$ with each unit cell of the IDC-membrane interface, which we indexed by the discrete coordinates (x_i, y_j) . It therefore seems reasonable that our circuit diagram should include a capacitor for each unit cell.³ In addition to these capacitances, we might try to account for the IDC geometry; an attempt at this is presented in Fig. (3.1.3) obtained by drawing a diagram on top of Fig. 3.1.1 (left).

It is certainly possible to write down Kirchhoff's equations for the IDC circuit sketched in Fig. 3.1.3 (left), but it is not likely to be a reasonable approach: Mathematical inconvenience aside, we do not necessarily know the parameters of the various inductive elements involved and, moreover, additional effects like mutual inductance have been neglected. In other words, the circuit in Fig. (3.1.3) includes a somewhat arbitrary selection of complications while leaving others out.

³More precisely, a capacitor should be included for each unit cell that contains a segment of the IDC. Unit cells that do not will not contribute to the interaction. On the other hand, unit cells that only contain a segment of the IDC, but no patch of membrane, will still contribute to the total capacitance.

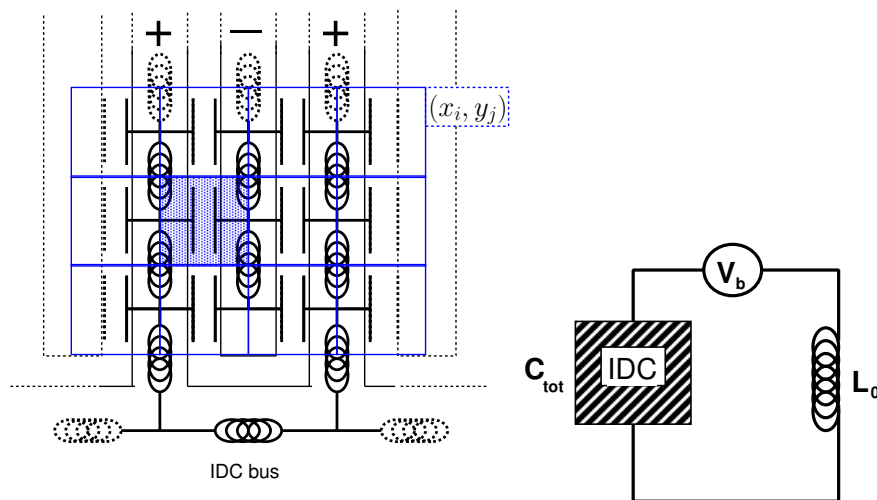


Figure 3.1.3: (Left) Attempt at converting Fig. 3.1.1 (left) into a circuit diagram using conventional symbols. Some of the capacitive unit cells (blue) are indicated; each is designated by a pair of coordinates (x_i, y_j) of the discretized grid. Each cell contains a capacitor that accounts for its individual capacitance, which only depends on the displacement $z(x_i, y_j)$ of the local patch of membrane directly above it (not shown). Inductors connect neighboring cells along the fingers as well as fingers of equal polarity along the bus. (Right) The LC circuit in which the IDC serves as the capacitive element. The inductance L_0 is large compared to any inductance arising internally in the IDC.

A more reasonable approach is to ask what effects we expect to be dominant in the larger perspective of the LC circuit in which the IDC enters, see Fig. 3.1.3 (right). The inductor in the main circuit has a large inductance L_0 compared to the inductances occurring internally in the IDC, $\{L_i\}_{i \in \mathbb{Z}_+}$. In the regime of interest $L_i/L_0 \ll 1$ we may effectively replace the IDC by an effective capacitance of C_{tot} and calculate the circuit resonance frequency as $\omega_{\text{LC}} = (L_0 C_{\text{tot}})^{-1/2}$; the associated circuit mode naturally involves current running through the main inductor, L_0 . It is essentially this mode of the circuit, that we are interested in coupling to a vibrational mode of the membrane.

But in order to set up a Hamiltonian description, we also need to include the other modes of the circuit. These modes rearrange charges within the IDC, with little or no current running through L_0 . For this reason they are expected to act on a much shorter timescale than that associated with L_0 , namely $1/\omega_{\text{LC}}$. For this reason we will henceforth refer to the “slow” circuit mode of frequency $\omega_{\text{slow}} = \omega_{\text{LC}}$ and the “fast” internal modes of the IDC, $\omega_{\text{fast},i}$. With regard to the membrane frequency, the typical situation is $\omega_{\text{mem}} \lesssim \omega_{\text{LC}}$, hence also corresponding to a relatively slow mode. That no current runs through L_0 when these modes act also implies that the net effect of the bias is expected to be zero for these modes, as they move as much charge “uphill”, against the bias, as they do “downhill”, with the bias.

Based on the above observations, we arrive at the following physical picture:

As the membrane moves, on the timescale $1/\omega_{\text{mem}}$, it will change the unit cell capacitances thereby rendering the charge configuration out of equilibrium. This will trigger both the slow and fast modes of the circuit. The fast internal modes of the IDC move charges between the various segments of the fingers so rapidly that their dynamics adiabatically follow the motion of the membrane. Given this timescale separation, the exact nature of the internal paths of the IDC is of less importance. Even though the fast modes will influence the dynamics of our modes of primary interest (the slow circuit mode and the membrane mode), this influence is likely to be minor compared to other effects. For these reasons, the diagram of Fig. 3.1.3 (left) can be said to be unnecessarily convoluted.

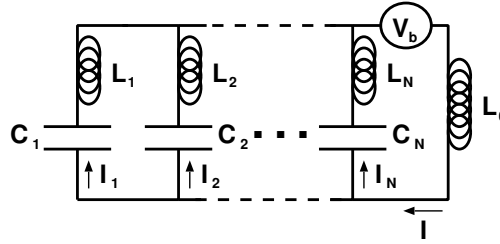


Figure 3.1.4: Simpler circuit diagram modeling the LC circuit including its IDC. Each capacitive unit cell is represented by a capacitor C_i (switching to a single index for brevity).

Instead we choose the circuit diagram shown in Fig. 3.1.4, assuming that we have segmented the interface into N unit cells. It retains the idea of representing each capacitive unit cell by a capacitor, but has the benefit of a much simpler topology compared to Fig 3.1.3. It can be expected to contain essentially the same physics in the regime $L_i/L_0 \ll 1$, where $\{L_i\}$ are the internal inductances of the IDC. On this basis, we will derive a Hamiltonian description of the circuit in what follows.

3.1.3.3 Classical Hamiltonian description

To obtain a classical Hamiltonian description of the circuit we will follow the standard approach: We write down the equations of motion and find the equivalent Lagrangian description, which, by means of the Legendre transform, yields the classical Hamiltonian.

Kirchhoff's circuit laws for our model circuit in Fig. 3.1.4 yield the N equations of motion

$$L_0 \sum_{j=1}^N \ddot{Q}_j + L_i \ddot{Q}_i + \frac{Q_i}{C_i} = V_b, \quad i \in \{1, \dots, N\}. \quad (3.1.10)$$

Note that the constraint imposed by Kirchhoff's junction rule, $I = \sum_{i=1}^N I_i$, has been used to eliminate the current through the inductive element L_0 , whereby the set of equations (3.1.10) is free of constraints. In this sense, the set $\{Q_i, \dot{Q}_i\}_{i \in \{1, \dots, N\}}$ can be considered generalized coordinates suitable for a Lagrangian formulation. By inspection, the following Lagrangian is seen to reproduce Eqs.

(3.1.10),

$$L = \sum_{j=1}^N \left[\frac{L_j \dot{Q}_j^2}{2} - \frac{Q_j^2}{2C_j} + Q_j V_b \right] + \frac{L_0}{2} \left(\sum_{j=1}^N \dot{Q}_j \right)^2, \quad (3.1.11)$$

as the corresponding Euler-Lagrange equations

$$\frac{d}{dt} \left(\frac{\partial L}{\partial \dot{Q}_i} \right) - \frac{\partial L}{\partial Q_i} = 0, \quad i \in \{1, \dots, N\}.$$

At this point it is appropriate to introduce vector notation, $\vec{Q} \equiv (Q_1, Q_2, \dots, Q_N)^T$, $\dot{\vec{Q}} \equiv (\dot{Q}_1, \dot{Q}_2, \dots, \dot{Q}_N)^T$, in terms of which the Lagrangian (3.1.11) may be written (in “kinetic - potential” form) as

$$L = \frac{1}{2} \dot{\vec{Q}}^T \underline{\underline{M}} \dot{\vec{Q}} - \left[\frac{1}{2} \vec{Q}^T \underline{\underline{D}} \vec{Q} - \vec{b}^T \vec{Q} V_b \right], \quad (3.1.12)$$

where we have defined the symmetric matrices

$$(\underline{\underline{M}})_{i,j} \equiv \delta_{i,j} L_i + L_0, \quad (\underline{\underline{D}})_{i,j} \equiv \delta_{i,j} \frac{1}{C_i}, \quad i, j \in \{1, \dots, N\} \quad (3.1.13)$$

and the vector $\vec{b} \equiv (1, 1, \dots, 1)^T \in \mathbb{R}^N$.

The canonical “momenta” associated with the set \vec{Q} are found from Eq. (3.1.12) to be

$$\vec{\phi} = \frac{\partial L}{\partial \dot{\vec{Q}}} = \underline{\underline{M}} \dot{\vec{Q}}, \quad (3.1.14)$$

for which the individual components are $\phi_i = L_i \dot{Q}_i + L_0 \sum_{j=1}^N \dot{Q}_j$, for explicitness. Eqs. (3.1.12) and (3.1.14) enables us to carry out the Legendre transform as:⁴

$$H_c(\vec{Q}, \vec{\phi}) = \dot{\vec{Q}}^T \vec{\phi} - L = \dot{\vec{Q}}^T \underline{\underline{M}} \dot{\vec{Q}} - L = \frac{1}{2} \dot{\vec{Q}}^T \underline{\underline{M}} \dot{\vec{Q}} + \left[\frac{1}{2} \vec{Q}^T \underline{\underline{D}} \vec{Q} - \vec{b}^T \vec{Q} V_b \right], \quad (3.1.15)$$

however, to arrive at a genuine Hamiltonian we must apply the change of variables $(\vec{Q}, \dot{\vec{Q}}) \rightarrow (\vec{Q}, \vec{\phi})$ to Eq. (3.1.15). Assuming $\underline{\underline{M}}$ to be invertible,⁵ we have $\dot{\vec{Q}} = \underline{\underline{M}}^{-1} \vec{\phi}$ from Eq. (3.1.14) from which the kinetic part of Eq. (3.1.15) transforms as

$$\frac{1}{2} \dot{\vec{Q}}^T \underline{\underline{M}} \dot{\vec{Q}} = \frac{1}{2} \vec{\phi}^T (\underline{\underline{M}}^{-1})^T \underline{\underline{M}} \underline{\underline{M}}^{-1} \vec{\phi} = \frac{1}{2} \vec{\phi}^T \underline{\underline{M}}^{-1} \vec{\phi},$$

using the fact that $\underline{\underline{M}}$, and hence $\underline{\underline{M}}^{-1}$, is symmetric. This completes the derivation of the classical Hamiltonian for our model circuit:

$$H_c(\vec{Q}, \vec{\phi}) = \frac{1}{2} \vec{\phi}^T \underline{\underline{M}}^{-1} \vec{\phi} + \frac{1}{2} \vec{Q}^T \underline{\underline{D}} \vec{Q} - \vec{b}^T \vec{Q} V_b. \quad (3.1.16)$$

⁴By noting that the Lagrangian (3.1.11) is of “kinetic - potential” form, $T - V$, where T is a quadratic form in the \dot{Q}_i eq. (RR) and V only depends on the Q_i

⁵The matrix $\underline{\underline{M}}$ is inverted in Appendix A.1, but we need not consider its entries explicitly at this point.

As discussed in section 3.1.1, the parametric coupling enters through the dependence of the unit cell capacities on position⁶ $C_i = C(z_i)$; henceforth, we will write this dependence explicitly when dealing with the components of the matrix $\underline{D} = \underline{D}(\vec{z})$. We now aim to approximate $C(z_i)$ by a truncated Taylor expansion around the classical equilibrium configuration. The latter is defined by the simultaneous set of equations $\dot{\vec{\phi}} = 0, \dot{\vec{\Pi}} = 0$ and we denote the solution to these equations $\{\vec{Q}^{(\text{eq})}, \vec{z}^{(\text{eq})}\}$. In preparation for expanding the interaction term around the equilibrium configuration we rewrite

$$\underline{D}(\vec{z}) = \underline{D}(\vec{z}^{(\text{eq})}) + \left(\underline{D}(\vec{z}) - \underline{D}(\vec{z}^{(\text{eq})}) \right) = \underline{D}^{(\text{eq})} + \underline{C}(\vec{z}; \vec{z}^{(\text{eq})}), \quad (3.1.17)$$

where we have defined $\underline{D}^{(\text{eq})} \equiv \underline{D}(\vec{z}^{(\text{eq})})$ and the coupling matrix $\underline{C}(\vec{z}; \vec{z}^{(\text{eq})}) \equiv \underline{D}(\vec{z}) - \underline{D}(\vec{z}^{(\text{eq})})$ (we will not always state the dependence on $\vec{z}^{(\text{eq})}$ explicitly). In component form, Eq. (3.1.17) amounts to nothing but $1/C(z_i) = 1/C_i^{(\text{eq})} + [1/C(z_i) - 1/C_i^{(\text{eq})}]$ (for the i 'th diagonal entry). Inserting Eq.(3.1.17) into the Hamiltonian (3.1.16) we get

$$H_c = \left[\frac{1}{2} \vec{\phi}^T \underline{M}^{-1} \vec{\phi} + \frac{1}{2} \vec{Q}^T \underline{D}^{(\text{eq})} \vec{Q} \right] - \vec{b}^T \vec{Q} V_b + \frac{1}{2} \vec{Q}^T \underline{C}(\vec{z}) \vec{Q} = H_{c,0} - \vec{b}^T \vec{Q} V_b + H_{\text{int}},$$

defining $H_{c,0}$ as the bracketed term and $H_{\text{int}} = \frac{1}{2} \vec{Q}^T \underline{C}(\vec{z}) \vec{Q}$. $H_{c,0}$ is the classical Hamiltonian for the non-interacting circuit with $C_i = C_i^{(\text{eq})}$ that will serve as our basis for quantizing the circuit. We would like to do so in terms of its normal modes, hence we must diagonalize $H_{c,0}$.

3.1.3.4 Diagonalizing the classical Hamiltonian of the non-interacting circuit, $H_{c,0}$

To this end, we introduce a canonical rescaling transformation that has the effect of rendering $\underline{D}^{(\text{eq})}$ proportional to the identity matrix; this has the benefit that we can afterwards diagonalize the kinetic term separately in order to diagonalize $H_{c,0}$. The transformation is given by the diagonal matrix $(\underline{S})_{i,j} \equiv \delta_{i,j} \sqrt{\frac{C_{\text{tot}}^{(\text{eq})}}{C_i^{(\text{eq})}}}$, where $C_{\text{tot}}^{(\text{eq})} \equiv \sum_{j=1}^N C_j^{(\text{eq})}$, leading to the new canonical variables $\vec{Q}' = \underline{S} \vec{Q}$, $\vec{\phi}' = \underline{S}^{-1} \vec{\phi}$. First, we consider the effect on $H_{c,0} - \vec{b}^T \vec{Q} V_b$ (saving H_{int} for later):

$$\begin{aligned} H_{c,0} - \vec{b}^T \vec{Q} V_b &= \frac{1}{2} \vec{\phi}'^T \underline{S}^T \underline{M}^{-1} \underline{S} \vec{\phi}' + \frac{1}{2} \vec{Q}'^T (\underline{S}^{-1})^T \underline{D}^{(\text{eq})} \underline{S}^{-1} \vec{Q}' - \vec{b}^T \underline{S}^{-1} \vec{Q}' V_b \\ &= \frac{1}{2} \vec{\phi}'^T \underline{M}'^{-1} \vec{\phi}' + \frac{1}{2 C_{\text{tot}}^{(\text{eq})}} \vec{Q}'^T \vec{Q}' - \vec{b}'^T \vec{Q}' V_b, \end{aligned} \quad (3.1.18)$$

where $\underline{M}'^{-1} \equiv \underline{S}^T \underline{M}^{-1} \underline{S}$ and $\vec{b}'^T \equiv \vec{b}^T \underline{S}^{-1} = (C_{\text{tot}}^{(\text{eq})})^{-1/2} (\sqrt{C_1^{(\text{eq})}}, \dots, \sqrt{C_N^{(\text{eq})}})$. The matrix appearing in the kinetic term, \underline{M}'^{-1} , is symmetric and hence diagonalizable by an orthogonal matrix \underline{R} , the rows of which are the normalized eigenvectors of \underline{M}'^{-1} so that $\underline{R}^{-1} = \underline{R}^T$. That is, $\underline{D}^{(\text{kin})} = \underline{R} \underline{M}'^{-1} \underline{R}^T$, where

⁶For brevity, we here write a single discrete index i rather than (i, j) .

$\underline{\underline{D}}^{(\text{kin})}$ is a diagonal matrix. The associated canonical transformation of the coordinates leads to $\vec{Q}'' = \underline{\underline{R}}\vec{Q}'$, $\vec{\phi}'' = \underline{\underline{R}}\vec{\phi}'$ resulting in the entire $H_{c,0}$ now being in diagonal form

$$H_{c,0} - \vec{b}'^T \vec{Q}' V_b = \frac{1}{2} \vec{\phi}'^T \underline{\underline{D}}^{(\text{kin})} \vec{\phi}'' + \frac{1}{2C_{\text{tot}}^{(\text{eq})}} \vec{Q}''^T \vec{Q}'' - \vec{b}'^T \underline{\underline{R}}^T \vec{Q}'' V_b, \quad (3.1.19)$$

from which the frequency of the i 'th mode can be read off to be $\omega_i^2 = (\underline{\underline{D}}^{(\text{kin})})_{i,i}/C_{\text{tot}}^{(\text{eq})}$.⁷

We will now consider the explicit expression for the kinetic term: In Appendix A.1 the matrix $\underline{\underline{M}}$, defined in Eq. (3.1.13), is inverted to find

$$(\underline{\underline{M}}^{-1})_{i,j} = \delta_{i,j} \frac{1}{L_i} - \frac{1}{L_i L_j} \left[\sum_{k=0}^N \frac{1}{L_k} \right]^{-1};$$

applying to this the scaling transformation defined by $\underline{\underline{S}}$ we get

$$(\underline{\underline{M}}'^{-1})_{i,j} = \frac{C_{\text{tot}}^{(\text{eq})}}{\sqrt{C_i^{(\text{eq})} C_j^{(\text{eq})}}} \left(\delta_{i,j} \frac{1}{L_i} - \frac{1}{L_i L_j} \left[\sum_{k=0}^N \frac{1}{L_k} \right]^{-1} \right). \quad (3.1.20)$$

The normal modes of the circuit, as modeled in Fig. 3.1.4, are the eigenvectors of this symmetric matrix and the associated eigenvalues $(\underline{\underline{D}}^{(\text{kin})})_{l,l}$ are related to the mode frequencies as $(\underline{\underline{D}}^{(\text{kin})})_{l,l} = \omega_l^2 C_{\text{tot}}^{(\text{eq})}$, using the notation introduced in connection with the formal diagonalization carried out above. We will not attempt to explicitly perform a full diagonalization of the matrix in Eq. (3.1.20). What we will do is to guess the 'slow' circuit mode, making use of the terminology introduced in course of the timescale discussion given in section 3.1.3.2. As discussed there, we expect only the slow mode to be affected by the DC voltage bias in the limit $\frac{L_i}{L_0} \rightarrow 0, i \in \{1, \dots, N\}$. On this basis we make the qualified guess that the vector \vec{b}' , that appeared in the rescaled bias term of Eq. (3.1.18), is the 'slow' normal mode eigenvector of $\underline{\underline{M}}'^{-1}$, Eq. (3.1.20). Calculating the product $\underline{\underline{M}}'^{-1} \vec{b}'$ we find for the i 'th component,

$$\sum_{j=1}^N (\underline{\underline{M}}'^{-1})_{i,j} (\vec{b}')_j = \sqrt{\frac{C_{\text{tot}}^{(\text{eq})}}{C_i^{(\text{eq})}}} \frac{1}{L_i} \left(1 - \left[\sum_{j=1}^N \frac{1}{L_j} \right] \left[\sum_{k=0}^N \frac{1}{L_k} \right]^{-1} \right);$$

the proportionality constant in the parenthesis (independent of i) may be restated in terms of the effective 'fast' inductance $L_{\text{fast}}^{-1} \equiv \sum_{j=1}^N L_j^{-1}$ as $1 - [1 + L_{\text{fast}}/L_0]^{-1}$ from which we see that in the limit $(L_{\text{fast}}/L_0) \rightarrow 0$, indeed \vec{b}' is the 'slow' eigenvector of $\underline{\underline{M}}'^{-1}$ with (zeroth order) eigenfrequency squared equal to zero, $\omega_{\text{slow}}^{2(0)} = 0$. This means that if we diagonalize the circuit Hamiltonian to zeroth order in L_{fast}/L_0 , one of the rows of the corresponding orthogonal

⁷This can be seen by subjecting the diagonalized Hamiltonian $H_{c,0}$ in Eq. (3.1.19) to the scaling transformation defined by $\underline{\underline{S}} = (L \underline{\underline{D}}^{(\text{kin})})^{-1/2}$, L being an arbitrary inductance, $\vec{Q} = \underline{\underline{S}} \vec{Q}'$, $\vec{\phi} = \underline{\underline{S}}^{-1} \vec{\phi}'$; this brings about the perhaps more familiar form $\frac{\vec{\phi}^2}{2L} + \frac{1}{2} L (\underline{\underline{D}}^{(\text{kin})}/C_{\text{tot}}^{(\text{eq})}) \vec{Q}^2$ analogous to $\frac{p^2}{2m} + \frac{1}{2} m \omega^2 x^2$ describing a mechanical oscillator.

transformation \underline{R} between the sets of canonical variables \vec{Q}' and \vec{Q}'' is given by \vec{b}' . Given the orthogonality of eigenvectors, any other normal mode, which is to say any 'fast' mode, will be unaffected by the bias term, $-\vec{b}'^T \underline{R}^T \vec{Q}'' V_b$, in the limit $(L_{\text{fast}}/L_0) \rightarrow 0$; to be explicit, the bias term simply projects out the 'slow' mode normal variable $-Q''_{\text{slow}} V_b$. Again, this is in line with the intuitive timescale discussion of section 3.1.3.2.

To verify that the circuit formalism is consistent with our expectations, we calculate the first order correction to ω_{slow} in the small parameter (L_{fast}/L_0) using perturbation theory. To this end we expand \underline{M}'^{-1} to lowest order in (L_{fast}/L_0) around zero,

$$(\underline{M}'^{-1})_{i,j} \approx \frac{C_{\text{tot}}^{(\text{eq})}}{\sqrt{C_i^{(\text{eq})} C_j^{(\text{eq})}}} \left(\delta_{i,j} \frac{1}{L_i} - \frac{L_{\text{fast}}}{L_i L_j} \left[1 - \frac{L_{\text{fast}}}{L_0} \right] \right)$$

from which we see that the leading order of the "perturbation" is

$$(\underline{V})_{i,j} = \frac{C_{\text{tot}}^{(\text{eq})}}{\sqrt{C_i^{(\text{eq})} C_j^{(\text{eq})}}} \frac{L_{\text{fast}}}{L_i L_j} \frac{L_{\text{fast}}}{L_0}.$$

Evaluating the expectation value of the perturbation with respect to the zeroth order 'slow' eigenvector \vec{b}' , we obtain the first order correction $\omega_{\text{slow}}^{2(1)}$ to the frequency squared ω_{slow}^2 (recall that $(\underline{D}^{(\text{kin})})_{l,l} = \omega_l^2 C_{\text{tot}}^{(\text{eq})}$)

$$\omega_{\text{slow}}^{2(1)} C_{\text{tot}}^{(\text{eq})} = \vec{b}'^T \underline{V} \vec{b}' = \sum_{i,j=1}^N \frac{L_{\text{fast}}}{L_i L_j} \frac{L_{\text{fast}}}{L_0} = \frac{1}{L_0},$$

from which we find $\omega_{\text{slow}}^2 \approx \omega_{\text{slow}}^{2(0)} + \omega_{\text{slow}}^{2(1)} = 0 + \frac{1}{L_0 C_{\text{tot}}^{(\text{eq})}} = \frac{1}{L_0 C_{\text{tot}}^{(\text{eq})}}$ in accordance with what we would expect from simple circuit theory in the $\frac{L_{\text{fast}}}{L_0} \rightarrow 0$ limit.

3.1.3.5 Equilibrium charges of the normal modes

We now find the equilibrium charge with respect to the normal modes \vec{Q}'' from Hamilton's equation $\dot{\vec{\phi}} = -\frac{\partial H}{\partial \vec{Q}''} = -\frac{\partial H_c}{\partial \vec{Q}''}$; noting that H_{int} vanishes at $\vec{z} = \vec{z}^{(\text{eq})}$ by construction, we see that

$$0 = \left. \frac{\partial H_c}{\partial \vec{Q}''} \right|_{\vec{Q}'' = \vec{Q}''^{(\text{eq})}, \vec{z} = \vec{z}^{(\text{eq})}} = \frac{1}{C_{\text{tot}}^{(\text{eq})}} \vec{Q}'' - \frac{\partial Q''_{\text{slow}}}{\partial \vec{Q}''} V_b,$$

the latter term being non-zero only for the 'slow' mode entry. Hence $Q''_{\text{slow}} = C_{\text{tot}}^{(\text{eq})} V_b$ while for all the remaining normal modes $Q''_{\text{fast},i} = 0$.

With the aim of obtaining a quantum description of the fluctuations around the equilibrium configuration $\{\vec{Q}'' = \vec{Q}''^{(\text{eq})}, \vec{z} = \vec{z}^{(\text{eq})}\}$, we perform the following shift of the canonical variables $\vec{Q}'' \rightarrow \vec{Q}''^{(\text{eq})} + \delta\vec{q}$ (which amounts to shifting Q''_{slow}) and similarly $\vec{z} \rightarrow \vec{z}^{(\text{eq})} + \delta\vec{z}$, the new canonical charge and position variables being $\delta\vec{q}$ and $\delta\vec{z}$ (the corresponding conjugate momenta being unaltered). Applying the shift to $H_{c,0} - Q''_{\text{slow}} V_b$, Eq. (3.1.19), and using the relation

$Q_{\text{slow}}''(\text{eq}) = C_{\text{tot}}^{(\text{eq})} V_b$ we see that all linear terms in $\delta\vec{q}$ (effectively δq_{slow}) drop out leaving a diagonal form

$$\begin{aligned} H_{c,0}(\delta\vec{q}, \vec{\phi}'') &= \frac{1}{2} \vec{\phi}''^T \underline{\underline{D}}^{(\text{kin})} \vec{\phi}'' + \frac{1}{2C_{\text{tot}}^{(\text{eq})}} \delta\vec{q}^T \delta\vec{q} + \frac{Q_{\text{slow}}''(\text{eq}) \delta q_{\text{slow}}}{C_{\text{tot}}^{(\text{eq})}} - (Q_{\text{slow}}''(\text{eq}) + \delta q_{\text{slow}}) V_b \\ &= \frac{1}{2} \vec{\phi}''^T \underline{\underline{D}}^{(\text{kin})} \vec{\phi}'' + \frac{1}{2C_{\text{tot}}^{(\text{eq})}} \delta\vec{q}^T \delta\vec{q} - Q_{\text{slow}}''(\text{eq}) V_b; \quad (3.1.21) \end{aligned}$$

the last term is constant and hence does not enter the equations of motion.

3.1.3.6 Effective interaction Hamiltonian

Finally, we return to the interaction term of the Hamiltonian, H_{int} . Performing the canonical transformations applied to $H_{c,0}$ above, $\vec{Q}' = \underline{\underline{S}}\vec{Q}$, $\vec{Q}'' = \underline{\underline{R}}\vec{Q}'$ and $\vec{Q}'' \rightarrow \vec{Q}''(\text{eq}) + \delta\vec{q}$, we have

$$H_{\text{int}} = \frac{1}{2} \vec{Q}^T \underline{\underline{C}}(\vec{z}) \vec{Q} = \frac{1}{2} (\vec{Q}''(\text{eq}) + \delta\vec{q})^T \underline{\underline{R}} \underline{\underline{C}}'(\vec{z}) \underline{\underline{R}}^T (\vec{Q}''(\text{eq}) + \delta\vec{q}), \quad (3.1.22)$$

defining the diagonal matrix $\underline{\underline{C}}'(\vec{z}) = \underline{\underline{S}}^{-1} \underline{\underline{C}}(\vec{z}) \underline{\underline{S}}^{-1}$ the i 'th diagonal component of which is $\frac{1}{C_{\text{tot}}^{(\text{eq})}} \left[\frac{C_i^{(\text{eq})}}{C(z_i)} - 1 \right]$. According to the strategy presented initially, we now Taylor expand $\frac{1}{C(z)}$ to second order around $z^{(\text{eq})}$ (dropping the subscript for brevity):

$$\begin{aligned} \frac{1}{C(z)} &\approx \frac{1}{C(z^{(\text{eq})})} + (z - z^{(\text{eq})}) \left[-\frac{1}{C^2(z)} \frac{dC}{dz} \right] \Big|_{z=z^{(\text{eq})}} \\ &\quad + \frac{1}{2} (z - z^{(\text{eq})})^2 \left[\frac{2}{C^3(z)} \left(\frac{dC}{dz} \right)^2 - \frac{1}{C^2(z)} \frac{d^2C}{dz^2} \right] \Big|_{z=z^{(\text{eq})}}. \end{aligned}$$

Defining the (inverse) characteristic length $(\xi_i^{(\text{eq})})^{-1} \equiv \left[-\frac{1}{C(z)} \frac{dC}{dz} \right] \Big|_{z=z_i^{(\text{eq})}}$ and the (inverse) area $(\alpha_i^{(\text{eq})})^{-1} \equiv \left[\frac{1}{C(z)} \frac{d^2C}{dz^2} \right] \Big|_{z=z_i^{(\text{eq})}}$ as well as the displacement from the equilibrium $\delta z_i \equiv z_i - z_i^{(\text{eq})}$, the components of $\underline{\underline{C}}'(\vec{z})$ are approximated by

$$(\underline{\underline{C}}'(\delta\vec{z}))_{i,j} \approx \delta_{i,j} \frac{1}{C_{\text{tot}}^{(\text{eq})}} \left[\frac{1}{\xi_i^{(\text{eq})}} \delta z_i + \frac{1}{2} \left[2 \left(\frac{1}{\xi_i^{(\text{eq})}} \right)^2 - \frac{1}{\alpha_i^{(\text{eq})}} \right] (\delta z_i)^2 \right]. \quad (3.1.23)$$

All information about coupling strengths and interaction induced frequency shifts is contained in this matrix $\underline{\underline{C}}'(\vec{z})$, Eq. (3.1.23). However, from the sandwich in which it appears in in Eq. (3.1.22) it is clear that we must consider the orthogonal transformation $\underline{\underline{R}}$ and the charge equilibrium shift to learn about the effect on the normal modes $\delta\vec{q}$.

In dealing with the interaction Hamiltonian we will now neglect certain terms based on the following physical argument: Applying a bias voltage V_b to the circuit results in a non-zero $Q_{\text{slow}}''(\text{eq})$ while the 'fast' mode equilibrium charges $Q_{\text{fast},i}''(\text{eq})$

remain zero as we saw in Section 3.1.3.5; thus, only processes corresponding to terms containing $Q_{\text{slow}}''^{(\text{eq})}$ in the interaction Hamiltonian (3.1.22) will be enhanced due to the bias. Therefore, we allow ourselves to neglect all non-enhanced terms. If we for definiteness take the 'slow' normal mode of the circuit to correspond to the N 'th entry of the vector $\delta\vec{q}$, then the enhanced terms will involve the entries of the N 'th row and column of the symmetric matrix $\underline{\underline{C}}''(\delta\vec{z}) \equiv \underline{\underline{R}}\underline{\underline{C}}'(\delta\vec{z})\underline{\underline{R}}^T$, these are

$$H_{\text{int}} \approx H_{\text{int,slow}} + H_{\text{int,fast}} = \frac{1}{2} [\underline{\underline{C}}''(\delta\vec{z})]_{N,N} (Q_{\text{slow}}''^{(\text{eq})} + \delta q_{\text{slow}})^2 + \sum_{j=1}^{N-1} \delta q_{\text{fast},j} [\underline{\underline{C}}''(\delta\vec{z})]_{j,N} (Q_{\text{slow}}''^{(\text{eq})} + \delta q_{\text{slow}}), \quad (3.1.24)$$

where $\delta q_{\text{fast},j} \equiv \delta q_j$, $\delta q_{\text{slow}} \equiv \delta q_N$ and we have named the term pertaining only to the 'slow' mode $H_{\text{int,slow}}$, while the remaining ones are combined in $H_{\text{int,fast}}$. Recalling that the N 'th row of $\underline{\underline{R}}$ is the eigenvector \vec{b}^T and noting that $\underline{\underline{C}}'(\delta\vec{z})$, Eq. (3.1.23), is diagonal we may evaluate the matrix element

$$\begin{aligned} [\underline{\underline{C}}''(\delta\vec{z})]_{N,N} &\equiv \sum_{i,j=1}^N [\underline{\underline{R}}]_{N,i} [\underline{\underline{C}}'(\delta\vec{z})]_{i,j} [\underline{\underline{R}}^T]_{j,N} = \sum_{i=1}^N [\underline{\underline{R}}]_{N,i}^2 [\underline{\underline{C}}'(\delta\vec{z})]_{i,i} \\ &= \sum_{i=1}^N \frac{C_i^{(\text{eq})}}{[C_{\text{tot}}^{(\text{eq})}]^2} \left[\frac{1}{\xi_i^{(\text{eq})}} \delta z_i + \frac{1}{2} \left[2 \left(\frac{1}{\xi_i^{(\text{eq})}} \right)^2 - \frac{1}{\alpha_i^{(\text{eq})}} \right] (\delta z_i)^2 \right]. \end{aligned} \quad (3.1.25)$$

The matrix elements $[\underline{\underline{C}}''(\delta\vec{z})]_{j,N}$, $1 \leq j < N$ cannot be evaluated individually without explicitly performing a full diagonalization of the circuit Hamiltonian. However, certain combinations of the elements may be evaluated by exploiting the completeness of the set of eigenvectors as we will demonstrate later, in Section 3.2.2.2. Let us now consider what physical effects arise from $H_{\text{int,slow}}$ and $H_{\text{int,fast}}$ respectively.

We start by examining $H_{\text{int,slow}}$ from which the most significant contributions are expected to arise; writing out the square parenthesis three distinct terms arise:

$$H_{\text{int,slow}} = \frac{1}{2} [\underline{\underline{C}}''(\delta\vec{z})]_{N,N} (Q_{\text{slow}}''^{(\text{eq})2} + 2Q_{\text{slow}}''^{(\text{eq})} \delta q_{\text{slow}} + \delta q_{\text{slow}}^2). \quad (3.1.26)$$

The first term only contains dynamical variables of the mechanical element; in view of Eq. (3.1.25), it has contributions of the type $\sim (\delta z \dots \delta z^2) Q_{\text{slow}}''^{(\text{eq})2}$ resulting in a shift in the equilibrium position of the membrane $\vec{z}^{(\text{eq})}$ from the configuration it would have in the absence of coupling. Additionally, the $\sim \delta z^2 Q_{\text{slow}}''^{(\text{eq})2}$ part also induces a mechanical frequency shift as we will consider in more detail below. Evidently, these effects scale like V_b^2 with the bias voltage.

The second term accounts for the bias enhanced coupling between the 'slow' circuit mode and the membrane $\sim \delta z \delta q_{\text{slow}} Q_{\text{slow}}''^{(\text{eq})}$, the strength of which is seen to scale linearly with the bias voltage V_b . The cubic terms $\sim \delta z^2 \delta q_{\text{slow}} Q_{\text{slow}}''^{(\text{eq})}$ also appearing will be neglected as they are higher order in the fluctuations around the equilibrium configuration which we will assume to be small. Regarding the

third term of Eq. (3.1.26), $(\delta z \dots \delta z^2)\delta q_{\text{slow}}^2$, we ignore it noting that it is both unenhanced and higher order in the fluctuations.

Turning now to the interactions involving the 'fast' modes we examine

$$H_{\text{int,fast}} = \sum_{j=1}^{N-1} [\underline{C}''(\delta \underline{z})]_{j,N} (\delta q_{\text{fast},j} Q_{\text{slow}}''^{(\text{eq})} + \delta q_{\text{fast},j} \delta q_{\text{slow}}). \quad (3.1.27)$$

Similar to what was found above for δq_{slow} , the first term gives rise to enhanced coupling between the mechanical element and the 'fast' circuit modes $\sim \delta z \delta q_{\text{fast},j} Q_{\text{slow}}''^{(\text{eq})}$. Given the fast timescale on which they evolve, as compared to the membrane dynamics, and the fact that we are not interested in the details of their evolution, we may consider eliminating these 'fast' modes adiabatically. The second term is unenhanced and higher order and hence neglected.

3.1.3.7 Quantizing the Hamiltonian

The framework developed above may serve to characterize circuit-mechanical systems including several modes from each subsystem. In this section we will demonstrate how to quantize the interacting system of an electric circuit mode and a single mechanical mode (a particular one of the drum modes for instance). The terms in the classical Hamiltonian leading to mechanical frequency shifts are assumed absorbed in $H_{\text{m},0}$ prior to quantization, this includes the shifts arising from the adiabatically eliminated 'fast' circuit modes.

We may quantize the total Hamiltonian (3.1.1) for the interacting circuit-membrane system according to the canonical quantization prescription by promoting the dynamical variables to operators obeying canonical commutation relations.⁸ As prepared for above, we will more precisely quantize the circuit and membrane fluctuations around the classical steady state configuration.

Noting that both $H_{\text{c},0}$ and $H_{\text{m},0}$ are formally equivalent to harmonic oscillators we may express the quantum Hamiltonian in terms of creation and annihilation operators,

$$\hat{H}/\hbar = \omega_{\text{slow}} \hat{a}_{\text{c}}^\dagger \hat{a}_{\text{c}} + \omega'_{\text{m}} \hat{a}_{\text{m}}^\dagger \hat{a}_{\text{m}} + \frac{g}{2} (\hat{a}_{\text{c}} + \hat{a}_{\text{c}}^\dagger) (\hat{a}_{\text{m}} + \hat{a}_{\text{m}}^\dagger),$$

where ω'_{m} is the shifted mechanical frequency and the coupling constant $\hbar g/2 = Gq_{0,\text{slow}} z_0$ is written in terms of the characteristic oscillator charge and length,⁹ $q_{0,\text{slow}} = \sqrt{\frac{\hbar}{2L_0\omega_{\text{slow}}}}$, $z_0 = \sqrt{\frac{\hbar}{2m\omega_{\text{m}}}}$ (quantifying their zero-point fluctuations).

3.1.4 Evaluating the capacitive unit cell

In this section we prepare for numerically evaluating the capacitive unit cell by rewriting relevant equations in dimensionless form. In setting up these equations, we also exploit the approximate symmetries discussed in Section 3.1.1: 1)

⁸While the quantization procedure used here is correct for $H_{\text{c},0}$ and $H_{\text{m},0}$ considered individually, it is not a completely rigorous way of obtaining the interaction Hamiltonian \hat{H}_{int} as discussed in the introduction of Section 3.1.

⁹It is not clear from the perturbative approach whether z_0 should be evaluated at the bare frequency ω_{m} or the shifted frequency ω'_{m} . The correction arising from evaluating at the latter is likely to be of the same order of magnitude as higher order corrections that we have neglected; hence it may be argued that ω_{m} is the more consistent choice.

reflection symmetry of the capacitive arrangement in the yz -planes bounding any unit cell, and 2) translational symmetry in the y -direction.

The strategy for calculating the unit cell capacitance is to first use Gauss' law and solve for the potential numerically. From this we can calculate the field and the energy stored in it. By equating this to $W = C_{\text{cell}}V_b^2/2$, where V_b is the DC bias voltage, we may solve for C_{cell} .

Gauss' law in terms of the electric displacement field \vec{D} and the free charge density ρ_f can be stated in terms of the electrostatic potential V as [10]

$$-\nabla_{\vec{r}} \cdot [\epsilon(\vec{r})\nabla_{\vec{r}}V(\vec{r})] = \rho_f(\vec{r}),$$

where $\epsilon(\vec{r})$ is the local electric permittivity and we have used the relation $\vec{D} = -\epsilon(\vec{r})\nabla_{\vec{r}}V(\vec{r})$ valid for linear dielectrics. Dividing through by ϵ_0V_b/L_p^2 and defining the dimensionless position $\tilde{\vec{r}} = \vec{r}/L_p$ and free charge density $\tilde{\rho}_f = (L_p^2/\epsilon_0V_b)\rho_f$, the equation can be stated in dimensionless form

$$-\nabla_{\tilde{\vec{r}}} \cdot [\epsilon_r(\tilde{\vec{r}})\nabla_{\tilde{\vec{r}}}(V(\tilde{\vec{r}})/V_b)] = \tilde{\rho}_f(\tilde{\vec{r}}), \quad (3.1.28)$$

where $\epsilon_r = \epsilon/\epsilon_0$ is the relative electric permittivity and we have used $\nabla_{\tilde{\vec{r}}} = L_p\nabla_{\vec{r}}$.

The form of Gauss' equation shown in Eq. (3.1.28) can be solved numerically for $V(\tilde{\vec{r}})/V_b$ by software such as MATLAB by means of the Finite Element Method (FEM) for given geometry, dielectric function and boundary conditions. But it is still left to derive a formula relating this numerical solution to the unit cell capacity. Proceeding as sketched above, we write down the energy stored in the field as a volume integral over a unit cell

$$W = \frac{1}{2} \int_{\text{cell}} dV \vec{E} \cdot \vec{D}. \quad (3.1.29)$$

At this point we need to make use of the symmetry considerations above. Given the translational symmetry in the y -direction, there can be no preferred direction along this axis and hence no field component. Furthermore, the symmetry dictates that the fields \vec{E} and \vec{D} must be uniform in the y -direction and, thus, specifically this is true within the cell volume integrated over in Eq. (3.1.29). Therefore, we may trivially integrate over that direction; doing so and reexpressing in terms of the potential we find

$$W = \frac{\Delta y}{2} \int_{\text{cell}} dx dz \vec{E} \cdot \vec{D} = \frac{\Delta y}{2} \int_{\text{cell}} dx dz \epsilon(\vec{r}) [\nabla_{\vec{r}}V(\vec{r})]^2, \quad (3.1.30)$$

which we now write in terms of the dimensionless solution $V(\tilde{\vec{r}})/V_b$ to Eq. (3.1.28) by switching to the dimensionless position $\tilde{\vec{r}} = (\tilde{x}, \tilde{y}, \tilde{z})$:

$$\begin{aligned} W &= \frac{\Delta y}{2} \epsilon_0 V_b^2 \int_{\text{cell}} d\tilde{x} d\tilde{z} L_p^2 \epsilon_r(\tilde{\vec{r}}) \left[\frac{1}{L_p} \nabla_{\tilde{\vec{r}}} V(\tilde{\vec{r}})/V_b \right]^2 \\ &= \frac{\Delta y}{2} \epsilon_0 V_b^2 \int_{\text{cell}} d\tilde{x} d\tilde{z} \epsilon_r(\tilde{\vec{r}}) \left[\nabla_{\tilde{\vec{r}}} V(\tilde{\vec{r}})/V_b \right]^2, \end{aligned}$$

where the characteristic length L_p has dropped out. Finally equating this to the expression $W = C_{\text{cell}}V_b^2/2$, we are led to define the dimensionless unit cell capacity \tilde{C}_{cell}

$$\tilde{C}_{\text{cell}} \equiv \frac{C_{\text{cell}}}{\epsilon_0 \Delta y} = \int_{\text{cell}} d\tilde{x}d\tilde{z}\epsilon_r(\tilde{r}) \left[\nabla_{\tilde{r}} V(\tilde{r})/V_b \right]^2,$$

which is the cell capacitance per unit length in the y -direction divided by the vacuum permittivity ϵ_0 . This is the quantity that follows most naturally from the numerical calculation. A MATLAB script for calculating \tilde{C}_{cell} for the membrane-IDC geometry is provided in Appendix B.

Whenever we wish to evaluate one of the formulas derived in this chapter numerically, we will make the substitution $C_{i,j} = C(z_{i,j}) = \epsilon_0 \Delta y \tilde{C}(\tilde{z}_{i,j})$ (having dropped the 'cell' label). Regarding the characteristic length and area defined in Section (3.1.3.6), we now define dimensionless versions of these in terms Δx , the width of the unit cell in the x -direction: $\tilde{\xi}_i^{(\text{eq})} \equiv \xi_i^{(\text{eq})}/\Delta x$ and $\tilde{\alpha}_i^{(\text{eq})} \equiv \alpha_i^{(\text{eq})}/(\Delta x)^2$. Since only relative variation of the capacitance enters these quantities, they can be determined (numerically) from the function $\tilde{C}(\tilde{z})$ as

$$(\tilde{\xi}_i^{(\text{eq})})^{-1} = \left[-\frac{1}{\tilde{C}(\tilde{z})} \frac{d\tilde{C}}{d\tilde{z}} \right] \Bigg|_{\tilde{z}=\tilde{z}_i^{(\text{eq})}} \quad \text{and} \quad (\tilde{\alpha}_i^{(\text{eq})})^{-1} = \left[\frac{1}{\tilde{C}(\tilde{z})} \frac{d^2\tilde{C}}{d\tilde{z}^2} \right] \Bigg|_{\tilde{z}=\tilde{z}_i^{(\text{eq})}}.$$

Note the following important outcome of the derivation: The considerations that led to Eq. (3.1.30) imply that the numerical calculation of the unit cell capacitance reduces to a 2-dimensional problem in the xz -plane. More specifically, we may consider each unit cell in terms of its projection into this plane, exactly as it is depicted in Fig. 3.1.1 (right). A single unit cell from this figure is reproduced in Fig. 3.1.5.

The appropriate boundary conditions to apply are as follows: The surfaces of the finger segments have fixed potentials so that the difference of these is unity (in the dimensionless quantity V/V_b). The vertical boundaries have no normal field component due to the approximate reflection symmetry around these discussed above. Moreover, the extent of the cell in the z -direction should be such that it is reasonable that the field has essentially died off at the boundary. This allows us to use the boundary condition of no normal field component on the horizontal boundaries as well.

If the membrane is taken to be a perfect conductor this can be accounted for by replacing the condition on the upper horizontal boundary by one at the lower membrane surface: Fixed potential of $(V_+ + V_-)/2V_b$, as follows from symmetry considerations.

3.2 Quantities of interest

Based on the framework developed above, we now extract formulas for the primary quantities that characterize the electromechanical interaction: The coupling constant and the induced mechanical frequency shift. These formulas rely

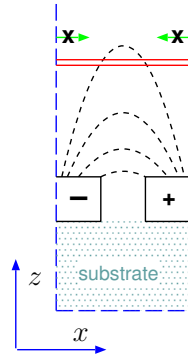


Figure 3.1.5: The xz -plane projection of a unit cell (blue). Solving this 2-dimensional scenario is sufficient to obtain the unit cell capacitance. The boundary condition of no normal field component on the vertical boundaries is indicated (green).

on knowledge about the static deflection of the membrane that occurs when the bias voltage is applied, i.e., its equilibrium configuration under these conditions. An algorithm for determining this equilibrium configuration is suggested in Section 3.2.3.

3.2.1 Electromechanical coupling strength

As identified in Section 3.1.3.6, the electromechanical coupling arises from the second term in Eq. (3.1.26),

$$[\underline{C}''(\delta\vec{z})]_{N,N} Q''_{\text{slow}}(\text{eq}) \delta q_{\text{slow}},$$

more specifically from the $\sim \delta\vec{z}\delta q_{\text{slow}}$ term that appears by inserting the explicit expression for the matrix element (3.1.25). Switching to a more natural labelling for the 2-dimensional grid of unit cells $\{(\tilde{x}_i, \tilde{y}_j)\}$, i.e., $i \rightarrow (i, j)$, and introducing the mode expansion (3.1.7) the coupling term takes the form

$$\sum_{i,j} \frac{C_{i,j}^{(\text{eq})}}{[C_{\text{tot}}^{(\text{eq})}]^2} \frac{1}{\xi_{i,j}^{(\text{eq})}} \delta z_{i,j} Q''_{\text{slow}}(\text{eq}) \delta q_{\text{slow}} = \sum_{m,n} \left[\sum_{i,j} V_b \frac{C_{i,j}^{(\text{eq})}}{C_{\text{tot}}^{(\text{eq})}} \frac{u_{m,n}(\tilde{x}_i, \tilde{y}_j)}{\xi_{i,j}^{(\text{eq})}} \right] \beta_{m,n} \delta q_{\text{slow}} \quad (3.2.1)$$

since $Q''_{\text{slow}}(\text{eq}) = C_{\text{tot}}^{(\text{eq})} V_b$. Eq. (3.2.1) accounts for the couplings of the 'slow' circuit mode with each of the spatial mechanical modes $u_{m,n}$ of canonical position $\beta_{m,n}$; the bracketed term is the coupling constant $G_{m,n}$ to mechanical mode (m, n) :

$$G_{m,n} \equiv \sum_{i,j} \frac{C_{i,j}^{(\text{eq})}}{C_{\text{tot}}^{(\text{eq})}} \left[\frac{V_b}{\xi_{i,j}^{(\text{eq})}} \right] u_{m,n}(\tilde{x}_i, \tilde{y}_j). \quad (3.2.2)$$

As suggested by the form of Eq. (3.2.2), $\{G_{m,n}\}$ can be thought of as coupling matrix elements between circuit and mechanical modes evaluated via discretized

position space integrals. The relation between G and the usual quantum Hamiltonian coupling constant g was given in Section 3.1.3.7,

$$\begin{aligned} g_{m,n} &= 2Gq_{0,\text{slow}}z_0/\hbar = \frac{1}{\sqrt{L_0\omega_{\text{slow}}m\omega_{\text{m}}}}G_{m,n} = \sqrt{\frac{C_{\text{tot}}^{(\text{eq})}\omega_{\text{slow}}}{m\omega_{\text{m}}}}G_{m,n} \\ &= \sqrt{\frac{\omega_{\text{slow}}}{m\omega_{\text{m}}}} \sum_{i,j} \frac{C_{i,j}^{(\text{eq})}}{\sqrt{C_{\text{tot}}^{(\text{eq})}}} \left[\frac{V_{\text{b}}}{\xi_{i,j}^{(\text{eq})}} \right] u_{m,n}(\tilde{x}_i, \tilde{y}_j), \end{aligned} \quad (3.2.3)$$

by use of the substitution $L_0^{-1} = C_{\text{tot}}^{(\text{eq})}\omega_{\text{slow}}^2$. In Eq. (3.2.3) we have evaluated the membrane mode oscillator length z_0 at the bare frequency ω_{m} (see footnote 9 on page 40).

3.2.2 Induced mechanical frequency shift

There are two bias enhanced contributions to the induced frequency shift of the membrane (in linear theory in the charge fluctuations):

- Due to coupling to the slow circuit mode whose equilibrium charge is enhanced by the applied DC bias voltage.
- Due to coupling to the fast internal modes of the capacitive element.

Of these two, we will derive a formula for the first while for the second we will indicate how evaluation can be approached.

3.2.2.1 Shift from slow circuit mode coupling

As discussed in Section 3.1.3.6, the mechanical frequency shift induced by the bias of the 'slow' circuit mode comes from the first term in $H_{\text{int,slow}}$ Eq. (3.1.26),

$$\frac{1}{2} [\underline{\underline{C''}}(\delta\vec{z})]_{N,N} Q_{\text{slow}}''^{(\text{eq})2},$$

more specifically its $(\delta\vec{z})^2$ part:

$$\frac{1}{4} V_{\text{b}}^2 \sum_{i,j} C_{i,j}^{(\text{eq})} \left[2 \left(\frac{1}{\xi_{i,j}^{(\text{eq})}} \right)^2 - \frac{1}{\alpha_{i,j}^{(\text{eq})}} \right] (\delta z_{i,j})^2,$$

using Eq. (3.1.25) with 2-dimensional indexing $i \rightarrow (i, j)$ and $Q_{\text{slow}}''^{(\text{eq})} = C_{\text{tot}}^{(\text{eq})} V_{\text{b}}$. To obtain an expression in terms of the canonical position variables of the membrane $\{\beta_{m,n}\}$, we insert the mode expansion (3.1.7), $\delta z_{i,j} = \sum_{m,n} \beta_{m,n} u_{m,n}(\tilde{x}_i, \tilde{y}_j)$, whereby the above expression becomes

$$V_{\text{b}}^2 \sum_{m,n} \sum_{m',n'} K_{(m,n);(m',n')} \beta_{m,n} \beta_{m',n'} \quad (3.2.4)$$

$$K_{(m,n);(m',n')} \equiv \frac{1}{4} \sum_{i,j} C_{i,j}^{(\text{eq})} \left[2 \left(\frac{1}{\xi_{i,j}^{(\text{eq})}} \right)^2 - \frac{1}{\alpha_{i,j}^{(\text{eq})}} \right] u_{m,n}(\tilde{x}_i, \tilde{y}_j) u_{m',n'}(\tilde{x}_i, \tilde{y}_j) \quad (3.2.5)$$

The quantities defined as $K_{(m,n);(m',n')}$ are coupling matrix elements between $\beta_{m,n}$ and $\beta_{m',n'}$ for $(m,n) \neq (m',n')$ while the diagonal elements, $(m,n) = (m',n')$, correspond to frequency shifts (both per bias voltage squared). Hence, we see that the voltage bias in general will result in coupling between the drum modes of the membrane, the strength of which can be determined by evaluating the appropriate matrix elements above.

Our focus here, however, are the frequency shifts, so we confine our attention to the diagonal terms of Eq. (3.2.4): $V_b^2 \sum_{m,n} K_{(m,n);(m,n)} \beta_{m,n}^2$. By adding these terms to the non-interacting mechanical Hamiltonian $H_{m,0}$ (or H_{mem}), Eq. (3.1.8), it will remain diagonalized and we can read off the shifted frequency $\omega'_{m,n}$ of mode (m,n) as the coefficient of the combined $\beta_{m,n}^2$ term

$$\begin{aligned} \frac{1}{2} m \omega_{m,n}^2 + V_b^2 K_{(m,n);(m,n)} &= \frac{1}{2} m \left[\omega_{m,n}^2 + \frac{2}{m} V_b^2 K_{(m,n);(m,n)} \right] \\ &\Rightarrow \omega'_{m,n} = \sqrt{\omega_{m,n}^2 + \frac{2}{m} V_b^2 K_{(m,n);(m,n)}}. \end{aligned}$$

The frequency shift must be small compared to the bare frequency for our perturbative approach to be valid, hence we can Taylor approximate the square root as

$$\omega'_{m,n} = \omega_{m,n} \sqrt{1 + \frac{2}{m \omega_{m,n}^2} V_b^2 K_{(m,n);(m,n)}} \approx \omega_{m,n} + \frac{1}{m \omega_{m,n}} V_b^2 K_{(m,n);(m,n)}$$

from which the frequency shift can be stated as $\Delta \omega_{m,n} \approx \frac{1}{m \omega_{m,n}} V_b^2 K_{(m,n);(m,n)}$. The shift is thus seen to be proportional to the bias voltage squared, V_b^2 .

3.2.2.2 Adiabatic shift from fast circuit modes

As discussed in Section 3.1.3.2, the fast modes of the capacitive element act on a much faster timescale than the mechanical mode and may therefore be adiabatically eliminated. This amounts to observing that these modes are always in their steady state w.r.t. the instantaneous mechanical configuration on our slower timescale of interest. This pseudo steady state for the j 'th fast mode is found from solving the following Hamilton's equations for $H_{c,0} + H_{\text{int,fast}}$, Eqs. (3.1.21) and (3.1.27),

$$\begin{aligned} 0 = -\dot{\phi}_{\text{fast},j}'' &= \frac{\partial [H_{c,0} + H_{\text{int,fast}}]}{\partial (\delta q_{\text{fast},j})} \Big|_{\delta q_{\text{fast},j} = \delta q_{\text{fast},j}^{(\text{adia})}} \approx \frac{\delta q_{\text{fast},j}^{(\text{adia})}}{C_{\text{tot}}^{(\text{eq})}} + Q_{\text{slow}}''^{(\text{eq})} [\underline{C}''(\delta \vec{z})]_{j,N} \\ &\Rightarrow \delta q_{\text{fast},j}^{(\text{adia})} \approx -C_{\text{tot}}^{(\text{eq})} Q_{\text{slow}}''^{(\text{eq})} [\underline{C}''(\delta \vec{z})]_{j,N}, \end{aligned}$$

ignoring terms not enhanced by the bias. We may now plug this adiabatic steady state back into $H_{c,0} + H_{\text{int,fast}}$, which gives rise to the following effective term in the Hamiltonian (ignoring terms $\sim (\delta \vec{z})^2 \delta q_{\text{slow}}$ that do not contribute to the frequency shift)

$$H_{\text{fast}}^{(\text{adia})} \equiv -\frac{1}{2} V_b^2 [C_{\text{tot}}^{(\text{eq})}]^3 \sum_{j=1}^{N-1} [\underline{C}''(\delta \vec{z})]_{j,N}^2. \quad (3.2.6)$$

While we cannot know the individual elements of \underline{C}'' appearing in this expression without explicitly performing a full diagonalization, we can evaluate the sum by exploiting the completeness of the eigenvectors $\mathbf{1} = \vec{b}'\vec{b}'^T + \sum_{j=1}^{N-1} \vec{e}_{\text{fast},j}\vec{e}_{\text{fast},j}^T$, where $\vec{e}_{\text{fast},j}^T$ is the j 'th row of the matrix \underline{R} that diagonalizes the kinetic matrix as considered earlier. In this way we find an expression for Eq. (3.2.6) in terms of known quantities

$$\begin{aligned} H_{\text{fast}}^{(\text{adia})} &= -\frac{1}{2}V_b^2[C_{\text{tot}}^{(\text{eq})}]^3\vec{b}'^T \left[\underline{C}''(\delta\vec{z}) \left(\sum_{j=1}^{N-1} \vec{e}_{\text{fast},j}\vec{e}_{\text{fast},j}^T \right) \underline{C}''(\delta\vec{z}) \right] \vec{b}' \\ &= -\frac{1}{2}V_b^2[C_{\text{tot}}^{(\text{eq})}]^3\vec{b}'^T \left[\underline{C}''(\delta\vec{z})(\mathbf{1} - \vec{b}'\vec{b}'^T)\underline{C}''(\delta\vec{z}) \right] \vec{b}' \\ &= -\frac{1}{2}V_b^2[C_{\text{tot}}^{(\text{eq})}]^3 \left([\underline{C}''^2(\delta\vec{z})]_{N,N} - [\underline{C}''(\delta\vec{z})]_{N,N}^2 \right). \end{aligned} \quad (3.2.7)$$

Note that $[\underline{C}''^2(\delta\vec{z})]_{N,N}$ can be determined from the diagonal matrix \underline{C}' (3.1.23) as $[\underline{RC}'^2(\delta\vec{z})\underline{R}^T]_{N,N}$, again only requiring knowledge of the slow eigenvector \vec{b}' . The diagonal matrix element $[\underline{C}''(\delta\vec{z})]_{N,N}$ has already been determined in Eq. (3.1.25). As we wish to determine the frequency shift induced by the fast circuit modes, we only retain terms of order $(\delta\vec{z})^2$ in Eq. (3.2.7) whereby we find

$$H_{\text{fast}}^{(\text{adia})} = -\frac{1}{2}V_b^2 \left[\sum_{i,j} \left(\frac{C_{i,j}^{(\text{eq})}}{[\xi_{i,j}^{(\text{eq})}]^2} \delta z_{i,j}^2 \right) - \frac{1}{C_{\text{tot}}^{(\text{eq})}} \left(\sum_{i,j} \frac{C_{i,j}^{(\text{eq})}}{\xi_{i,j}^{(\text{eq})}} \delta z_{i,j} \right)^2 \right]. \quad (3.2.8)$$

The remainder of the calculation proceeds in complete parallel to that given in the previous section from Eq. (3.2.5) and on. The first term of Eq. (3.2.8) exactly cancels the frequency shift contribution from the first term of Eq. (3.2.5) pertaining to the 'slow' mode interaction, while the second term of Eq. (3.2.8) contributes the shift $g_{m,n}^2/(2\omega_{\text{slow}})$ to the mechanical mode (m, n) .

3.2.3 Static deflection of the mechanical element

Our derivation of the interaction Hamiltonian in Section 3.1.3.6 is based on a Taylor expansion around the classical equilibrium configuration of the system $\{\vec{Q}''^{(\text{eq})}, z^{(\text{eq})}(\tilde{x}, \tilde{y})\}$. Due to the bias voltage V_b , this equilibrium is shifted from that of the non-interacting circuit and membrane, say, $\{\vec{Q}''^{(0)}, z^{(0)}(\tilde{x}, \tilde{y})\}$. As a first approximation one can assume $z^{(\text{eq})}(\tilde{x}, \tilde{y}) \approx z^{(0)}(\tilde{x}, \tilde{y})$, i.e. a flat membrane, whereby $\vec{Q}''^{(\text{eq})} = \vec{Q}''^{(0)}$ accordingly. This is the approach we will take in Section 3.3 in demonstrating the calculation scheme.

However, in this section we propose an iterative algorithm for determining $\{\vec{Q}''^{(\text{eq})}, z^{(\text{eq})}(\tilde{x}, \tilde{y})\}$.¹⁰ The idea is the following: Rather than expanding the capacitance around $z^{(\text{eq})}(\tilde{x}, \tilde{y})$, which we do not know, we expand around the flat membrane $z^{(0)}(\tilde{x}, \tilde{y}) = 0$ (hereby defining the origin of the z -axis). The relevant Hamiltonian can be obtained from Eq. (3.1.19) by replacing $C_{\text{tot}}^{(\text{eq})} \rightarrow C_{\text{tot}}^{(0)}$, the latter being the total capacitance evaluated at $z^{(0)}(\tilde{x}, \tilde{y})$.

¹⁰The algorithm sketched here has not yet been implemented, therefore its numerical convergence and stability properties are unknown.

Based on this we now wish to generate an estimate of the equilibrium charge $\bar{Q}''^{(0)}$, but to avoid dealing with simultaneous equations of $\bar{Q}''^{(\text{eq})}$ and $z^{(\text{eq})}$, we do so for fixed $z = z^{(0)}(\tilde{x}, \tilde{y})$. That is, we evaluate Hamilton's equation at $z^{(0)}(\tilde{x}, \tilde{y})$ (our best estimate so far) rather than $z^{(\text{eq})}(\tilde{x}, \tilde{y})$:

$$0 = \left. \frac{\partial H_c}{\partial \bar{Q}''} \right|_{\bar{Q}'' = \bar{Q}''^{(0)}, z = z^{(0)}} = \frac{1}{C_{\text{tot}}^{(0)}} \bar{Q}'' - \frac{\partial Q''_{\text{slow}}}{\partial \bar{Q}''} V_b,$$

from which we get the estimate $\bar{Q}''^{(0)}$ which has components $Q''_{\text{slow}}^{(0)} = C_{\text{tot}}^{(0)} V_b$ and $Q''_{\text{fast},j}^{(0)} = 0$; note that the contribution from H_{int} vanished as we evaluated at the expansion ‘‘point’’ $z = z^{(0)}(\tilde{x}, \tilde{y})$. We proceed by finding a new estimate for the membrane configuration $z^{(1)}(\tilde{x}, \tilde{y})$ for fixed $\bar{Q}'' = \bar{Q}''^{(0)}$. Given this, we consider a new Hamiltonian for which the capacitance is expanded around $z^{(1)}(\tilde{x}, \tilde{y})$ and so on. We note that the k 'th estimate of the equilibrium charge, based on $z^{(k)}(\tilde{x}, \tilde{y})$, is $Q''_{\text{slow}}^{(k)} = C_{\text{tot}}^{(k)} V_b$ and $Q''_{\text{fast},j}^{(k)} = 0$.

We write down Hamilton's equation for the $(k+1)$ 'th correction to the membrane equilibrium configuration by considering the drum mode Hamiltonian (3.1.8) and the interaction Hamiltonian (3.1.24) expanded around $z^{(k)}(\tilde{x}, \tilde{y})$ and evaluated at $\bar{Q}''^{(k)}$; the latter is

$$H_{\text{int}}^{(k)} \Big|_{\bar{Q}'' = \bar{Q}''^{(k)}} = \frac{1}{2} V_b^2 \sum_{i,j} C_{i,j}^{(k)} \left[\frac{1}{\xi_{i,j}^{(k)}} \delta z_{i,j} + \frac{1}{2} \left[2 \left(\frac{1}{\xi_{i,j}^{(k)}} \right)^2 - \frac{1}{\alpha_{i,j}^{(k)}} \right] (\delta z_{i,j})^2 \right],$$

where $\delta z_{i,j}$ is the deviation from $z^{(k)}(\tilde{x}_i, \tilde{y}_j)$. Expressing this in terms of drum modes, Hamilton's equation for $\dot{p}_{m,n} = 0$ takes the form

$$0 = \frac{\partial}{\partial \beta_{m,n}} \left[H_{\text{mem}} + H_{\text{int}}^{(k)} \Big|_{\bar{Q}'' = \bar{Q}''^{(k)}} \right] \Big|_{\beta_{m,n} = \delta \beta_{m,n}^{(k+1)}} = m \omega_{m,n}^2 \delta \beta_{m,n}^{(k+1)} + \frac{1}{2} V_b^2 \sum_{i,j} C_{i,j}^{(k)} \left[\frac{1}{\xi_{i,j}^{(k)}} + \left[2 \left(\frac{1}{\xi_{i,j}^{(k)}} \right)^2 - \frac{1}{\alpha_{i,j}^{(k)}} \right] \sum_{m',n'} \delta \beta_{m',n'}^{(k+1)} u_{m',n'}(\tilde{x}_i, \tilde{y}_j) \right] u_{m,n}(\tilde{x}_i, \tilde{y}_j),$$

or, in matrix, form

$$0 = (m \underline{\omega}^2 + V_b^2 \underline{S}) \delta \vec{\beta}^{(k+1)} + V_b^2 \vec{v}, \quad (3.2.9)$$

where we have condensed (m, n) into a single integer index and defined

$$[\underline{\omega}]_{(m,n;m',n')} \equiv \delta_{m,m'} \delta_{n,n'} \omega_{m,n}; \quad [\vec{v}]_{(m,n)} \equiv \frac{1}{2} \sum_{i,j} \frac{C_{i,j}^{(k)}}{\xi_{i,j}^{(k)}} u_{m,n}(\tilde{x}_i, \tilde{y}_j);$$

$$[\underline{S}]_{(m,n;m',n')} \equiv \frac{1}{2} \sum_{i,j} C_{i,j}^{(k)} \left[2 \left(\frac{1}{\xi_{i,j}^{(k)}} \right)^2 - \frac{1}{\alpha_{i,j}^{(k)}} \right] u_{m,n}(\tilde{x}_i, \tilde{y}_j) u_{m',n'}(\tilde{x}_i, \tilde{y}_j).$$

Inverting Eq. (3.2.9) we obtain the $(k+1)$ 'th correction to the estimate of the equilibrium configuration

$$\delta \vec{\beta}^{(k+1)} = - \left(\frac{m}{V_b^2} \underline{\omega}^2 + \underline{S} \right)^{-1} \vec{v},$$

yielding the $(k + 1)$ 'th estimate

$$z^{(k+1)}(\tilde{x}, \tilde{y}) = \sum_{m,n} \left(\sum_{i=1}^{k+1} \delta\beta_{m,n}^{(i)} \right) u_{m,n}(\tilde{x}, \tilde{y}). \quad (3.2.10)$$

as the sum of all corrections to the flat membrane configuration, $z^{(0)}(\tilde{x}, \tilde{y}) = 0$.

3.3 Application to experiment

We end this chapter by giving a brief demonstration of actual calculations. As mentioned in the introduction, the procedure is originally developed for the interface of a membrane and an interdigitated capacitor, the setup which was used to illustrate the derivation. This interface is currently being investigated experimentally in the membrane group at QUANTOP, NBI with the aim of implementing the transduction scheme proposed in Ref. [27] (and which was mentioned in Section 2.4). The current, preliminary experiments focus on characterizing the electromechanical coupling between the interdigitated capacitor and membranes of various compositions.

The account given here does not pretend to be a full analysis and represents work in progress.

3.3.1 Description of the experiment

The setup mainly consists of a vibrating membrane mounted above an Inter-Digitated Capacitor (IDC), the scenario also considering in e.g. Fig. 3.1.1. We will consider square membranes and IDCs of equal area, but sacrificing some IDC finger segments is likely to be necessary to allow for simultaneous optomechanical interaction. An example unit cell of the setup is shown in Fig. 3.3.1, it is largely equivalent to that considered in Fig. 3.1.5. The IDC is placed on a substrate whose dielectric response will tend to decrease the coupling to the membrane, since this stray capacitance diminishes the relative capacitance changes induced by the membrane movement.

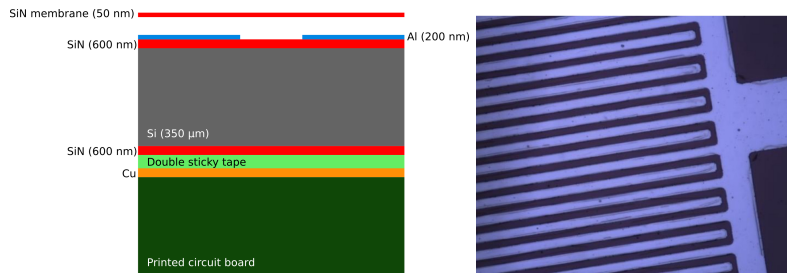


Figure 3.3.1: (Left) Unit cell of the membrane-IDC interface. (Right) Microscope image of the fingers of an interdigitated capacitor. Images provided by Tolga Bagci.

The LC circuit mode is brought into resonance with the fundamental mode of the membrane by picking an appropriate inductance L and hence no AC drive field is required to achieve $\omega_{LC} = \omega_{1,1}$.

The above setup has been realized with membranes of different compositions, primarily two types: The first type is the SiN membrane which may be considered a linear dielectric and hence is straightforward to model within our calculational scheme. The second type is the hybrid SiGraphene membrane, obtained from the former by adding a layer of doped graphene on the side of the membrane facing the IDC. The electrical properties of such hybrid membranes are difficult to model precisely and will depend on the doping level. The carrier density may even depend on the bias voltage which would additionally complicate the picture.

The SiGraphene membranes offer stronger coupling than their SiN counterparts and the effort is therefore focused on the former type. From the calculational side, the approach will be to model them as perfect conductors. This can be accommodated for by imposing appropriate boundary conditions as explained in Section 3.1.4.

3.3.2 Experimental parameters and data

The numerical calculations will be based on the parameter set presented in Table 3.1. The normal distance between the fingers and the plane in which the membrane is mounted varies between the different realizations. As mentioned above, we take $\omega_{LC} = \omega_{1,1}$ and consider the membrane and IDC squares of equal side length.

membrane	mass m	freq. $\omega_{1,1}$	thickness	side length L
	$4 \cdot 10^{-8} \text{g}$	810 KHz	50 nm	0.5 mm
IDC finger	width	gap	height	
	$5 \mu\text{m}$	$4 \mu\text{m}$	200 nm	

Table 3.1: Parameter set of the experiments that enter the numerical calculations. The relative dielectric constant of the pure SiN membranes were taken to be $\epsilon_r = 7.6$ while for the substrate the value $\epsilon_r = 4.2$ was used, corresponding to glass.

The electromechanical coupling strength has so far not been measured successfully in these experiments, so we will not be able to compare calculated values to the experiment. Nonetheless, we will present the results of the calculation below.

The mechanical frequency shift due to the interaction, on the other hand, has been measured for several membrane-IDC setups of which two examples are shown in Fig. 3.3.2. These show a characteristic $\propto -\alpha V_b^2$ behavior in agreement with our formalism, see Section 3.2.2.1. We will therefore calculate α below and compare with the experimental fits (those in Fig. 3.3.2 and others).

3.3.3 Numerical calculations

Our numerical calculation applies the above parameter set to the unit cell in Fig. 3.1.5. For this calculation, we use as the characteristic length L_p the periodicity of the finger pattern, i.e., the center-to-center distance of fingers of the same polarity. Note that this interval contains two unit cells, $L_p = 2\Delta x$.

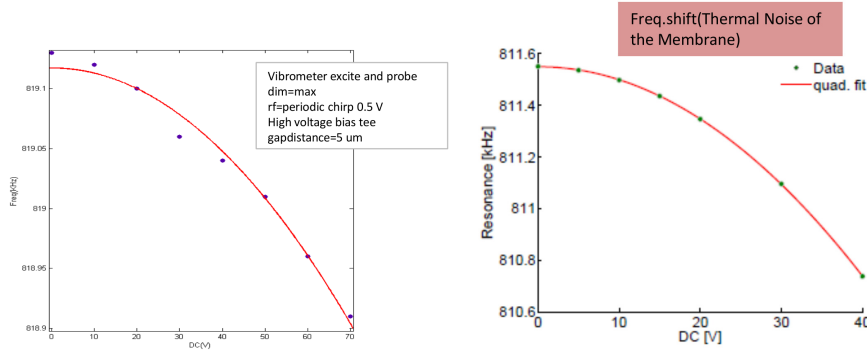


Figure 3.3.2: Experimental measurements of the bias induced mechanical frequency shift fitted to parabolas.

In Fig. 3.3.3 the dimensionless unit cell capacity \tilde{C}_{cell} is plotted as a function of normal distance (in units of L_p) between the top of the fingers and the plane in which the membrane is mounted; both membrane types are represented, SiN and perfect conductor, respectively. In principle, all information we need is contained in this plot as we may estimate its first and second derivatives. This will allow us to calculate the characteristic lengths and areas, $\tilde{\xi}$ and $\tilde{\alpha}$.¹¹

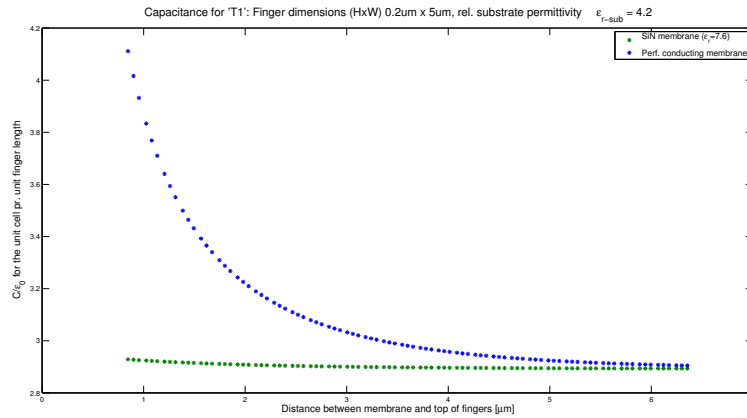


Figure 3.3.3: Dimensionless capacitance of the unit cell, SiN and perfectly conducting membranes, respectively.

Below we demonstrate how to apply the formulas derived in Section 3.2 to calculate the frequency shift and the coupling strength based on the quantities \tilde{C}_{cell} , $\tilde{\xi}$ and $\tilde{\alpha}$. Afterwards we plot the results and compare with experimental data.

¹¹In practice it is necessary to make convergence tests by varying the grid size of the FEM calculation as well as the delta involved in estimating derivatives numerically.

3.3.3.1 Mechanical frequency shift

We will only take into account the main contribution to the shift of the fundamental membrane mode which arises from the voltage bias of the 'slow' mode, see Section 3.2.2.1. To this end, we need to evaluate the (1, 1) diagonal element of the matrix K defined in Eq. (3.2.5). As a lowest order calculation we do this assuming the equilibrium configuration of the membrane to be unaltered by the applied bias voltage, that is, it remains flat $z_{i,j}^{(\text{eq})} = z_{\text{flat}}$; under this assumption, the quantities $\{C_{i,j}^{(\text{eq})} = C_{\text{flat}}\}$, $\{\xi_{i,j}^{(\text{eq})} = \xi_{\text{flat}}\}$ and $\{\alpha_{i,j}^{(\text{eq})} = \alpha_{\text{flat}}\}$ also become uniform in the membrane coordinates $(\tilde{x}_i, \tilde{y}_j)$ whereby the matrix elements of K takes the form

$$K_{(m,n):(m',n')} = \frac{1}{4}C_{\text{flat}} \left[2 \left(\frac{1}{\xi_{\text{flat}}} \right)^2 - \frac{1}{\alpha_{\text{flat}}} \right] \sum_{i,j} u_{m,n}(\tilde{x}_i, \tilde{y}_j) u_{m',n'}(\tilde{x}_i, \tilde{y}_j). \quad (3.3.1)$$

The only $(\tilde{x}_i, \tilde{y}_j)$ dependence being in the drum modes, we may take the continuum limit of the sum and exploit the orthonormality property Eq. (3.1.6)

$$\begin{aligned} \sum_{i,j} u_{m,n}(\tilde{x}_i, \tilde{y}_j) u_{m',n'}(\tilde{x}_i, \tilde{y}_j) &\rightarrow \\ \left(\frac{2L}{L_p} \right)^2 \int_0^1 \int_0^1 d\tilde{x} d\tilde{y} u_{m,n}(\tilde{x}_i, \tilde{y}_j) u_{m',n'}(\tilde{x}_i, \tilde{y}_j) &= \left(\frac{2L}{L_p} \right)^2 \delta_{m,m'} \delta_{n,n'}. \end{aligned}$$

As a side remark, the diagonal nature of this expression shows that in the flat membrane approximation, the bias does not induce direct coupling between the drum modes. With the sum evaluated, the diagonal elements of K , Eq (3.3.1), become

$$K_{(m,n):(m,n)} = \frac{1}{4}C_{\text{flat}} \left[2 \left(\frac{1}{\xi_{\text{flat}}} \right)^2 - \frac{1}{\alpha_{\text{flat}}} \right] \left(\frac{2L}{L_p} \right)^2,$$

which is independent of (m, n) . The frequency shifts are then, as derived in Section 3.2.2.1,

$$\Delta\omega_{m,n} \approx \frac{1}{m\omega_{m,n}} V_b^2 K_{(m,n):(m,n)} = \frac{V_b^2}{2} \frac{\tilde{C}_{\text{cell}}(z_{\text{flat}}) \epsilon_0}{m\omega_{m,n}} \frac{L^2}{L_p^3} \left[2 \left(\frac{1}{\tilde{\xi}(z_{\text{flat}})} \right)^2 - \frac{1}{\tilde{\alpha}(z_{\text{flat}})} \right] \quad (3.3.2)$$

where we have introduced the dimensionless quantities that are the output of the numerical calculation via $C_{\text{flat}} = \tilde{C}_{\text{cell}}(z_{\text{flat}}) \epsilon_0 L_p / 2$, $\xi_{\text{flat}} = \tilde{\xi}(z_{\text{flat}}) L_p$ and $\alpha_{\text{flat}} = \tilde{\alpha}(z_{\text{flat}}) L_p^2$. From Eq. (3.3.2) we may specifically calculate the contribution to the shift of the fundamental drum mode, $(m, n) = (1, 1)$, by evaluating at its bare frequency.

3.3.3.2 Electromechanical coupling strength

To calculate the coupling strength $g_{1,1}$ between the circuit mode and the fundamental mode of the membrane we apply formula (3.2.3). For simplicity and as a lowest order result, we approximate the equilibrium configuration of the membrane to be flat $\{z_{i,j}^{(\text{eq})} = z_{\text{flat}}\}_{i,j}$, entailing equality among the values of

$\{C_{i,j}^{(\text{eq})} = C_{\text{flat}}\}_{i,j}$, $\{\xi_{i,j}^{(\text{eq})} = \xi_{\text{flat}}\}_{i,j}$ as these are only functions of $z_{i,j}^{(\text{eq})}$ within the approximations of our framework. In turn, we have $C_{\text{tot}}^{(\text{eq})} = \sum_{i,j} C_{i,j}^{(\text{eq})} = NC_{\text{flat}}$, where N is the number of unit cells. Under these circumstances, formula (3.2.3) yields

$$g_{1,1} = \sqrt{\frac{\omega_{\text{slow}}}{m\omega_{\text{m}}}} \sum_{i,j} \frac{C_{\text{flat}}}{\sqrt{NC_{\text{flat}}}} \left[\frac{V_{\text{b}}}{\xi_{\text{flat}}} \right] u_{1,1}(\tilde{x}_i, \tilde{y}_j) = \sqrt{\frac{\omega_{\text{slow}}}{m\omega_{\text{m}}}} \sqrt{\frac{C_{\text{flat}}}{N}} \frac{V_{\text{b}}}{\xi_{\text{flat}}} \sum_{i,j} u_{1,1}(\tilde{x}_i, \tilde{y}_j) \quad (3.3.3)$$

Since the only position dependence left is in the mechanical mode function, we may perform the sum over the unit cells by taking the continuum limit $\sum_{i,j} u_{1,1}(\tilde{x}_i, \tilde{y}_j) \rightarrow (\Delta\tilde{x}\Delta\tilde{y})^{-1} \int_0^1 \int_0^1 d\tilde{x}d\tilde{y} u_{1,1}(\tilde{x}_i, \tilde{y}_j) = (2L/L_{\text{p}})^2(8/\pi^2)$. At this point we will introduce the dimensionless quantities that are output by the numerical computation, these enter via $C_{\text{flat}} = \tilde{C}_{\text{cell}}(z_{\text{flat}})\epsilon_0 L_{\text{p}}/2$ and $\xi_{\text{flat}} = \tilde{\xi}(z_{\text{flat}})L_{\text{p}}$. These steps along with the substitution $N = (2L/L_{\text{p}})^2$ turn Eq. (3.3.3) into

$$g_{1,1} = \sqrt{\frac{\omega_{\text{slow}}}{m\omega_{\text{m}}}} \sqrt{\tilde{C}_{\text{cell}}(z_{\text{flat}})\epsilon_0} \frac{V_{\text{b}}}{\tilde{\xi}(z_{\text{flat}})} \frac{\sqrt{2}L}{L_{\text{p}}^{3/2}} \frac{8}{\pi^2},$$

which we evaluate assuming $\omega_{\text{slow}} = \omega_{\text{m}}$.

3.3.4 Numerical results and comparison

3.3.4.1 Frequency shift

In Fig. 3.3.4 we have plotted our calculated frequency shift coefficients $\propto -V_{\text{b}}^2$ for a perfectly conducting membrane, our best available model for SiGraphene membranes. The experimental values are plotted alongside. A rough estimate of the numerical accuracy of the calculation is $\pm 10\%$. The measured frequency shifts are seen to be consistently larger than the calculated ones, thereby apparently outperforming a perfect conductor.

The frequency shift has also been calculated for a pure SiN membrane mounted at the distance $5.04\mu\text{m}$ from the top of the fingers. The calculated value is seen to be $\sim 20\%$ smaller than the measured value:

	Calculated	Measured
Frequency shift, $\Delta\nu = -\alpha V_{\text{b}}^2$	$\alpha = 4.5 \cdot 10^{-2} \text{Hz}/\text{V}^2$	$\alpha = 5.5 \cdot 10^{-2} \text{Hz}/\text{V}^2$

The above comparison shows that the calculated and measured values are of comparable magnitude, which is encouraging. However, a better understanding of the uncertainties of the parameters and the measurement process is required for a more detailed comparison to be meaningful. Measuring the shift for membranes which are truly good conductors and comparing to SiGraphene data could provide an indication of whether our modeling of the latter is reasonably accurate.

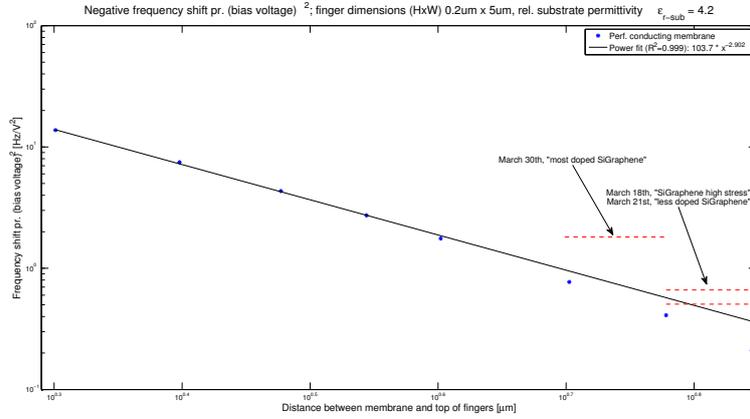


Figure 3.3.4: Calculated negative frequency shift per bias voltage squared for a perfectly conducting membrane, loglog scale. Fitted coefficients from SiGraphene experiments plotted for comparison (the membrane to IDC distance is known within $1\mu\text{m}$).

3.3.4.2 Coupling strength

Given the reasonable correspondance between calculation and measurement above for the case of frequency shifts, we now present our prediction for the electromechanical coupling constant (per bias voltage). It is plotted for the case of a perfectly conducting membrane in Fig. 3.3.5.

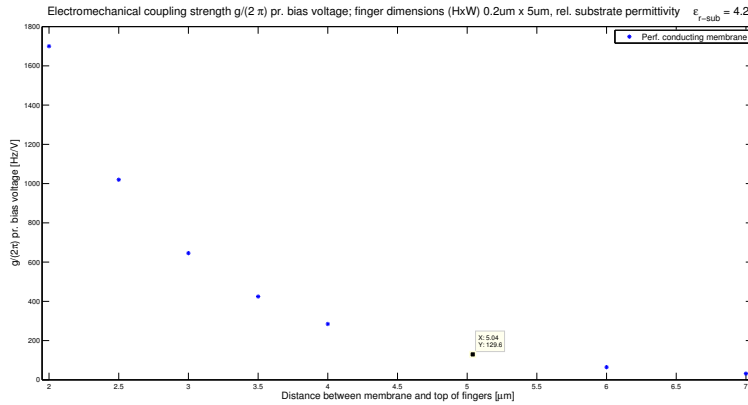


Figure 3.3.5: Coupling strength per bias voltage for perfectly conducting membranes. Plotted as a function of normal distance (in units of L_p) from fingers to the plane in which the membrane is mounted.

For the pure SiN membrane mounted at the distance $5.04\mu\text{m}$ our calculation predicts

	Calculated
Coupling strength pr. bias voltage, $g/2\pi V_b$	7.6 Hz/V

Chapter 4

Quantum noise theory

This chapter provides the conceptual and methodical basis for the cooling analysis in Chapter 5. In Section 4.1 we give a discussion of the notion of “a system coupled to a reservoir” and how a consistent quantum noise theory may be formulated based on this idea. We then go on to derive the quantum Langevin equation in the white noise limit. Based on this, in Section 4.2 we derive exact formulas for the steady state occupancies of coupled harmonic oscillators subjected to white noise. Finally, in Section 4.3, we present a formalism for obtaining effective quantum Langevin equations for subsystems weakly coupled to other system degrees of freedom.

4.1 Effective equations of motion for a system coupled to a Markovian reservoir

In this section we derive an effective equation of motion - the *quantum Langevin equation* - for a quantum system influenced by its environment, as will be the case in any realistic physical situation. It must be stressed, however, that in the context of quantum noise theory, “the environment” should not be associated solely with *undesired* influences impinging on the physical system of interest, although this is certainly a prominent subset of environmental influences. Rather, we shall define “the environment” as being made up of all degrees of freedom amenable to a *reservoir* (or *bath*) description, as will be detailed below. Employing such descriptions allow for the derivation of highly economical effective equations of motion.

The fact that the influence of a reservoir need not be detrimental to a quantum optical system has come to be realized recently. One of the major challenges in the quest for building capable quantum computers, a prominent objective in the field of quantum optics, is indeed posed by the decoherence that results from unwanted coupling to environmental degrees of freedom. Nonetheless, recent years have seen a growing number of proposals to exploit the effects of coupling to *engineered reservoirs* in the quantum optical setting. Interesting examples include topological quantum memories based on engineered dissipation [21] and dissipative state preparation [13]. Thus, influences of “the environment” are not necessarily harmful if we are able to cleverly engineer at least parts of it.

The resulting formalism will reflect a stochastic theory of *quantum noise*. Effective quantum noise equations of various generality can be derived [9]; in the derivation we will give here, approximations will be made that are valid in the majority of quantum optical situations. To be specific, we will derive the *quantum white noise* Langevin equation in the Rotating Wave Approximation (RWA). Fortunately, this approach brings about significant simplification over more general quantum Langevin equations; most notably, we avoid the issue of the divergences that arise from the asymptotically rising quantum noise spectrum. The origin of the divergences is the zero-point quantum fluctuations of the infinite number of modes in the environment; renormalization in one form or another would be required to obtain physical results.

It should also be pointed out that alternative approaches exist to achieving an effective description of the system-environment scenario. Rather than deriving *Heisenberg-Langevin* equations (i.e., effective Heisenberg equations), one can develop effective evolution equations in terms of the reduced density operator of the system, namely so-called *master equations*. The master equation formalism allow more naturally for reservoirs that do not consist of bosonic harmonic oscillators, whereas this is the specific basis on which the quantum Langevin equation is derived. Having said that, it is possible, in the Markovian limit, to formulate a bosonic oscillator bath equivalent to any meaningful reservoir that may occur in the master equation formalism; hence, the two approaches can be considered equivalent in this limit.

4.1.1 Physical systems and their environments

Suppose we are faced with the task of writing down the Hamiltonian governing the evolution of a quantum mechanical experiment at hand; which degrees of freedom to include? Of course, we will make sure to account for those serving a purpose in the experimental scheme, i.e., degrees of freedom that are relevant by design; typical examples in quantum optics are the internal states of an ensemble of atoms or a particular field mode of an electromagnetic cavity. However, these “intentional” degrees of freedom will inevitably have undesirable couplings to additional degrees of freedom, resulting, generally, in degradation of the performance of the experiment; for instance, undesirable degrees of freedom could be the motional states of atoms or free space radiation modes. Given these two (roughly defined) classes of contributions to the Hamiltonian, it might be tempting to presume that we should think of the former as constituting “the system” while the latter plays the role of “the environment”. This distinction is certainly meaningful - ‘idealized description’ versus ‘additional realistic complications’ - but it is not relevant for the purposes of this account of quantum noise theory.

The virtue of quantum noise theory, of which the quantum Langevin equation is a particular instance, is to extract the essence of the *effect* of certain degrees of freedom, thereby obtaining an effective description of the remaining degrees of freedom. Whether the effect of the eliminated degrees of freedom might be utile or of detrimental character need not concern us in developing the formalism. The alternative to employing the noise formalism for a given problem would be to write down the full set of quantum mechanical equations of motion for all degrees of freedom, and from there attempt to solve for the unitary evolution of

the system. This is, in fact, the starting point for the development of quantum noise theory, that is to say, it is a theory *within* the existing framework of quantum mechanics. From there, quantum noise theory goes on to consider the limit where the full set of equations of motion can be reformulated as stochastic equations. Not surprisingly, this requires us to make certain assumptions about the degrees of freedom that we wish to account for in an effective, stochastic manner. As a consequence of this, we cannot draw the line between “system” and “environment” arbitrarily.

For our purposes, *reservoir* will be taken to mean a large assembly of degrees of freedom with the following characteristics:

1. A broad, dense spectrum suited for a continuum description,
2. Weak coupling to the system given by a smooth function of frequency,
3. The state of the “large” reservoir is essentially unchanged by its interaction with the “relatively small” system,
4. It is *Markovian*: On the timescale on which the system evolves, the reservoir has no “memory” of the previous states of the system, i.e., on the aforementioned timescale the effect of the reservoir on the system depends only on the instantaneous state of the system.

These conditions will be specified more precisely in course of the derivation below. It is possible to derive more general quantum Langevin equations by relaxing some of the requirements listed above, but this will not interest us here.

A common mathematical model for the environment is an ensemble of bosonic harmonic oscillators. It is especially common within quantum optics due to the fact that the electromagnetic modes are excellently described by such a model; moreover, in the large cavity limit their spectrum will be a quasi-continuum. In fact, assuming such an ensemble of oscillators is the standard basis for deriving the quantum Langevin equation.

4.1.2 Classical Langevin equations: Brownian motion

The Langevin equation originates from classical stochastic theory and we will here briefly consider the problem of classical Brownian motion to illustrate the structure of the Langevin equation.

A tiny (classical) particle suspended in water can, under a microscope, be observed to undergo so-called Brownian motion due to the stochastic momentum kicks it receives from the smaller, lighter water molecules. Solving this problem by means of Newtonian equations of motion for the particle and all the water molecules is a formidable task and this approach is not likely to yield much physical insight, although it could be the starting point for a numerical simulation. Given that we are interested in the motion of the particle only, an effective equation of motion is desirable; this is provided by the Langevin equation for the problem at hand:

$$\dot{p}(t) = -\eta p(t) + f(t), \quad (4.1.1)$$

where $p(t)$ is the momentum of the particle, η is the drag coefficient and $f(t)$ accounts for the randomness of the momentum kicks (the equation is stated one-dimensionally for simplicity). The viscous drag term, $-\eta p$, models the damping of the particle's motion, which is, microscopically, the average effect resulting from collisions with many water molecules assumed to be in thermal equilibrium. But this cannot be the full story, as the stochastic nature of the collisions necessarily entails deviations from this average, thereby preventing the particle from coming to rest; for this reason, the stochastic *Langevin force* $f(t)$ must be present in the equation (4.1.1) representing these fluctuations. Averaged over a time interval where many collisions take place, the Langevin force must vanish, $\langle f(t) \rangle = 0$, if we assume the motion of the water molecules to be isotropically distributed. Its two-time auto-correlation function, however, is a non-zero function of the time difference and is typically written in terms of the diffusion coefficient D as

$$\langle f(t)f(t') \rangle \propto Dg(t-t'). \quad (4.1.2)$$

While it follows from $\langle f(t) \rangle = 0$ that the Langevin force will not influence the average momentum, it will alter the mean square momentum as a result of Eq. (4.1.2). The normalized function $g(t-t')$ characterizes how fast the random force component fluctuates; its shape is a peak centered around $t-t' = 0$ (given that we are dealing with a thermal bath). If it takes many collisions to produce any appreciable effect on the particle, we may consider the evolution on this timescale, which is long compared to that of a single collision; from this point of view, $f(t)$ varies very rapidly and can be taken delta-correlated with itself, i.e., $g(t-t') = \delta(t-t')$. Put differently, there is essentially no change in $p(t)$ on the timescale of a single collision (over which $f(t)$ is hardly delta-correlated) and we can therefore coarse-grain over several such collisions.¹ This is the *white noise* limit, which is also the limit we will consider in the quantum treatment below. Note that under the conditions stated in the above it is reasonable to assume that the thermal equilibrium of the water molecules is not significantly disturbed. This, combined with the weak individual influence of the many collisions, allows for a plausible reservoir treatment of the body of water.

The Langevin equation, Eq. (4.1.1), thus gives us an intuitive way of thinking about the net effect of the particle's interaction with the immense number of water molecules; we see that the coupling to this reservoir effectively induces two complementary effects on the system: *Dissipation* of energy into the reservoir and *input of fluctuations/noise* from the reservoir.

We would now like to derive similar effective equations within the framework of quantum mechanics where only the essence of the effect of environment on the system remains while the details of the evolution of the environment degrees of freedom are left out. It is indeed possible, and the quantum Langevin equation even maintains the structure of the classical counterpart, Eq. (4.1.1). But a quantum theory must necessarily have additional structure given its operator nature and status of being a more general theory; this is the subject of the following section.

¹In writing the drag term of Eq. (4.1.1) as simply $-\eta p$, we have actually already assumed $p(t)$ to be essentially constant over the timescale of single collisions. Generally, the drag term has a memory of the history of the particle: $\dot{p}(t) \sim -\int_{-\infty}^t h(t-t')p(t')dt'$.

4.1.3 Requirements for quantum noise theory

In establishing a quantum noise theory there are some requirements to be fulfilled for it to be consistent with well-established physical theories: Classical statistical mechanics and, of course, quantum mechanics. Regarding the first, we must require that the quantum noise theory agrees with statistical mechanics in the appropriate limit, which is the regime where the fundamentally quantized nature of the system becomes irrelevant; this can usually be phrased formally as $\hbar \rightarrow 0$. The primary constraint that arises as a consequence of being in the quantum setting is the requirement of preserving canonical commutation relations. Since we will be altering the standard Heisenberg equations of motion, we risk ruining the algebraic structure specified by the commutation relations as we evolve the system according to our modified equations. We will explore this matter in the following.

A simple way of demonstrating that care must be exerted in formulating a consistent quantum theory of noise is to naïvely add in the damping to the Heisenberg equation of motion and consider the consequences: Let us consider, as a typical quantum optical example, a 2-level atom interacting with a free space radiation field initially in its vacuum state (i.e. effectively at zero temperature, $T = 0$). Here we can treat the internal degree of freedom of the atom as our system and the radiation field modes as constituting the reservoir. The decay rate γ of the atom into the free space continuum of radiation modes is given by the *Wigner-Weisskopf* result for spontaneous emission. Then, given this quantity, how do we formulate a consistent effective quantum description? The internal state of the atom can be described in terms of the Heisenberg picture evolution of the usual Pauli operators $\hat{\sigma}^+ = |2\rangle\langle 1|$, $\hat{\sigma}^- = |1\rangle\langle 2|$ and $\hat{\sigma}_z = |2\rangle\langle 2| - |1\rangle\langle 1|$. Proceeding naïvely, we add by hand a decay term proportional to γ to the free evolution Heisenberg equation, thereby obtaining

$$\dot{\hat{\sigma}}^- = -i\omega_a \hat{\sigma}^- - \frac{\gamma}{2} \hat{\sigma}^-, \quad (4.1.3)$$

ω_a being the transition frequency of the atom (and the time dependence of the operators has been suppressed). From the operator definitions we find, algebraically, the same-time commutation relation $[\hat{\sigma}^+(t), \hat{\sigma}^-(t)] = \hat{\sigma}_z(t)$, for all t . However, according to Eq. (4.1.3) and its Hermitian conjugate,

$$\begin{aligned} \frac{d}{dt} [\hat{\sigma}^+(t), \hat{\sigma}^-(t)] &= [\dot{\hat{\sigma}}^+(t), \hat{\sigma}^-(t)] + [\hat{\sigma}^+(t), \dot{\hat{\sigma}}^-(t)] \\ &= (i\omega_a - \frac{\gamma}{2}) [\hat{\sigma}^+(t), \hat{\sigma}^-(t)] + (-i\omega_a - \frac{\gamma}{2}) [\hat{\sigma}^+(t), \hat{\sigma}^-(t)] = -\gamma [\hat{\sigma}^+(t), \hat{\sigma}^-(t)], \end{aligned}$$

implying that this commutator decays exponentially in time, or equivalently, $\dot{\hat{\sigma}}_z(t) = -\gamma \hat{\sigma}_z(t)$ leading to the unphysical conclusion that the probability of finding the atom to be in one of its two states does not remain unity. A similar attempt in the case of a bosonic harmonic oscillator, with annihilation operator $\hat{a}(t)$, results likewise in a decaying same-time commutator $[\hat{a}, \hat{a}^\dagger] \neq 1$. These fiascos warrant a more careful derivation.

Such a treatment will reveal, as hinted at above, that the quantum formalistic requirement of the commutation relation lies behind the principle of dissipation and noise input being inseparable in the quantum realm. That is, if a

system has a decay channel to a reservoir, then inevitably the system will be subjected to fluctuations from the reservoir. This is true even for a reservoir at zero temperature, $T = 0$, because, independently of temperature, its quantum mechanical zero-point fluctuations are present, ensuring the preservation of the commutations relations as it turns out.

4.1.4 Derivation of the quantum Langevin equation

Finally, we will derive the quantum Langevin equation in the white noise limit, which is the quantum generalization of Eq. (4.1.1) subject to the assumption made in that section. The white noise limit is an idealization that captures the essence of high frequency/narrow bandwidth situations in the presence of weak coupling; it is therefore an adequate description of many quantum optical scenarios. Under these conditions we can make the Rotating Wave Approximation, neglecting terms of very rapidly varying phase; as mentioned in the introduction of section 4.1, this makes for a drastically simplified formalism free of diverging integrals in need of renormalization.

The quantum Langevin equation is a reformulation of the usual Heisenberg equation of motion in the presence of a reservoir. The Langevin derivation assumes a reservoir well-described by an ensemble of bosonic harmonic oscillators with a dense, quasi-continuous spectrum; in addition, we shall make the assumptions listed in section 4.1.1, which will be introduced as we go along.

We consider a Hamiltonian of the form

$$\hat{H} = \hat{H}_{\text{sys}} + \hat{H}_{\text{bath}} + \hat{H}_{\text{int}}, \quad (4.1.4)$$

that is subdivided into free evolution terms of the system and bath degrees of freedom, \hat{H}_{sys} and \hat{H}_{bath} respectively, as well as a term \hat{H}_{int} coupling the two subsets.

4.1.4.1 System-reservoir coupling

The coupling, \hat{H}_{int} , will be assumed to be linear in the reservoir operators as is standard for the Langevin derivation. This precludes direct application of the formalism to, for instance, scattering processes assisted by a phonon reservoir; in this case, the master equation formalism must be employed to account for the temperature dependence of such processes. However, linear coupling occurs naturally in the interaction between matter and electromagnetic fields and we let this case serve as inspiration in the derivation. Accordingly, to see how we might define \hat{H}_{int} in Eq. (4.1.4), we take a look at the Hamiltonian of this situation which may be written in terms of the set of bath oscillators $\{\hat{q}_n, \hat{p}_n\}$ in the form

$$\hat{H}' = \hat{H}_{\text{sys}} + \frac{1}{2} \sum_n [(\hat{p}_n - g_n \hat{S}_c)^2 + \omega_n^2 \hat{q}_n^2], \quad (4.1.5)$$

where \hat{S}_c is the Hermitian system operator entering the coupling and g_n is the coupling strength to the n 'th mode. The interaction is manifested through the modification of the canonical bath momenta $\hat{p}_n \rightarrow \hat{p}_n - g_n \hat{S}_c$ (so-called *minimal*

coupling), which is a different form compared to Eq. (4.1.4), but we see that we may take \hat{H}_{int} to be of the form

$$\hat{H}_{\text{int}} \sim - \sum_n g_n \hat{p}_n \hat{S}_c. \quad (4.1.6)$$

In the following, we will take the system coupling operator to have the form $\hat{S}_c \propto (\hat{c} + \hat{c}^\dagger)$; if \hat{c} is a harmonic oscillator annihilation operator this corresponds to “position” coupling, $\hat{S}_c \propto \hat{x}$. The bath will be described in terms of its normal mode operators $\{\hat{b}_n, \hat{b}_n^\dagger\}$. Based on Eq. (4.1.6) we write down the interaction Hamiltonian

$$\hat{H}_{\text{int}} = -i\hbar \sum_n k_n (\hat{b}_n - \hat{b}_n^\dagger) (\hat{c} + \hat{c}^\dagger), \quad (4.1.7)$$

using $\hat{p}_n \propto (\hat{b}_n - \hat{b}_n^\dagger)$ and where the coupling constants k_n have been assumed real without loss of generality.

4.1.4.2 Rotating Wave Approximation

We now go on to make the assumption that the interaction, \hat{H}_{int} , is weak compared to the free evolution terms, \hat{H}_{sys} and \hat{H}_{bath} ; this is very often a justified assumption in quantum optics which typically involves THz frequencies. Thus, the time evolution of any operator will be its free evolution subject to some slight perturbation. Based on this observation, we rewrite \hat{H}_{int} in terms of slowly varying operators defined by factoring out the free evolution, $\hat{B}_n \equiv e^{i\omega_n t} \hat{b}_n$, $\hat{C} \equiv e^{i\omega_c t} \hat{c}$ and their Hermitian conjugates:

$$\hat{H}_{\text{int}} = -i\hbar \sum_n k_n \left[\hat{B}_n \hat{C} e^{-i(\omega_n + \omega_c)t} - \hat{B}_n^\dagger \hat{C} e^{i(\omega_n - \omega_c)t} \right] + \text{H.c.}, \quad (4.1.8)$$

implicitly assuming \hat{c} to be an eigenoperator of \hat{H}_{sys} . The exponential factors have the arguments $\pm i(\omega_n \pm' \omega_c)$; given that the operators \hat{B}_n, \hat{C} vary slowly compared to the timescale of ω_c^{-1} , the terms containing $\exp[\pm i(\omega_n + \omega_c)t]$ will have effectively averaged to zero on the timescale of the evolution of the aforementioned operators. Meanwhile, the sum over terms containing $\exp[\pm i(\omega_n - \omega_c)t]$ includes a range of near-resonant terms, $\omega_n \approx \omega_c$. On this basis we make the Rotating Wave Approximation in dropping the rapidly rotating terms $\exp[\pm i(\omega_n + \omega_c)t]$ in Eq. (4.1.8) and revert to the original operators \hat{b}_n, \hat{c} :

$$\hat{H}_{\text{int}} = i\hbar \sum_n k_n (\hat{b}_n^\dagger \hat{c} - \hat{c}^\dagger \hat{b}_n). \quad (4.1.9)$$

4.1.4.3 Quasi-continuum transition

Neglecting the zero-point energy of the bath oscillators, their free evolution Hamiltonian is

$$\hat{H}_{\text{bath}} = \sum_n \hbar \omega_n \hat{b}_n^\dagger \hat{b}_n. \quad (4.1.10)$$

We now assume the spectrum of the bath oscillators to be so dense that it essentially forms a continuum and wish to transform eqs. (4.1.9) and (4.1.10) accordingly. The bath ladder operators obey the usual bosonic commutation

relations $[\hat{b}_l, \hat{b}_m^\dagger] = \delta_{l,m}$, $[\hat{b}_l, \hat{b}_m] = 0$, $[\hat{b}_l^\dagger, \hat{b}_m^\dagger] = 0$; in order for us to achieve the continuum limit commutation relation

$$[\hat{b}(\omega), \hat{b}^\dagger(\omega')] = \delta(\omega - \omega'), \quad (4.1.11)$$

we need to make the correspondance $\hat{b}_n \rightarrow (\frac{dn}{d\omega})^{-\frac{1}{2}} \hat{b}(\omega)$, where $\frac{dn}{d\omega}$ is the density of states. Making the transition $\sum_n \rightarrow \int d\omega (\frac{dn}{d\omega})$, eqs. (4.1.9) and (4.1.10) transform as

$$\begin{aligned} \hat{H}_{\text{int}} &= i\hbar \sum_n k_n (\hat{b}_n^\dagger \hat{c} - \hat{c}^\dagger \hat{b}_n) \rightarrow i\hbar \int_0^\infty d\omega \kappa(\omega) (\hat{b}^\dagger(\omega) \hat{c} - \hat{c}^\dagger \hat{b}(\omega)) \\ \hat{H}_{\text{bath}} &= \sum_n \hbar \omega_n \hat{b}_n^\dagger \hat{b}_n \rightarrow \int_0^\infty d\omega \hbar \omega \hat{b}^\dagger(\omega) \hat{b}(\omega), \end{aligned}$$

where the coupling function $\kappa(\omega)$ of dimension $\sqrt{\text{frequency}}$ arises as $k_n (\frac{dn}{d\omega})^{\frac{1}{2}} \rightarrow \kappa(\omega)$; note that $\hat{b}(\omega)$ has dimension $\sqrt{1/\text{frequency}}$ as can be seen from its commutation relation.

4.1.4.4 Formal integration and first Markov approximation

The Heisenberg equation of motion $\dot{\hat{a}}(t) = -(i/\hbar)[\hat{a}(t), \hat{H}]$ for any system operator \hat{a} is

$$\dot{\hat{a}}(t) = -\frac{i}{\hbar} [\hat{a}(t), \hat{H}_{\text{sys}}] + \int_0^\infty d\omega \kappa(\omega) \left[\hat{b}^\dagger(\omega, t) [\hat{a}(t), \hat{c}(t)] - [\hat{a}(t), \hat{c}^\dagger(t)] \hat{b}(\omega, t) \right], \quad (4.1.12)$$

since any system operator $\hat{a}(t)$ commutes with all bath operators evaluated at the same time t , $\{\hat{b}(\omega, t), \hat{b}^\dagger(\omega, t)\}$. Using this fact once again along with Eq. (4.1.11), we similarly obtain the equation of motion for $\hat{b}(\omega, t)$:

$$\dot{\hat{b}}(\omega, t) = -i\omega \hat{b}(\omega, t) + \kappa(\omega) \hat{c}(t). \quad (4.1.13)$$

Integrating this equation formally, we obtain

$$\hat{b}(\omega, t) = e^{-i\omega(t-t_0)} \hat{b}(\omega, t_0) + \int_{t_0}^t e^{-i\omega(t-t')} \kappa(\omega) \hat{c}(t') dt',$$

which we substitute into the equation of motion for \hat{a} , Eq. (4.1.12), resulting in

$$\begin{aligned} \dot{\hat{a}}(t) &= -\frac{i}{\hbar} [\hat{a}(t), \hat{H}_{\text{sys}}] \\ &+ \int_0^\infty d\omega \kappa(\omega) \left[e^{i\omega(t-t_0)} \hat{b}^\dagger(\omega, t_0) [\hat{a}(t), \hat{c}(t)] - [\hat{a}(t), \hat{c}^\dagger(t)] e^{-i\omega(t-t_0)} \hat{b}(\omega, t_0) \right] \\ &+ \int_{t_0}^t dt' \int_0^\infty d\omega \kappa^2(\omega) \left[e^{i\omega(t-t')} \hat{c}^\dagger(t') [\hat{a}(t), \hat{c}(t)] - [\hat{a}(t), \hat{c}^\dagger(t)] e^{-i\omega(t-t')} \hat{c}(t') \right]. \end{aligned} \quad (4.1.14)$$

We now make the *first Markov approximation* in assuming that the coupling function is a constant: $\kappa(\omega) = \sqrt{\frac{\gamma}{2\pi}}$. To proceed, we will need, out of mathematical convenience, to extend the lower limit of the frequency integrals in

Eq. (4.1.14) to $-\infty$. This amounts to adding negative energy bath modes to the Hamiltonian, which does not make physical sense. On the other hand, according to the discussion given in section 4.1.4.2, these added terms will be far off-resonant relative to \hat{c} and are thus heavily suppressed. The two assumptions just introduced allow us to exploit the relation $\int_{-\infty}^{\infty} d\omega e^{i\omega(t-t')} = 2\pi\delta(t-t')$, whereby Eq. (4.1.14) simplifies to

$$\begin{aligned} \dot{\hat{a}}(t) &= -\frac{i}{\hbar}[\hat{a}(t), \hat{H}_{\text{sys}}] \\ &+ \sqrt{\frac{\gamma}{2\pi}} \int_{-\infty}^{\infty} d\omega \left[e^{i\omega(t-t_0)} \hat{b}^\dagger(\omega, t_0) [\hat{a}(t), \hat{c}(t)] - [\hat{a}(t), \hat{c}^\dagger(t)] e^{-i\omega(t-t_0)} \hat{b}(\omega, t_0) \right] \\ &+ \gamma \int_{t_0}^t dt' [\delta(t-t') \hat{c}^\dagger(t') [\hat{a}(t), \hat{c}(t)] - [\hat{a}(t), \hat{c}^\dagger(t)] \delta(t-t') \hat{c}(t')] \\ &= -\frac{i}{\hbar} [\hat{a}, \hat{H}_{\text{sys}}] + [\hat{a}, \hat{c}] \left(\sqrt{\gamma} \hat{b}_{\text{in}}^\dagger + \frac{\gamma}{2} \hat{c}^\dagger \right) - [\hat{a}, \hat{c}^\dagger] \left(\sqrt{\gamma} \hat{b}_{\text{in}} + \frac{\gamma}{2} \hat{c} \right), \end{aligned} \quad (4.1.15)$$

suppressing the time dependence in the final line, where all operators are evaluated at time t . In the above equation, we have introduced the noise input operator

$$\hat{b}_{\text{in}}(t) \equiv \frac{1}{\sqrt{2\pi}} \int_{-\infty}^{\infty} d\omega e^{-i\omega(t-t_0)} \hat{b}(\omega, t_0). \quad (4.1.16)$$

Eq. (4.1.15) is the quantum Langevin equation; because of the Rotating Wave Approximation, it is valid in a narrow bandwidth around the free evolution frequency of the system according to section 4.1.4.2. Remarkably, Eq. (4.1.15) is a first order differential equation, meaning that, in principle, the time evolution of any system operator can be determined when initial conditions have been specified. Since it only depends on the instantaneous state of \hat{a} , there is no “memory” of previous system states influencing the evolution. However, to finish the derivation, we need to concern ourselves with the properties of the noise input operator, $\hat{b}_{\text{in}}(t)$.

4.1.4.5 White noise limit

The equation (4.1.15) is only really stochastic to the extent that we specify an incoherent input, $\hat{b}_{\text{in}}(t)$, which depends only on the bath state at time t_0 : $\hat{b}(\omega, t_0)$; we will, furthermore, take the combined state of system and reservoir to factorize at time t_0 . Quantum white noise, in analogy to Eq. (4.1.2), corresponds to

$$\langle \hat{b}_{\text{in}}^\dagger(t) \hat{b}_{\text{in}}(t') \rangle = \bar{n}_{\text{bath}}(\omega_{\text{sys}}) \delta(t-t'), \quad \langle \hat{b}_{\text{in}}(t) \hat{b}_{\text{in}}^\dagger(t') \rangle = [\bar{n}_{\text{bath}}(\omega_{\text{sys}}) + 1] \delta(t-t'), \quad (4.1.17)$$

where $\bar{n}_{\text{bath}}(\omega_{\text{sys}}) = [\exp(\hbar\omega_{\text{sys}}/k_{\text{B}}T) - 1]^{-1}$ is the mean bath occupancy evaluated at the free evolution frequency of \hat{a} . Generally for a thermal bath state (at time t_0), we would have

$$\langle \hat{b}^\dagger(\omega, t_0) \hat{b}(\omega', t_0) \rangle = \bar{n}_{\text{bath}}(\omega) \delta(\omega - \omega'), \quad \langle \hat{b}(\omega, t_0) \hat{b}^\dagger(\omega', t_0) \rangle = [\bar{n}_{\text{bath}}(\omega) + 1] \delta(\omega - \omega'). \quad (4.1.18)$$

Evaluating $\langle \hat{b}_{\text{in}}^\dagger(t) \hat{b}_{\text{in}}(t') \rangle$ and $\langle \hat{b}_{\text{in}}(t) \hat{b}_{\text{in}}^\dagger(t') \rangle$ based on eqs. (4.1.18) and the definition Eq. (4.1.16) we would find the inverse Fourier transforms of $\bar{n}_{\text{bath}}(\omega)$ and

$[\bar{n}_{\text{bath}}(\omega) + 1]$, respectively. However, if we argue that we are only interested in the evolution of \hat{a} in a narrow bandwidth around ω_{sys} (outside which our derivation in fact fails to be valid), then our system only sees a small part of $\bar{n}_{\text{bath}}(\omega)$, $\omega \approx \omega_{\text{sys}}$, which we take to be essentially flat, $\bar{n}_{\text{bath}}(\omega) \approx \bar{n}_{\text{bath}}(\omega_{\text{sys}})$. In this *quantum white noise* approximation we arrive at eqs. (4.1.17).

4.1.4.6 Harmonic oscillator

An application of the quantum Langevin equation that will be important to us is the case where the system is a bosonic harmonic oscillator degree of freedom. In this case $\hat{a} = \hat{c}$ and $\hat{H}_{\text{sys}} = \hbar\omega_{\text{sys}}\hat{a}^\dagger\hat{a}$; Eq. (4.1.15) yields

$$\dot{\hat{a}} = \left[-i\omega_{\text{sys}} - \frac{\gamma}{2} \right] \hat{a} - \sqrt{\gamma}\hat{b}_{\text{in}}. \quad (4.1.19)$$

The analogy to the classical Langevin equation, Eq. (4.1.1), is obvious and the intuitive interpretation of the effective environment description, discussed in section 4.1.2, carries over to the quantum case. Additionally, as also discussed above, we have seen how the noise term is integral to formulating a consistent quantum theory of noise, attesting to the fact that dissipation and fluctuations are closely connected phenomena. By integrating Eq. (4.1.19) formally and evaluating $[\hat{a}(t), \hat{a}^\dagger(t)]$, this commutator is indeed seen to maintain the canonical relation as required [3].

4.2 Steady state occupancies of coupled harmonic oscillators subjected to white noise

The steady state occupancy can be thought of as the effective temperature of a single mode. Therefore, calculating this quantity will be central to the cooling analysis given in Chapter 5, where we will consider various situations. As a mathematical preliminary, we will in this section determine the steady state occupancy of coupled harmonic oscillators subjected to white noise. Such a set of oscillators is governed by Langevin equations of the form (4.1.19) coupled to one another. Harmonic oscillators are unique for the fact that this problem is exactly solvable.

We will give two different mathematical procedures for obtaining this solution: The first one is derived in the time-domain by solving a Lyapunov equation, while the second one goes via Fourier space to solve the equations of motion. Each procedure has its advantages and disadvantages: For the one carried out in the time-domain, it is straightforward (but perhaps tedious) to evaluate the result; however, the calculation itself offers little physical insight (although the result hopefully does). On the contrary, the calculation that works in frequency space reveals significantly more of the physics as it can be phrased in terms of auto-correlation functions and susceptibilities. The latter method is the most common in the context of cavity mechanics, employed in e.g. Refs. [18, 7]. Furthermore, it is closely related to the effective formalism for weakly coupled subsystems presented in Section 4.3.

4.2.1 Time-domain solution via the Lyapunov equation

We consider the case where the equations of motion for the set of $2N$ operators $\{\hat{a}_i, \hat{a}_i^\dagger\}_{i \in \{1, \dots, N\}}$. By defining vectors with operator entries these can be stated as

$$\dot{\mathbf{v}}(t) = -M\mathbf{v}(t) - \mathbf{N}(t), \quad (4.2.1)$$

where $\mathbf{v} \equiv (\hat{a}_1, \dots, \hat{a}_N; \hat{a}_1^\dagger, \dots, \hat{a}_N^\dagger)^T$ (suppressing the time-dependence, t) the mutual interaction of which are accounted for by the time-independent matrix $M \in \mathbb{C}^{2N \times 2N}$ and the vector $\mathbf{N}(t)$ contains mutually uncorrelated white noise Langevin operators. Each oscillator may be directly coupled to several independent reservoirs; we therefore define the i 'th of the first N components of the noise vector as $[\mathbf{N}(t)]_i \equiv \sum_j \sqrt{\gamma_{i,j}} \hat{f}_{i,j}(t)$, $i \in \{1, \dots, N\}$, for which

$$\langle \hat{f}_{i,j}^\dagger(t) \hat{f}_{i',j'}(t') \rangle = \delta_{i,i'} \delta_{j,j'} \delta(t-t') n_{i,j} \quad \text{and} \quad (4.2.2)$$

$$\langle \hat{f}_{i,j}(t) \hat{f}_{i',j'}^\dagger(t') \rangle = \delta_{i,i'} \delta_{j,j'} \delta(t-t') [n_{i,j} + 1], \quad (4.2.3)$$

while any correlators of the forms $\langle f f' \rangle, \langle f^\dagger f'^\dagger \rangle$ are assumed to vanish as will be the case for thermal reservoirs (but not for squeezed sources, see Ref. [3]). The duality $\hat{a}_i \leftrightarrow \hat{a}_i^\dagger$ requires the last N components of the noise vector to be the Hermitian conjugate of first N components, $[\mathbf{N}(t)]_{i+N} = [\mathbf{N}(t)]_i^\dagger = \sum_j \sqrt{\gamma_{i,j}} \hat{f}_{i,j}^\dagger(t)$, $i \in \{1, \dots, N\}$ (this duality, of course, puts similar requirements on the matrix M). For each Langevin operator appearing in the i 'th component of the noise vector, there will be a corresponding decay term in $(M)_{i,i} \sim \sum_j \frac{\gamma_{i,j}}{2}$ as required in order to have a consistent quantum white noise theory (see Eq. (4.1.19) and the discussion given in section 4.1).

Integrating Eq. (4.2.1) formally, we obtain

$$\mathbf{v}(t) = - \int_{-\infty}^t dt' e^{-(t-t')M} \mathbf{N}(t'), \quad (4.2.4)$$

where we have taken the lower limit t_0 to $-\infty$ because we are not interested in transient phenomena; for any finite $t_0 \leq t$, Eq. (4.2.4) would include the decaying term $e^{-(t-t_0)M} \mathbf{v}(t_0)$ depending on the initial state of \mathbf{v} . In order to be able to project out single components of \mathbf{v} , we now specify explicitly its basis vectors, $\{\mathbf{e}_i\}_{i \in \{1, \dots, 2N\}}$: In terms of these, the definition of \mathbf{v} can be restated as $\mathbf{v} \equiv \sum_{i=1}^N [\hat{a}_i \mathbf{e}_i + \hat{a}_i^\dagger \mathbf{e}_{N+i}]$. Forming outer products of the basis vectors, we introduce the projectors $P_i \equiv \mathbf{e}_i \mathbf{e}_i^\dagger \in \mathbb{C}^{2N \times 2N}$, $i \in \{1, \dots, 2N\}$ obeying $\sum_{i=1}^{2N} P_i = \mathbf{1} \in \mathbb{C}^{2N \times 2N}$, the identity matrix.

From Eq. (4.2.4) we can now easily write down the steady state occupancies of any of the oscillators $i \in \{1, \dots, N\}$ as

$$\begin{aligned} n_i^{(\text{ss})} &= \langle \hat{a}_i^\dagger(t) \hat{a}_i(t) \rangle = \langle \mathbf{v}^\dagger(t) P_i \mathbf{v}(t) \rangle \\ &= \int_{-\infty}^t dt' \int_{-\infty}^t dt'' \langle \mathbf{N}^\dagger(t') e^{-(t-t')M^\dagger} P_i e^{-(t-t'')M} \mathbf{N}(t'') \rangle. \end{aligned} \quad (4.2.5)$$

Inserting resolutions of the identity $\mathbf{1} = \sum_{i=1}^{2N} P_i = \sum_{i=1}^{2N} \mathbf{e}_i \mathbf{e}_i^\dagger$ we effectively revert to an explicit component expression for the vectors and matrices.

$$\begin{aligned} & \langle \mathbf{N}^\dagger(t') e^{-(t-t')M^\dagger} P_i e^{-(t-t'')M} \mathbf{N}(t'') \rangle \\ &= \sum_{k,k'=1}^{2N} \langle \mathbf{N}^\dagger(t') \mathbf{e}_k \mathbf{e}_k^\dagger e^{-(t-t')M^\dagger} P_i e^{-(t-t'')M} \mathbf{e}_{k'} \mathbf{e}_{k'}^\dagger \mathbf{N}(t'') \rangle. \end{aligned}$$

This allows us to move around terms as long as we observe the commutation relations of quantum operators. In this way the above expression can be written:

$$\sum_{k,k'=1}^{2N} \mathbf{e}_k^\dagger e^{-(t-t')M^\dagger} P_i e^{-(t-t'')M} \mathbf{e}_{k'} \langle \mathbf{N}^\dagger(t') \mathbf{e}_k \mathbf{e}_{k'}^\dagger \mathbf{N}(t'') \rangle. \quad (4.2.6)$$

Evaluating the noise correlator in Eq. (4.2.6) using Eqs. (4.2.2) we find for $1 \leq k, k' \leq N$

$$\begin{aligned} \langle \mathbf{N}^\dagger(t') \mathbf{e}_k \mathbf{e}_{k'}^\dagger \mathbf{N}(t'') \rangle &= \sum_{j,j'} \sqrt{\gamma_{k,j} \gamma_{k',j'}} \langle \hat{f}_{k,j}^\dagger(t') \hat{f}_{k',j}(t'') \rangle \\ &= \sum_{j,j'} \sqrt{\gamma_{i,j} \gamma_{i',j'}} \delta_{k,k'} \delta_{j,j'} \delta(t' - t'') n_{k,j} = \sum_j \gamma_{k,j} n_{k,j} \delta_{k,k'} \delta(t' - t''), \end{aligned} \quad (4.2.7)$$

while for $N+1 \leq k, k' \leq 2N$

$$\begin{aligned} \langle \mathbf{N}^\dagger(t') \mathbf{e}_k \mathbf{e}_{k'}^\dagger \mathbf{N}(t'') \rangle &= \sum_{j,j'} \sqrt{\gamma_{(k-N),j} \gamma_{(k'-N),j'}} \langle \hat{f}_{(k-N),j}^\dagger(t') \hat{f}_{(k'-N),j}(t'') \rangle \\ &= \sum_j \gamma_{(k-N),j} [n_{(k-N),j} + 1] \delta_{k,k'} \delta(t' - t''); \end{aligned} \quad (4.2.8)$$

if k and k' are not in the same range, $\{1, \dots, N\}$ or $\{N+1, \dots, 2N\}$, the statement after Eqs. (4.2.2) implies the noise correlator in the last expression of Eq. (4.2.6) to be zero. Plugging these results into Eq. (4.2.6) we get

$$\begin{aligned} & \langle \mathbf{N}^\dagger(t') e^{-(t-t')M^\dagger} P_i e^{-(t-t'')M} \mathbf{N}(t'') \rangle \\ &= \delta(t' - t'') \sum_{k=1}^N \left[\mathbf{e}_k^\dagger e^{-(t-t')M^\dagger} P_i e^{-(t-t'')M} \mathbf{e}_k \left(\sum_j \gamma_{k,j} n_{k,j} \right) \right. \\ & \quad \left. + \mathbf{e}_{k+N}^\dagger e^{-(t-t')M^\dagger} P_i e^{-(t-t'')M} \mathbf{e}_{k+N} \left(\sum_j \gamma_{k,j} [n_{k,j} + 1] \right) \right]. \end{aligned}$$

Finally, we plug this expression into Eq. (4.2.5) which allows us to carry out one of the time integrals yielding

$$\begin{aligned} n_i^{(\text{ss})} &= \int_{-\infty}^0 d\tau \sum_{k=1}^N \left[\mathbf{e}_k^\dagger e^{\tau M^\dagger} P_i e^{\tau M} \mathbf{e}_k \left(\sum_j \gamma_{k,j} n_{k,j} \right) \right. \\ & \quad \left. + \mathbf{e}_{k+N}^\dagger e^{\tau M^\dagger} P_i e^{\tau M} \mathbf{e}_{k+N} \left(\sum_j \gamma_{k,j} [n_{k,j} + 1] \right) \right], \end{aligned} \quad (4.2.9)$$

having switched the integration variable of the remaining time integral $t' \rightarrow \tau = -(t - t')$.

The integral in Eq. (4.2.9) is now solved by finding the antiderivative $G(\tau)$ of the matrix valued function $g(\tau) = e^{\tau M^\dagger} P_i e^{\tau M}$. Using the ansatz $G(\tau) = e^{\tau M^\dagger} \Gamma e^{\tau M}$ we obtain by differentiation $G'(\tau) = e^{\tau M^\dagger} [M^\dagger \Gamma + \Gamma M] e^{\tau M}$; thus, demanding $G'(\tau) = g(\tau)$ we arrive at the *Lyapunov equation* for the unknown matrix Γ

$$M^\dagger \Gamma + \Gamma M = P_i. \quad (4.2.10)$$

This equation has a unique solution if and only if the matrices M and $-M^\dagger$ have no eigenvalues in common [4]. The fact that $|\det(M - \mathbb{1}\lambda)| = |\det(-M^\dagger + \mathbb{1}\lambda^*)|$ leads to the following relation between respective characteristic polynomials of M and $-M^\dagger$

$$\det[M - \mathbb{1}\lambda] = 0 \Leftrightarrow \det[-M^\dagger - (-\mathbb{1}\lambda^*)] = 0,$$

which is to say that if λ is an eigenvalue of M then $-\lambda^*$ is an eigenvalue of $-M^\dagger$. The above criterion then translates into the statement that M must not have two eigenvalues such that $\lambda_i = -\lambda_j^*$, i.e., with equal imaginary parts and opposite real parts. Specifically, this will be true if all eigenvalues have positive real parts as will be true if the couplings are not too large. For our purposes in the following chapter, where we assume to be in a regime where the Rotating Wave Approximation is valid for the oscillator couplings, $g \ll \omega$, a solution does exist. Existence conditions for more general calculations can be established using the Routh-Hurwitz criterion [5].

Assuming that the equation has a unique solution we note from its Hermitian conjugate, $M^\dagger \Gamma^\dagger + \Gamma^\dagger M = P_i$ (note that $P_i = P_i^\dagger$), that we must have $\Gamma = \Gamma^\dagger$, that is, Γ is Hermitian. From this it follows that Eq. (4.2.10) may be restated as $\Gamma M + (\Gamma M)^\dagger = P_i$. From the latter form we see that the Lyapunov matrix equation in general constitutes the following number of independent linear equations in the entries of Γ : $2N$ real equations from the diagonal terms and $[(2N)^2 - 2N]/2$ complex equations from the off-diagonal (upper or lower) triangular terms; in total, this amounts to $(2N)^2$ real, linear equations.

Given that we have solved the Lyapunov equation for Γ we know the antiderivative of the integral in Eq. (4.2.9) and can hence evaluate $\int_{-\infty}^0 d\tau e^{\tau M^\dagger} P_i e^{\tau M} = \left[e^{\tau M^\dagger} \Gamma e^{\tau M} \right]_{-\infty}^0 = \Gamma$ as the decay terms of M will make the lower limit contribution vanish. Eq. (4.2.9) now reads

$$n_i^{(\text{ss})} = \sum_{k=1}^N \left[(\Gamma)_{k,k} \left(\sum_j \gamma_{k,j} n_{k,j} \right) + (\Gamma)_{k+N,k+N} \left(\sum_j \gamma_{k,j} [n_{k,j} + 1] \right) \right], \quad (4.2.11)$$

which is our final result for the steady state occupancies. Note that only the (real) diagonal elements of Γ enter, rendering the right-hand side of Eq. (4.2.11) manifestly real as required.

4.2.2 Frequency-domain solution

We now present an alternative method of solution that makes use of the Fourier representation of the problem. Given that the matrix M in Eq. (4.2.1) is time-

independent, it is straightforward to obtain the Fourier transformed version of that equation using $\mathcal{F}_{t \rightarrow \omega}[\dot{\mathbf{v}}(t)] = i\omega \mathcal{F}_{t \rightarrow \omega}[\mathbf{v}(t)]$:

$$i\omega \tilde{\mathbf{v}}(\omega) = -M \tilde{\mathbf{v}}(\omega) - \tilde{\mathbf{N}}(\omega), \quad (4.2.12)$$

where, using the vector notation introduced in the previous section, we must define

$$\tilde{\mathbf{v}}(\omega) \equiv \sum_{i=1}^N \left[\tilde{a}_i(\omega) \mathbf{e}_i + \tilde{b}_i^\dagger(\omega) \mathbf{e}_{N+i} \right] \equiv \mathcal{F}[\mathbf{v}(t)] \equiv \frac{1}{\sqrt{2\pi}} \int_{-\infty}^{\infty} e^{-i\omega t} \sum_{i=1}^N \left[\hat{a}_i(t) \mathbf{e}_i + \hat{a}_i^\dagger(t) \mathbf{e}_{N+i} \right],$$

where $\tilde{b}_i^\dagger(\omega) \equiv \tilde{a}_i^\dagger(-\omega)$. Assuming the matrix $M + i\omega \mathbb{I}$ to be invertible, we solve Eq. (4.2.12)

$$\tilde{\mathbf{v}}(\omega) = -(M + i\omega \mathbb{I})^{-1} \tilde{\mathbf{N}}(\omega). \quad (4.2.13)$$

To be able to demonstrate more clearly how the method of this section relates to the structured reservoir formalism in the following section, we proceed by determining an expression for the Fourier transform of correlation functions of the type $\langle \hat{a}_i^\dagger(\tau) \hat{a}_i(\tau') \rangle$ (where $i \in \{1, \dots, N\}$):²

$$\begin{aligned} & \int_{-\infty}^{\infty} d\tau \langle \hat{a}_i^\dagger(\tau) \hat{a}_i(\tau') \rangle e^{-i\omega \tau} = - \int_{-\infty}^{\infty} d\omega' \langle \tilde{b}_i^\dagger(\omega) \mathbf{e}_i^\dagger (M + i\omega' \mathbb{I})^{-1} \tilde{\mathbf{N}}(\omega') \rangle \\ & = \sum_{k, k'=1}^{2N} \int_{-\infty}^{\infty} d\omega' \langle \tilde{\mathbf{N}}^\dagger(-\omega) \mathbf{e}_k \mathbf{e}_k^\dagger [(M - i\omega \mathbb{I})^{-1}]^\dagger \mathbf{e}_i \mathbf{e}_i^\dagger (M + i\omega' \mathbb{I})^{-1} \mathbf{e}_{k'} \mathbf{e}_{k'}^\dagger \tilde{\mathbf{N}}(\omega') \rangle, \end{aligned} \quad (4.2.14)$$

where we have used the definition of the Fourier transform, the solution Eq. (4.2.13) as well as its inverse Fourier transform evaluated at $\tau' = 0$; furthermore we have inserted resolutions of the identity $\mathbb{1} = \sum_{k=1}^{2N} \mathbf{e}_k \mathbf{e}_k^\dagger$. As exploited previously in Eq. (4.2.6), the component form of Eq. (4.2.14) allows us to consider individually the terms $\langle \tilde{\mathbf{N}}^\dagger(-\omega) \mathbf{e}_k \mathbf{e}_k^\dagger \tilde{\mathbf{N}}(\omega') \rangle$ for $k, k' \in \{1, \dots, 2N\}$; in the quantum white noise limit we find (in parallel to Eqs. (4.2.7) and (4.2.8) in the previous section),

$$\langle \tilde{\mathbf{N}}^\dagger(-\omega) \mathbf{e}_k \mathbf{e}_k^\dagger \tilde{\mathbf{N}}(\omega') \rangle = \begin{cases} \sum_j \gamma_{k,j} n_{k,j} \delta_{k,k'} \delta(\omega + \omega') & \text{for } 1 \leq k, k' \leq N \\ \sum_j \gamma_{(k-N),j} [n_{(k-N),j} + 1] \delta_{k,k'} \delta(\omega + \omega') & \text{for } N+1 \leq k, k' \leq 2N \\ 0 & \text{otherwise.} \end{cases}$$

Inserting this into Eq. (4.2.14) and taking advantage of the delta functions, we find

$$\begin{aligned} & \sum_{k=1}^N \left[\left(\sum_j \gamma_{k,j} n_{k,j} \right) [(M - i\omega \mathbb{I})^{-1}]_{k,i}^\dagger [(M - i\omega \mathbb{I})^{-1}]_{i,k} \right. \\ & \quad \left. + \left(\sum_j \gamma_{k,j} [n_{k,j} + 1] \right) [(M - i\omega \mathbb{I})^{-1}]_{k+N,i}^\dagger [(M - i\omega \mathbb{I})^{-1}]_{i,k+N} \right], \end{aligned}$$

²Using the symmetric definition of the Fourier transform with a factor of $1/\sqrt{2\pi}$ in each direction for annihilation and creation operators.

using the component notation $A_{i,j} \equiv \mathbf{e}_i^\dagger A \mathbf{e}_j$ for the matrices. But since $[A^\dagger]_{i,j} = A_{j,i}^*$, we arrive at the following manifestly real expression for the Fourier transformed correlation function

$$\begin{aligned} & \int_{-\infty}^{\infty} d\tau \langle \hat{a}_i^\dagger(\tau) \hat{a}_i(\tau' = 0) \rangle e^{-i\omega\tau} \\ &= \sum_{k=1}^N \left[\left(\sum_j \gamma_{k,j} n_{k,j} \right) \left| [(M - i\omega\mathbb{I})^{-1}]_{i,k} \right|^2 + \left(\sum_j \gamma_{k,j} [n_{k,j} + 1] \right) \left| [(M - i\omega\mathbb{I})^{-1}]_{i,k+N} \right|^2 \right], \end{aligned} \quad (4.2.15)$$

Performing the inverse Fourier transform of this expression,³ we may determine the steady state occupancy of mode i as $n_i^{(\text{ss})} = \langle \hat{a}_i^\dagger(\tau = 0) \hat{a}_i(\tau' = 0) \rangle_{\text{ss}}$, where the 'ss' subscript indicates that we neglect transients. Note that the location of the poles are given by the characteristic polynomial of M .

It is interesting to compare this result to the time-domain solution, Eq. (4.2.11). The connection that appears between the solution to the Lyapunov equation and the inverse Fourier transform is non-trivial. We remark that, except for the final inverse Fourier transform, this procedure is identical to that of determining effective reservoir occupancies presented below in section 4.3.

4.3 Effective description of weakly coupled subsystems

In Section 4.1 an effective description of Markovian reservoirs was developed. With this formalism as our basis, we will now consider somewhat more complex scenarios. Specifically, we shall consider a subsystem coupled *indirectly* to Markovian reservoirs via a number of discrete system modes. We will aim, under suitable conditions, to eliminate the explicit dynamics of these intermediate modes from our equations. Thus, as we will see, our subsystem of interest will then effectively be coupled to a *structured reservoir*.

The motivation for this derivation is easily explained in light of the previous section, where we considered coupled systems only involving harmonic oscillators (and their reservoirs). As soon as we add degrees of freedom to the system that do not have a bosonic harmonic oscillator description, the exact derivations above will fail. Hence, in this case we need to look for an alternative, approximative approach. But even if we do consider a system comprised only of harmonic oscillators, as in the previous section, the exact solution may be hard to gain physical insight from. Thus, also for this reason, rather than out of sheer mathematical necessity, can it be appropriate to turn to the structured reservoir approach.

³In principle, one can proceed by using Cauchy's theorem. This requires a suitable analytical continuation of Eq. (4.2.15), the residues of which must be evaluated at the poles situated in one of the complex half-planes. However, this requires determining the poles as the roots of the complex polynomial $\det(M - i\omega\mathbb{I}) = 0$, for which there is no closed-form expression for general N . Except for the simple case of two oscillators, the only manageable approach to inverting Eq. (4.2.15) is by the procedure summarized in Appendix A.6 of Ref. [11].

We will now give a more thorough description of the scenario from which we will extract a structured reservoir formalism. Similar to the situation considered in the previous section, our system includes n harmonic oscillators arbitrarily coupled to one another,⁴ $\{\hat{R}_i, \hat{R}_i^\dagger\}_{i \in \{1 \dots n\}}$. As was the case previously, the oscillators are each coupled to one or more Markovian reservoirs. Additionally, the system includes a degree of freedom of primary interest. It is assumed weakly coupled to a single one of the oscillators, say, that represented by \hat{R}_1 . More precisely, the coupling is weak compared to the timescale on which the oscillators decay. Furthermore, also the decay rate of the subsystem of interest is assumed small in comparison to those governing the oscillators. It is this timescale separation that allows for a sensible description of the oscillators and their reservoirs as one combined structured reservoir from the point of view of the subsystem of interest. As such, the approach can be thought of as simultaneous adiabatic elimination of the rapidly decaying degrees of freedom. For an illustration of the structured reservoir perspective, see Fig. 5.2.1 on page 82 (in which the 'target' subsystem is the one of interest).

The approach we will follow is that employed by Stannigel et al. [25] to eliminate the degrees of freedom of optomechanical transducers (connecting stationary and photonic qubits). This is very similar to the subsystem we will seek to eliminate in Chapter 5.

4.3.1 Structured reservoirs of bosonic harmonic oscillator degrees of freedom

The elimination procedure used in Ref. [25] is stated therein to various degrees of generality.⁵ We will closely follow the example of a specific elimination carried out in paper, where the system of interest (not to be eliminated) is a 2-level system; we will, however, generalize the calculation slightly to accommodate for the cases of having as our system of interest either a harmonic oscillator degree of freedom or any system diagonalized by an angular momentum basis within some j -subspace. That is to say, we will consider target systems whose free evolution is given by a Hamiltonian of either of the following two forms:

$$\hat{H}_{t,\text{free}} = \hbar\omega_t \hat{a}_t^\dagger \hat{a}_t; \quad \hat{H}_{t,\text{free}} = \omega_t \hat{J}_z^{(j)},$$

where $\hat{J}_z^{(j)}$ is the z component of the angular momentum operator in the j subspace. The objective is to achieve effective equations of motion for the annihilation and creation operators $\hat{a}_t, \hat{a}_t^\dagger$ in the harmonic oscillator case, and for $\hat{J}_z^{(j)}$ and the ladder operators $\hat{J}_\pm^{(j)}$ in the angular momentum case. The free evolution of the annihilation and lowering operators, respectively, are given by

$$\dot{\hat{a}}_t(t) = \frac{i}{\hbar} [\hat{H}_{t,\text{free}}, \hat{a}_t] = -i\omega_t \hat{a}_t(t); \quad \dot{\hat{J}}_-^{(j)}(t) = \frac{i}{\hbar} [\hat{H}_{t,\text{free}}, \hat{J}_-^{(j)}] = -i\omega_t \hat{J}_-^{(j)}(t), \quad (4.3.1)$$

which follow from the commutation relations $[\hat{a}_t, \hat{a}_t^\dagger] = 1$ and $[\hat{J}_z^{(j)}, \hat{J}_\pm^{(j)}] = \pm \hbar \hat{J}_\pm^{(j)}$. The similarity of Eqs. (4.3.1) makes it possible to state them as a

⁴Although the stability considerations mentioned in Section 4.2.1 apply.

⁵The most general statement of the elimination procedure is given in Appendix A of the paper, while a specific elimination is carried out in a step-by-step manner in Section II, D.

single equation,

$$\dot{\hat{S}}(t) = -i\omega_t \hat{S}(t), \quad (4.3.2)$$

where \hat{S} is the relevant target system operator, \hat{a}_t or $\hat{J}_-^{(j)}$; henceforth, we will use this unified notation. The coupling to the subsystem which we wish to treat as a structured reservoir is assumed to be of the beam splitter type⁶

$$\hat{H}_{\text{coupl}} = \frac{\hbar g_{\text{res}}}{2} (\hat{S}^\dagger \hat{R}_1 + \hat{R}_1^\dagger \hat{S}), \quad (4.3.3)$$

where \hat{R}_1 is an annihilation operator of the structured reservoir subsystem (labelled by '1' for later convenience) and the coupling constant g_{res} has been taken real without any loss of generality.

The equations of motion for the n discrete harmonic oscillator modes of the structured reservoir subsystem can be stated in a vectorial form separating 1) coupling among these n oscillators, 2) coupling to the target system, and 3) Langevin noise terms accounting for heating of the oscillators from their Markovian reservoirs. To arrive at this form, we introduce, in parallel with [25], the vectors of operators

$$\begin{aligned} \mathbf{v} &= (\hat{R}_1, \hat{R}_2, \dots, \hat{R}_n, \hat{R}_1^\dagger, \hat{R}_2^\dagger, \dots, \hat{R}_n^\dagger)^T, \quad \mathbf{S} = (\hat{S}, 0, \dots, 0, -\hat{S}^\dagger, 0, \dots, 0)^T, \\ \mathbf{N} &= (\sqrt{\gamma_1} \hat{f}_1, \sqrt{\gamma_2} \hat{f}_2, \dots, \sqrt{\gamma_n} \hat{f}_n, \sqrt{\gamma_1} \hat{f}_1^\dagger, \sqrt{\gamma_2} \hat{f}_2^\dagger, \dots, \sqrt{\gamma_n} \hat{f}_n^\dagger)^T, \end{aligned} \quad (4.3.4)$$

where only the 1st and $(n+1)$ 'th components of \mathbf{S} are non-zero, reflecting the structure of Eq. (4.3.3). The desired equations of motion for structured reservoir is then

$$\dot{\mathbf{v}}(t) = -M\mathbf{v}(t) - i\frac{g_{\text{res}}}{2}\mathbf{S}(t) - \mathbf{N}(t), \quad (4.3.5)$$

where the matrix $M \in \mathbb{C}^{2n \times 2n}$ contains the internal couplings and complex energies of the n structured reservoir oscillators.

Taking the same approach as usual when deriving Heisenberg-Langevin equations, we formally integrate the equations of motion for the reservoir degrees of freedom; as we are not interested in the transients from any initial state of the structured reservoir, we let the lower bound of the time integral tend to $-\infty$:

$$\mathbf{v}(t) = \int_{-\infty}^t dt' e^{-(t-t')M} \left[-i\frac{g_{\text{res}}}{2}\mathbf{S}(t') - \mathbf{N}(t') \right]. \quad (4.3.6)$$

The first term of the integrand accounts for the influence of the target system on the structured reservoir, while the second accounts for the stochastic heating from the white-noise reservoirs. Had there been no coupling to the target system, $g_{\text{res}} = 0$, only the latter term would remain, which leads us to introduce $\mathbf{v}_{\text{free}}(t) = -\int_{-\infty}^t dt' e^{-(t-t')M} \mathbf{N}(t')$, the free steady state solution for the structured reservoir (after all transients have died out).

So far we have assumed nothing about the relationship between the respective timescales of the target system and the structured reservoir nor the strength of their mutual coupling constant g_{res} , but this is exactly what we will need to do in order proceed towards an effective, structured reservoir description.

⁶In neglecting counter-rotating terms we have made the Rotating Wave Approximation, which is reasonable for this weak coupling derivation.

We will assume g_{res} to be either much smaller than the decay rate of any normal mode of the n oscillators or much smaller than the detuning between the target system and the nearest normal mode. Under this condition, the n oscillators will adiabatically follow the target system due to their much faster timescale. Put differently, to lowest order in g_{res} , the n oscillators will have no memory of the history of the target system's state: $\mathbf{v}(t)$ will only depend on the instantaneous state $\mathbf{S}(t)$ of the target system. To see this, consider Eq. (4.3.6): Any deviation of $\mathbf{S}(t')$ from free evolution will be due to its coupling to the n oscillators, therefore any aggregate process that feeds the influence of \mathbf{v} on \mathbf{S} back into \mathbf{v} at a later time will be of at least second order in the small parameter g_{res} and hence negligible.⁷ Thus, to lowest order in the reservoir couplings of the target system, it is permissible to let $\mathbf{S}(t')$ in Eq. (4.3.6) be equal to its free evolution as given by the solution to Eq. (4.3.2): $\hat{S}(t') = e^{-i\omega_{\text{t}}(t'-t)}\hat{S}(t)$ (the Hermitian conjugate of which gives the free evolution for \hat{S}^\dagger).

Furthermore, to have our effective, structured reservoir description fit within the Markovian framework, we will need to assume that the total effective decay rate of the target system, $\sum_i \gamma_{\text{t},i}$, is much less than the decay rate of (or detuning w.r.t.) any normal mode of the n oscillators; this in order for our structured reservoir to, essentially, appear as white noise to the target system, i.e. with an essentially flat occupancy function, $n_{\text{res}}(\omega)$, over the bandwidth of the target system around $\omega = \omega_{\text{t}}$.

With these assumptions in place, we can perform the integration of the $\int_{-\infty}^t dt' e^{-(t-t')M} \mathbf{S}(t')$ term in equation (4.3.6); separating out the matrix product between the exponentiated matrix and the vector \mathbf{S} and focusing on the \hat{R}_1 component, motivated by the assumed form of the coupling, Eq. (4.3.3), we get

$$\begin{aligned} & \int_{-\infty}^t dt' \left([e^{(t'-t)[M-i\omega_{\text{t}}\mathbb{I}}]_{1,1} \hat{S}(t) - [e^{(t'-t)[M+i\omega_{\text{t}}\mathbb{I}}]_{1,n+1} \hat{S}^\dagger(t) \right) \\ &= \left(\left[\frac{e^{(t'-t)[M-i\omega_{\text{t}}\mathbb{I}}]}{M-i\omega_{\text{t}}\mathbb{I}} \right]_{1,1} \right)_{t'=-\infty}^{t'=t} \hat{S}(t) - \left(\left[\frac{e^{(t'-t)[M+i\omega_{\text{t}}\mathbb{I}}]}{M+i\omega_{\text{t}}\mathbb{I}} \right]_{1,n+1} \right)_{t'=-\infty}^{t'=t} \hat{S}^\dagger(t) \\ &= [(M-i\omega_{\text{t}}\mathbb{I})^{-1}]_{1,1} \hat{S}(t) - [(M+i\omega_{\text{t}}\mathbb{I})^{-1}]_{1,n+1} \hat{S}^\dagger(t). \end{aligned}$$

Putting this together with the relevant free reservoir evolution component, $\hat{R}_{1,\text{free}}(t) \equiv [\mathbf{v}_{\text{free}}(t)]_1$, the first component of Eq. (4.3.6) is

$$\hat{R}_1(t) = \hat{R}_{1,\text{free}}(t) - i \frac{g_{\text{res}}}{2} \left([(M-i\omega_{\text{t}}\mathbb{I})^{-1}]_{1,1} \hat{S}(t) - [(M+i\omega_{\text{t}}\mathbb{I})^{-1}]_{1,n+1} \hat{S}^\dagger(t) \right), \quad (4.3.7)$$

which can then be substituted into the full equations of motion for the target system to obtain the desired effective description. One may want to drop the $\hat{S}^\dagger(t)$ term in Eq. (4.3.7) as this will give rise to counter-rotating terms in the effective equations of motion for the target system operators, this amounting to a Rotating Wave Approximation. In that case, the induced effective decay rate

⁷If, additionally, the target system is coupled weakly to another reservoir with coupling strength g'_{res} , the influence of this reservoir (via the target system) on the n oscillators will also be of higher order $\propto g'_{\text{res}}g_{\text{res}}$ and hence negligible.

and frequency shift due to the coupling to the structured reservoir are

$$\gamma_{\text{res}} = \frac{g_{\text{res}}^2}{2} \text{Re} [(M - i\omega_t \mathbb{I})^{-1}]_{1,1} \quad \text{and} \quad \Delta_{\text{res}} = \frac{g_{\text{res}}^2}{4} \text{Im} [(M - i\omega_t \mathbb{I})^{-1}]_{1,1}, \quad (4.3.8)$$

as seen by substituting $\hat{R}_1(t)$, Eq. (4.3.7), into the full equation of motion for $\hat{S}(t)$. The $\hat{R}_{1,\text{free}}(t)$ term captures the heating from the structured reservoir and, after having performed the substitution of Eq. (4.3.7), it will be natural to define a structured reservoir Langevin operator proportional to this term, $\hat{F}_{\text{res}}(t) \equiv -i \frac{g_{\text{res}}}{2\sqrt{\gamma_{\text{res}}}} \hat{R}_{1,\text{free}}(t)$. Given our time-scale assumption above, $\hat{F}_{\text{res}}(t)$ can be considered delta function correlated, $\langle \hat{F}_{\text{res}}^\dagger(t) \hat{F}_{\text{res}}(t') \rangle = n_{\text{res}}(\omega_t) \delta(t - t')$ and $\langle \hat{F}_{\text{res}}(t) \hat{F}_{\text{res}}^\dagger(t') \rangle = [n_{\text{res}}(\omega_t) + 1] \delta(t - t')$, with the relevant occupation number being that evaluated at the target system frequency:[25]

$$\begin{aligned} n_{\text{res}}(\omega_t) &\equiv 2\text{Re} \int_0^\infty dt \langle \hat{F}_{\text{res}}^\dagger(t) \hat{F}_{\text{res}}(t' = 0) \rangle e^{-i\omega_t t} \\ &= \int_{-\infty}^\infty dt \langle \hat{F}_{\text{res}}^\dagger(t) \hat{F}_{\text{res}}(t' = 0) \rangle e^{-i\omega_t t}. \end{aligned} \quad (4.3.9)$$

This can be determined in Fourier space as a weighted sum involving certain entries of the matrix $(M - i\omega_t \mathbb{I})^{-1}$ as demonstrated in Section 4.2.2, specifically Eq. (4.2.15).

Chapter 5

Extending cavity-mechanical cooling

In this chapter we will explore whether it is possible to exploit the successful technique of cavity-assisted sideband cooling of mechanical motion, discussed in Section 2.2, to cool other degrees of freedom. As emphasized in the survey presented in Chapter 2, the assisting electromagnetic cavity can be of either optical or electrical nature. Due to the respective frequency ranges involved, each of these has its specific advantages and disadvantages of technical as well as intrinsic character.

5.1 Main ideas and preliminaries

In cavity-mechanical cooling scenarios, or extensions thereof, the effective temperature of a mode being cooled results from a competition between the effective temperatures of the reservoirs affecting the system. (In this qualitative discussion, by “effective temperature” we mean the average occupancy.) Moreover, if we approach the ground state regime, quantum zero-point fluctuations previously masked by thermal effects will become significant and eventually define the lower limit on the cooling achievable. However, we will restrict our focus to the former aspect: The competition between thermal reservoirs of different effective temperatures.

Similar to what we considered in the mathematical context of Sections 4.2 and 4.3, the general scenario we have in mind is the following: A multi-component system (involving several mutually coupled degrees of freedom) where each component, or subsystem, is subject to individual environmental influences; this is illustrated in Fig. 5.1.1. What we would like to understand is how these environmental influences propagate or distribute among the various system degrees of freedom. This will enable us to engineer the system to behave in accordance with our purposes. For the degenerate case of a single-component system, the answer is contained in a simple Langevin equation like Eq. (4.1.19). In the multi-component case, several such Langevin equations will be coupled. The fact that several indirect decay paths are now available to the system can lead to interesting interference phenomena, as we will see below.

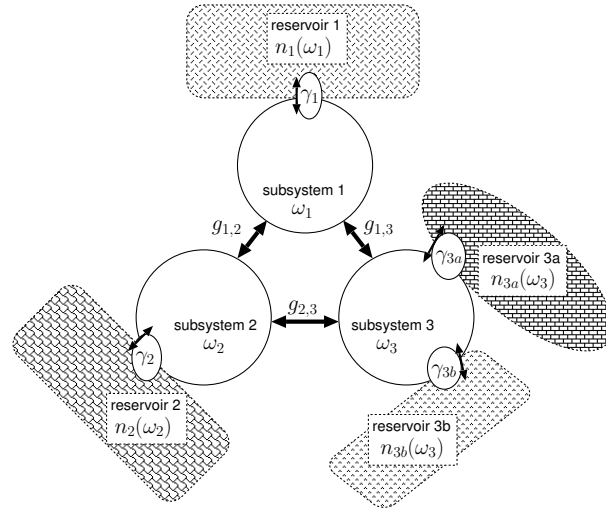


Figure 5.1.1: Three-component system with each subsystem coupled directly to either one or two reservoirs. The influences of the reservoirs will propagate via the coherent couplings $g_{i,j}$ and thereby affect subsystems to which they are not directly coupled.

What intuition do we have about such a situation? As already stressed in Section 2.2, our definition of “cooling” does not coincide entirely with the usual notion related to bulk temperatures. Let us, nevertheless, consider the familiar cooling scenario of a regular fridge. We may depict this in a diagram resembling Fig. 5.1.1, although here we will allow ourselves to be somewhat vague about the distinction ‘system vs. reservoir’. The cooling cycle of the fridge is competing with the room temperature environment in its task of cooling the contents (see Fig. 5.1.2). The food is not in direct contact with the cooling element of the fridge, rather, the food is cooled by cooling the air residing inside the fridge. If we refrain from opening the fridge and let the cooling cycle be continually active, eventually the temperature of the food (and the surrounding air) will reach a common steady state temperature which is a compromise between the cooling and heating mechanisms. As suggested in Fig. 5.1.2, we may think of the cooling cycle and the external room temperature air, respectively, as reservoirs directly coupled to the internal body of air (an ancillary system component) which, in turn, is coupled to the food (the primary system component). This fridge scenario will serve as a point of comparison below.

The above argument relies on thermodynamic intuition, which may or may not remain valid for our kind of few-mode cooling. As it turns out, few-mode cooling will be seen to allow for effects that contradict the above picture. Translated into the language of the fridge scenario, we may in fact cool the food without necessarily cooling the air in the fridge.

As a preliminary, however, we will in the following sections start out by considering simple versions of Fig. 5.1.1, illustrating the generic few-mode cooling scenario.

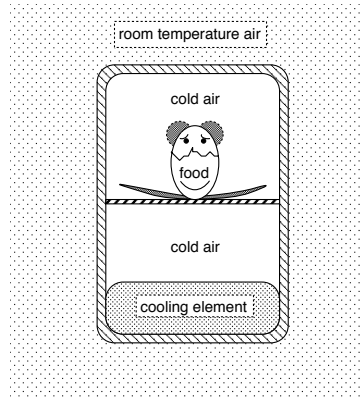


Figure 5.1.2: A regular fridge cooling its contents (food surrounded by air) below the temperature of the surroundings with which it competes.

5.1.1 Single-component system

To begin with, it is worth considering the steady state occupancy that arises in the situation where a single bosonic oscillator mode is directly coupled to a number of reservoirs. Here we will consider the case of two independent (white noise) reservoirs as illustrated in Fig. 5.1.3.

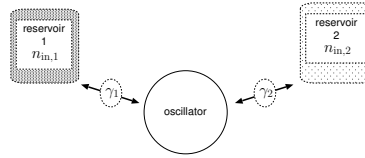


Figure 5.1.3: A single mode coupled at rates γ_1, γ_2 to two independent reservoirs of occupancy $n_{\text{in},1}, n_{\text{in},2}$, respectively.

The Heisenberg-Langevin equation for this situation is (in a rotating frame w.r.t. the oscillator frequency)

$$\dot{\hat{c}}(t) = -\frac{1}{2} [\gamma_1 + \gamma_2] \hat{c}(t) - \sqrt{\gamma_1} \hat{c}_{\text{in},1}(t) - \sqrt{\gamma_2} \hat{c}_{\text{in},2}(t), \quad (5.1.1)$$

where $\langle \hat{c}_{\text{in},i}^\dagger(t) \hat{c}_{\text{in},j}(t') \rangle = \delta_{i,j} n_{\text{in},i} \delta(t - t')$ as in Eq. (4.1.17). Integrating Eq. (5.1.1) formally, we obtain (neglecting transients)

$$\hat{c}(t) = \int_{-\infty}^t dt' e^{-\frac{1}{2}(\gamma_1 + \gamma_2)(t-t')} [-\sqrt{\gamma_1} \hat{c}_{\text{in},1}(t') - \sqrt{\gamma_2} \hat{c}_{\text{in},2}(t')],$$

from which we find the steady state mean occupancy of the oscillator by making use of the auto-correlation functions of the mutually uncorrelated reservoirs:

$$\begin{aligned} n_{\text{HO}}^{(\text{ss})} &= \langle \hat{c}^\dagger(t) \hat{c}(t) \rangle_{\text{ss}} = \int_{-\infty}^t dt' \int_{-\infty}^t dt'' e^{-\frac{1}{2}(\gamma_1 + \gamma_2)[(t-t') + (t-t'')] \delta(t' - t'') [\gamma_1 n_{\text{in},1} + \gamma_2 n_{\text{in},2}] \\ &= \int_{-\infty}^t dt' e^{-(\gamma_1 + \gamma_2)(t-t')} [\gamma_1 n_{\text{in},1} + \gamma_2 n_{\text{in},2}] = \frac{\gamma_1 n_{\text{in},1} + \gamma_2 n_{\text{in},2}}{\gamma_1 + \gamma_2}, \end{aligned} \quad (5.1.2)$$

a weighted average of the two reservoir occupancies. We will recognize the same structure in corresponding expressions for the less simple scenarios to be considered below. In the following section we increase the complexity by adding in another subsystem.

5.1.2 Direct cooling of an LC circuit

As stated at the very beginning of this chapter, our aim is to explore the idea of using the increasingly well-established technique of cavity-mechanical cooling to achieve cooling of other degrees of freedom. Such an extension of cavity-mechanical cooling must of course involve the coupling of the mechanical mode to our cooling target in one way or another. The simplest imaginable way is to arrange for a direct coupling between the two (if technically possible); this is the scheme depicted in Fig. 5.1.4. We will examine it to identify its limiting factors as well as to build intuition about few-mode cooling. It will serve as benchmark and a basis for understanding more involved cooling schemes.

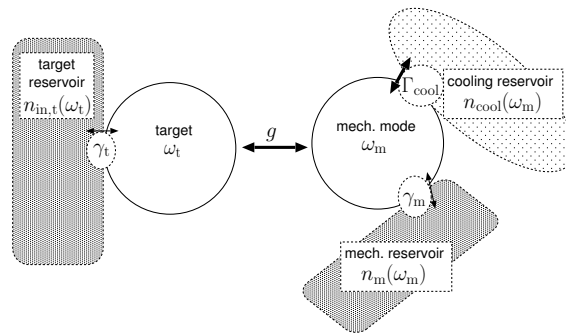


Figure 5.1.4: Using the cavity-mechanical cooling mechanism to cool a target degree of freedom directly coupled to the mechanical mode. The cavity-assisted cooling mechanism is modeled as a low-temperature reservoir. Thermal reservoirs are coupled to the target and mechanical modes competing with the cooling.

This 'direct' cooling scheme is nothing but a slightly more abstract formulation of the proposal put forward in Ref. [27], which was presented in Section 2.4: The extension of optical cavity-assisted cooling of a mechanical mode to an LC circuit via capacitive coupling. For definiteness, we will consider this specific realization of the scheme in Fig. 5.1.4 for the remainder of the discussion. However, it should be kept in mind that, in principle, any degree of freedom modelled mathematically as a bosonic harmonic oscillator may take the place of the LC circuit mode in the calculation below. Thus, in addition to the electrical LC circuit, possible candidates for 'direct' cooling targets include any electromagnetic cavities compatible with the parametric coupling discussed in Section 2.2.1. Even though we here consider cooling of a bosonic harmonic oscillator (the LC circuit mode), the scheme is also meaningful for target systems with different mathematical descriptions. This might be a relevant application of the scheme as the direct coupling between mechanical membranes and electronic

spin or charge qubits is being contemplated in the context of optomechanics [26]. We take the LC circuit and the membrane to be on resonance with each other (this may have to be realized using an AC drive bridging the frequency gap). The Heisenberg-Langevin equations describing the mechanical membrane (\hat{a}) coupled on-resonance to the LC circuit (\hat{b}) are, within the Rotating Wave Approximation (both in the electro-mechanical coupling as well as in all environmental couplings),

$$\begin{aligned}\dot{\hat{a}} &= -\frac{1}{2}(\gamma_m + \Gamma_{\text{cool}})\hat{a} - \sqrt{\gamma_m}\hat{a}_{\text{in},m} - \sqrt{\Gamma_{\text{cool}}}\hat{a}_{\text{in,cool}} - ig_m\hat{b} \\ \dot{\hat{b}} &= -\frac{1}{2}\gamma_{\text{LC}}\hat{b} - \sqrt{\gamma_{\text{LC}}}\hat{b}_{\text{in,LC}} - ig_m^*\hat{a},\end{aligned}\quad (5.1.3)$$

where the Langevin operators $\hat{a}_{\text{in},m}, \hat{b}_{\text{in,LC}}$ are white noise idealizations of the thermal reservoirs with auto-correlators given by Eqs. (4.1.17). Eqs. (5.1.3) are the mathematical expression of Fig. 5.1.4 (with $\gamma_t \rightarrow \gamma_{\text{LC}}, g \rightarrow g_m$).

5.1.2.1 Exact solution for the LC occupancy

The exact steady state occupancy of the LC circuit (within the Rotating Wave Approximation) can be evaluated by solving Eqs. (5.1.3) using either of the methods presented in section 4.2; they both yield the formula:

$$n_{\text{LC}}^{(\text{ss})} = \frac{\gamma_{\text{LC}}n_{\text{LC}} + \frac{4|g_m|^2}{\gamma_m + \Gamma_{\text{cool}}} \left(\frac{\gamma_{\text{LC}}n_{\text{LC}} + \gamma_m n_m + \Gamma_{\text{cool}}n_{\text{cool}}}{\gamma_{\text{LC}} + \gamma_m + \Gamma_{\text{cool}}} \right)}{\gamma_{\text{LC}} + \frac{4|g_m|^2}{\gamma_m + \Gamma_{\text{cool}}}}, \quad (5.1.4)$$

Inspired by Eq. (5.1.2) for the single-oscillator scenario, the result is stated in the suggestive form of a weighted average (of weighted averages), and this is at least one possible angle on the result. It is therefore tempting to interpret the term of Eq. (5.1.4) in parenthesis, which is a weighted average of occupancies, as an effective occupancy of some sort,

$$n_{\text{eff}} \equiv \frac{\gamma_{\text{LC}}n_{\text{LC}} + \gamma_m n_m + \Gamma_{\text{cool}}n_{\text{cool}}}{\gamma_{\text{LC}} + \gamma_m + \Gamma_{\text{cool}}}.$$

Pursuing this logic for a moment, we define the corresponding rate, $\gamma_{\text{eff}} \equiv 4|g_m|^2/(\gamma_m + \Gamma_{\text{cool}})$, in terms of which we can restate Eq. (5.1.4) as

$$n_{\text{LC}}^{(\text{ss})} = \frac{\gamma_{\text{LC}}n_{\text{LC}} + \gamma_{\text{eff}}n_{\text{eff}}}{\gamma_{\text{LC}} + \gamma_{\text{eff}}}. \quad (5.1.5)$$

Now, if we imagine increasing $|g_m|$, and thus γ_{eff} , from zero, Eq. (5.1.5) indicates that $n_{\text{LC}}^{(\text{ss})}$ interpolates between two regimes dominated by n_{LC} and n_{eff} , respectively. What is misleading about Eq. (5.1.5) is that, in view of Eq. (5.1.2) above, we seem to suggest that the LC circuit is coupled at a rate γ_{eff} to an effective reservoir of occupancy n_{eff} . As is seen from its definition, n_{eff} depends significantly on parameters pertaining to the LC and this conflicts with the notion of a reservoir as defined in section 4.1.1; specifically the reservoir property of being essentially unaltered by its interaction with the system. We now consider limiting cases.

5.1.2.2 Adiabatic limit

Physically, this is the same limited that we considered in deriving the structured reservoir formalism in Section 4.3. In the limit where the membrane equilibrates rapidly with its environment $\gamma_m + \Gamma_{\text{cool}} \gg \gamma_{\text{LC}}, |g_m|$, the membrane can be adiabatically eliminated from the LC equation of motion. This results in an induced decay rate of γ_{eff} , exactly the quantity appearing in Eqs. (5.1.4, 5.1.5). Assuming the “intrinsic” membrane heating to be insignificant compared to that of the LC, which is reasonable in practice due to the usually large mechanical Q -factors, the steady state LC occupancy is (for $n_{\text{cool}} \approx 0$)

$$n_{\text{LC}}^{(\text{ss})} \approx \frac{\gamma_{\text{LC}}}{\gamma_{\text{eff}} + \gamma_{\text{LC}}} n_{\text{LC}} = \left[1 + \frac{4|g_m|^2}{\gamma_{\text{LC}}(\gamma_m + \Gamma_{\text{cool}})} \right]^{-1} n_{\text{LC}}$$

in the adiabatic limit, which also follows from Eq. (5.1.4). For fixed $|g_m|$, the result suggests that we should keep Γ_{cool} as small as possible without violating the criteria for the adiabatic limit to be valid.

5.1.2.3 Strong coupling limit

In the regime of strong coupling, defined by $|g_m| > \sqrt{\gamma_{\text{LC}}(\gamma_m + \Gamma_{\text{cool}})}/2$, the LC and mechanical degrees of freedom hybridize. As we enter this regime, it is no longer natural to understand the physics in terms of dynamical variables describing either the LC or the membrane separately; rather, the natural basis is that of the normal modes of the system. The fact that, due to the strong coupling, we cannot influence, say, the membrane without thereby also affecting the LC makes it reasonable that we have to consider their collective response to get a clear picture of the physics. As an extension to this, if we are well into the strong coupling regime, it cannot be significant which part of the system, LC or membrane, we subject to reservoir coupling; this is indeed what we see in the $|g_m| \rightarrow \infty$ limit of Eq. (5.1.4):

$$n_{\text{LC}}^{(\text{ss})} \rightarrow \frac{\gamma_{\text{LC}} n_{\text{LC}} + \gamma_m n_m + \Gamma_{\text{cool}} n_{\text{cool}}}{\gamma_{\text{LC}} + \gamma_m + \Gamma_{\text{cool}}}, \quad (5.1.6)$$

showing that the influences entering the system via the membrane are on equal footing with that of the reservoir directly in contact with the LC. If we again take the intrinsic membrane heating to be negligible (and set $n_{\text{cool}} \approx 0$), the LC steady state occupancy in the strong coupling limit, Eq. (5.1.6), reduces to $n_{\text{LC}}^{(\text{ss})} \approx \frac{\gamma_{\text{LC}}}{\gamma_m + \Gamma_{\text{cool}}} n_{\text{LC}}$ (additionally assuming $\gamma_m + \Gamma_{\text{cool}} \gg \gamma_{\text{LC}}$, as required for appreciable cooling). This result suggests that we should make Γ_{cool} as large as possible (at least within the regime of validity for the limit under consideration). Note that for the Rotating Wave Approximation to remain valid, we must require $|g_m| \ll \omega_m$ in order for the counter-rotating terms (that we are neglecting) not to become resonant. Thus, in taking the limit $|g_m| \rightarrow \infty$ above it is understood that $|g_m|$ should be sufficiently small that we can ignore such counter-rotating terms.

5.1.2.4 Optimal cooling rate Γ_{cool}

We will now determine the optimal value of the cavity-induced cooling rate Γ_{cool} experienced by the membrane. We do so by minimizing the exact expression

for the LC occupancy $n_{\text{LC}}^{(\text{ss})}$, Eq. (5.1.4), for fixed electromechanical coupling strength g_{m} ; solving $\left. \frac{\partial n_{\text{LC}}^{(\text{ss})}}{\partial \Gamma_{\text{cool}}} \right|_{\Gamma_{\text{cool}}=\Gamma_{\text{cool}}^{(\text{opt})}} = 0$ we find

$$\Gamma_{\text{cool}}^{(\text{opt})} = \sqrt{\left(1 + \frac{\gamma_{\text{m}}}{\gamma_{\text{LC}}}\right) (\gamma_{\text{m}} \gamma_{\text{LC}} + 4|g_{\text{m}}|^2)} \approx \sqrt{\gamma_{\text{m}} \gamma_{\text{LC}} + 4|g_{\text{m}}|^2} = 2|g_{\text{m}}| \sqrt{1 + \frac{1}{C_{\text{m}}}}, \quad (5.1.7)$$

introducing the electromechanical *cooperativity* $C_{\text{m}} \equiv 4|g_{\text{m}}|^2 / (\gamma_{\text{m}} \gamma_{\text{LC}})$ (more precisely the unloaded cooperativity, i.e., for $\Gamma_{\text{cool}} = 0$). In Eq. (5.1.7) we once again made the approximation $\gamma_{\text{m}} \ll \gamma_{\text{LC}}$ which is very reasonable since mechanical Q -factors usually exceed those of LC circuits by several orders of magnitude (as pointed out in Chapter 2). In the large cooperativity limit, $C_{\text{m}} \gg 1$, required for appreciable cooling, Eq. (5.1.7) simplifies to

$$\Gamma_{\text{cool}}^{(\text{opt})} \approx 2|g_{\text{m}}|, \quad (C_{\text{m}} \gg 1).$$

Taking note of how these quantities, Γ_{cool} and g_{m} , enter the equations of motion (5.1.3), we reach the following physically reasonable conclusion: It is not possible to drain the LC circuit of excitations at a rate faster than the bottleneck set by the electromechanical coupling $2|g_{\text{m}}|$. Increasing Γ_{cool} beyond this value broadens the mechanical level unnecessarily with the effect of decoupling the mechanical mode from the LC mode. This optimal value of Γ_{cool} is seen to be a compromise between the values suggested by the respective limiting results above. The resulting minimal occupancy in the large cooperativity limit is (again ignoring γ_{m} and setting $n_{\text{cool}} \approx 0$)

$$n_{\text{LC}}^{(\text{ss})} \Big|_{\text{opt}} \approx \frac{\gamma_{\text{LC}} + \left[\frac{1}{2|g_{\text{m}}|} + \frac{1}{\gamma_{\text{LC}}} \right]^{-1}}{\gamma_{\text{LC}} + 2|g_{\text{m}}|} n_{\text{LC}} \approx \frac{\gamma_{\text{LC}}}{|g_{\text{m}}|} n_{\text{LC}}. \quad (5.1.8)$$

Later, we will return to Eq. (5.1.8) as a point of comparison.

5.1.3 Cooling via a link

We will now consider an extension of the cooling scheme considered in the previous section: Rather than connecting our cooling target directly to the mechanical degree of freedom, it is connected indirectly via a 'link' degree of freedom as might be necessitated by technical circumstances that prevent a direct coupling to the target. Hence, the cooling system under consideration consists of three components: The *target* subsystem, which we would like to cool, the *link* subsystem and the *mechanical* subsystem; see Fig. 5.1.5. As we will consider later, the 'target' could for example be an atomic spin or a mechanical degree of freedom not amenable to direct cavity-assisted cooling. For the 'link' we have an electromagnetic cavity in mind, for instance an LC electrical circuit.

These subsystems are coupled to individual reservoirs whereby they attain certain linewidths. Each subsystem is coupled to an "intrinsic" reservoir accounting for the inevitable, generally unwanted environmental influences; we denote the resulting intrinsic widths γ_{t} , γ_{link} and γ_{m} , respectively. Additionally,

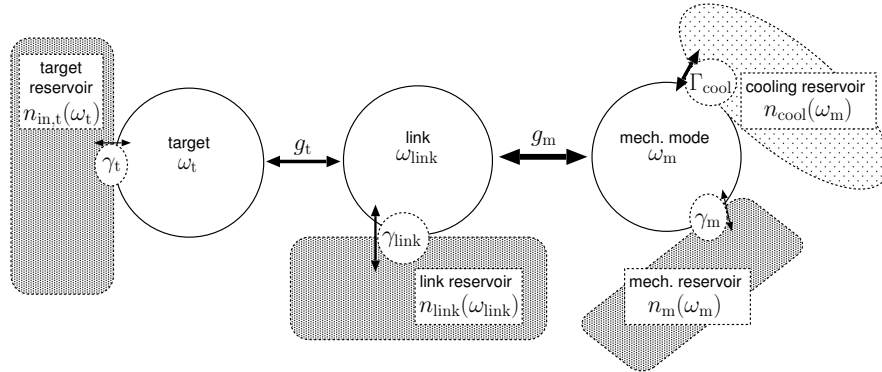


Figure 5.1.5: The ‘indirect’ cooling scheme in which an intermediate link mediates the cavity-assisted cooling from the mechanical mode to the target.

the mechanical subsystem is intentionally coupled to a low-occupancy cooling reservoir, inducing another width contribution, Γ_{cool} , in the mechanical subsystem. The latter is an effective description of the cavity-assisted cooling mechanism. Regarding the relative magnitudes of these widths we assume $\gamma_t \ll \gamma_{\text{link}}, (\gamma_m + \Gamma_{\text{cool}})$, that is, the target subsystem is long-lived (relatively isolated from its environment) compared to the other degrees of freedom in the system. We also assume the target to be weakly coupled to the link, $|g_t| \ll \gamma_{\text{link}}$. In order to achieve effective cooling of the target, we will need the influence of the low-occupancy cooling reservoir to be significant compared to that of the intrinsic reservoirs of relatively high occupancy ($n_{\text{cool}} \ll n_t, n_{\text{link}}, n_m$). The link subsystem mediates cooling from the mechanical subsystem to the target, but also contributes with heating from its own reservoir. An interesting question is what the net effect on the target is, specifically, which combinations of parameters determine its steady state occupancy? Furthermore, to what extent can we tilt the balance between these competing effects? In consideration of the analogy to how cooling (in the prosaic sense) is distributed in a fridge - from the cooling element via the air in fridge to the food - we may ask if efficient cooling of the link subsystem is a prerequisite to achieving cooling of the target system to which it is coupled. In course of the analysis below, we will see that this is not the case.

The cooling scheme of Fig. 5.1.5 described in the above paragraph will now be related explicitly to the opto- and electro-mechanical techniques and setups treated in Chapter 2. As already hinted at, the mechanical component connected to the cold reservoir is the mechanical degree of freedom of a cavity-assisted mechanical cooling setup. The cold reservoir is a highly simplified description of the net cooling effect on the membrane induced by the cavity radiation pressure interaction. As discussed in Chapter 2, the electromagnetic cavity may be either optical or electrical. If we intend to implement the above cooling scheme in a room temperature setup, then the obvious choice for the cavity would be an optical one. Its advantage comes from the fact that the thermal occupancy at optical frequencies is virtually zero at room temperature; thus, $n_{\text{cool}} \approx 0$ to a good approximation (ignoring technical laser noise) which fits well with

our scheme. As discussed in Section 2.2, superconducting electrical microwave circuits have their advantages, in spite of their lower frequencies, if one is willing to work with a cryogenic setup. The second, “intrinsic” reservoir coupled to the mechanical mode in Fig. 5.1.5 is simply a model of the thermal, environmental influences already discussed in Section 2.2.

The ‘indirect’ cooling scheme presented above will be the main focus of the remainder of the analysis.

5.2 Structured reservoir description of the ‘indirect’ cooling system

Depending on the nature of the target and link systems, the ‘indirect’ cooling scheme outlined in Section 5.1.3 may or may not be describable in terms of exactly solvable equations. In the special case where we deal only with bosonic harmonic oscillators, the methods of Section 4.2 may be used to solve for the exact steady state occupancies, but these solutions are not easy to interpret in general. Therefore we will now derive an effective mathematical description of the ‘indirect’ cooling system using the structured reservoir formalism developed in Section 4.3, that captures the physics of the scheme in a certain limit. This effective formalism may then afterwards be applied to various target systems of interest.

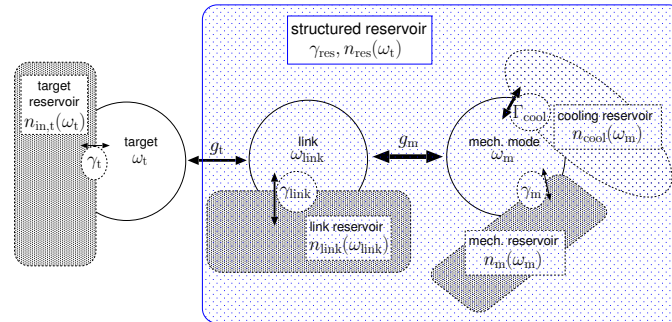


Figure 5.2.1: The ‘indirect’ cooling system considered as a structured reservoir. In the limit $\gamma_t, |g_t| \ll \gamma_{\text{link}}, (\gamma_m + \Gamma_{\text{cool}})$, the target will effectively see a reservoir characterized by the parameters $\gamma_{\text{res}}, n_{\text{res}}(\omega_t)$.

The point of view of the effective formalism is illustrated in Fig. 5.2.1: We replace the cooling system with a structured reservoir of effective occupation number $n_{\text{res}}(\omega_t)$, to which the target decays at a rate γ_{res} . These quantities are then incorporated into the effective equation for whatever target system is being considered (this can be either a master equation or a Heisenberg-Langevin equation). Such an effective reservoir description will not always be an appropriate picture. It relies on the interaction rates of the target system being slow compared to those of the cooling system degrees of freedom, $\gamma_t, |g_t| \ll \gamma_{\text{link}}, (\gamma_m + \Gamma_{\text{cool}})$.¹ We assume these conditions to be fulfilled, but we

¹More precisely, γ_t and $|g_t|$ must be small compared compared to the decay rate of any normal mode of the cooling system or the detuning to the nearest such normal mode.

shall later examine the stability of the effective theory as we depart from the ideal limit for $\gamma_t, |g_t|$.

The structured reservoir formalism of Section 4.3 requires us to evaluate certain expressions for the “free” cooling system, in the absence of interaction with the target (this obviously relies on the aforementioned conditions to be an appropriate description). This procedure yields the pair of effective parameters, $\gamma_{\text{res}}, n_{\text{res}}(\omega_t)$. By making the Rotating Wave Approximation in the link coupling, the equations of motion for the “free” cooling system are exactly of the form considered in connection with ‘direct’ LC circuit cooling above, Eqs. (5.1.3) (although these were specifically for the resonant case). We restate them here in matrix form for general detunings using the parameter labels of Figs. 5.1.5 and 5.2.1,

$$\begin{pmatrix} \dot{\hat{a}} \\ \dot{\hat{b}} \end{pmatrix} = - \underbrace{\begin{pmatrix} \frac{1}{2}(\gamma_m + \Gamma_{\text{cool}}) + i\omega_m & ig_m \\ ig_m^* & \frac{1}{2}\gamma_{\text{link}} - i\Delta \end{pmatrix}}^M \underbrace{\begin{pmatrix} \hat{a} \\ \hat{b} \end{pmatrix}}^{\mathbf{v}} - \underbrace{\begin{pmatrix} \sqrt{\gamma_m}\hat{a}_{\text{in},m} + \sqrt{\Gamma_{\text{cool}}}\hat{a}_{\text{in},\text{cool}} \\ \sqrt{\gamma_{\text{LC}}}\hat{b}_{\text{in},\text{LC}} \end{pmatrix}}^{\mathbf{N}}, \quad (5.2.1)$$

where Δ is the effective detuning between drive and resonance for the link cavity (see Section 2.2.1). Eq. (5.2.1) is a specific instance of Eq. (4.3.5). In this regard, note that in the (cooling system) Rotating Wave Approximation, annihilation operators only couple to annihilation operators. This means that these can be solved for separately; thus the simplified form of Eq. (5.2.1). By taking the Hermitian conjugate of the former solutions, the solutions for the creation operators are produced (as always).

First we determine the effective rate γ_{res} using Eq. (4.3.8): In our case it translates into $\gamma_{\text{res}} = 2g_t^2 \text{Re} [(M - i\omega_t \mathbb{I})^{-1}]_{2,2}$ since $\frac{g_{\text{res}}}{2} \rightarrow g_t$ and the target is coupled to \hat{b} (which has been assigned to the second vector entry). Using Kramer’s formula (stated in Appendix A.1), we find

$$[(M - i\omega_t \mathbb{I})^{-1}]_{2,2} = \frac{\frac{1}{2}(\gamma_m + \Gamma_{\text{cool}}) + i(\omega_m - \omega_t)}{[\frac{1}{2}(\gamma_m + \Gamma_{\text{cool}}) + i(\omega_m - \omega_t)][\frac{1}{2}\gamma_{\text{link}} - i(\Delta + \omega_t)] + |g_m|^2} \Rightarrow \quad (5.2.2)$$

$$\gamma_{\text{res}} = g_t^2 \frac{\gamma_{\text{link}} + |g_m|^2 \frac{(\gamma_m + \Gamma_{\text{cool}})}{\frac{1}{4}(\gamma_m + \Gamma_{\text{cool}})^2 + \delta^2}}{\frac{1}{4} \left(\gamma_{\text{link}} + |g_m|^2 \frac{(\gamma_m + \Gamma_{\text{cool}})}{\frac{1}{4}(\gamma_m + \Gamma_{\text{cool}})^2 + \delta^2} \right)^2 + \left(\tilde{\Delta} - |g_m|^2 \frac{\delta}{\frac{1}{4}(\gamma_m + \Gamma_{\text{cool}})^2 + \delta^2} \right)^2}, \quad (5.2.3)$$

where we have introduced the bare target-link detuning $\tilde{\Delta} \equiv -(\Delta + \omega_t)$ and the bare target-mechanics detuning $\delta \equiv \omega_m - \omega_t$. These quantities are illustrated in Fig. 5.2.2, where also the relative magnitude of the linewidths are indicated qualitatively. We ignore the frequency shift induced by the reservoir interaction Δ_{res} , given by Eq. (4.3.8), as it does not influence the results obtained for a single target degree of freedom coupled to broad (essentially white noise) reservoirs.

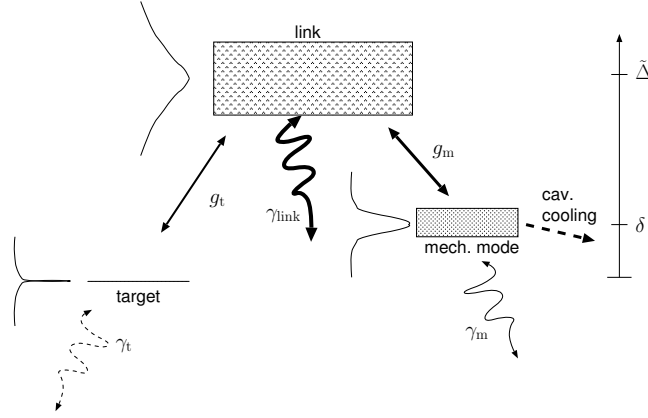


Figure 5.2.2: Bare level diagram for the ‘indirect’ cooling scheme. The very narrow target level is coupled via the rapidly decaying link to the cooling broadened mechanical mode.

Next, we proceed to determine the effective occupation number $n_{\text{res}}(\omega_t)$ of the structured reservoir from Eq. (4.3.9). This involves the Langevin operator $\hat{F}_{\text{res}}(t) \equiv -i \frac{g_t}{\sqrt{\gamma_{\text{res}}}} \hat{b}_{\text{free}}(t)$, defined in terms of the ‘free’ link annihilation operator, i.e., with the target decoupled, $g_t \rightarrow 0$. Hence, the evolution of \hat{b}_{free} is governed only by the coupling to other bosonic oscillators as well as quantum white noise reservoirs; this simplifies the description considerably. Since we have made the Rotating Wave Approximation in the link-mechanical coupling, M is block diagonal with two $N \times N$ blocks; this makes the second term within the brackets of formula Eq. (4.2.15) vanish in our case. Hence, Eq. (4.3.9) reads

$$\begin{aligned} n_{\text{res}}(\omega_t) &= \frac{g_t^2}{\gamma_{\text{res}}} \int_{-\infty}^{\infty} dt \langle \hat{b}_{\text{free}}^\dagger(t) \hat{b}_{\text{free}}(t=0) \rangle e^{-i\omega_t t} \\ &= \frac{g_t^2}{\gamma_{\text{res}}} \sum_{k=1}^2 \left(\sum_j \gamma_{k,j} n_{k,j} \right) |[(M - i\omega\mathbb{I})^{-1}]_{2,k}|^2, \end{aligned} \quad (5.2.4)$$

which leaves the task of determining the matrix element $[(M - i\omega\mathbb{I})^{-1}]_{2,1} = \frac{-ig_m^*}{\det(M - i\omega\mathbb{I})}$ since the diagonal component was already determined in Eq. (5.2.2). Note that the terms γ_{res} , $|[(M - i\omega\mathbb{I})^{-1}]_{2,k}|^2$ are all inversely proportional to $|\det(M - i\omega\mathbb{I})|^2$ so that this factor drops out and we are left with

$$\begin{aligned} n_{\text{res}}(\omega_t) &= \frac{(\gamma_{\text{link}} n_{\text{link}}) \left| \frac{1}{2}(\gamma_m + \Gamma_{\text{cool}}) + i\delta \right|^2 + (\gamma_m n_m + \Gamma_{\text{cool}} n_{\text{cool}}) |g_m|^2}{\gamma_{\text{link}} \left| \frac{1}{2}(\gamma_m + \Gamma_{\text{cool}}) + i\delta \right|^2 + (\gamma_m + \Gamma_{\text{cool}}) |g_m|^2} \\ &= \frac{\gamma_{\text{link}} n_{\text{link}} + \frac{|g_m|^2 (\gamma_m + \Gamma_{\text{cool}})}{\frac{1}{4}(\gamma_m + \Gamma_{\text{cool}})^2 + \delta^2} \left(\frac{\gamma_m n_m + \Gamma_{\text{cool}} n_{\text{cool}}}{\gamma_m + \Gamma_{\text{cool}}} \right)}{\gamma_{\text{link}} + \frac{|g_m|^2 (\gamma_m + \Gamma_{\text{cool}})}{\frac{1}{4}(\gamma_m + \Gamma_{\text{cool}})^2 + \delta^2}}. \end{aligned} \quad (5.2.5)$$

This is the effective mean occupancy of the structured reservoir from the point of view of a long-lived target system subjected to the ‘indirect’ scheme.

It is interesting to compare this result to the exact (RWA) result for the steady state occupancy of the target in the ‘direct’ scheme; this was obtained in Section

5.1.2, Eq. (5.1.4), for the resonant case (with an LC circuit mode as target for definiteness). We now juxtapose the two for ease of comparison (setting $\delta = 0$ in Eq. (5.2.5)):

$$n_{\text{LC}}^{(\text{ss})} = \frac{\gamma_{\text{LC}} n_{\text{LC}} + \frac{4|g_{\text{m}}|^2}{\gamma_{\text{m}} + \Gamma_{\text{cool}}} \left(\frac{\gamma_{\text{LC}} n_{\text{LC}} + \gamma_{\text{m}} n_{\text{m}} + \Gamma_{\text{cool}} n_{\text{cool}}}{\gamma_{\text{LC}} + \gamma_{\text{m}} + \Gamma_{\text{cool}}} \right)}{\gamma_{\text{LC}} + \frac{4|g_{\text{m}}|^2}{\gamma_{\text{m}} + \Gamma_{\text{cool}}}} \quad (5.2.6)$$

$$n_{\text{res}} = \frac{\gamma_{\text{link}} n_{\text{link}} + \frac{4|g_{\text{m}}|^2}{\gamma_{\text{m}} + \Gamma_{\text{cool}}} \left(\frac{\gamma_{\text{m}} n_{\text{m}} + \Gamma_{\text{cool}} n_{\text{cool}}}{\gamma_{\text{m}} + \Gamma_{\text{cool}}} \right)}{\gamma_{\text{link}} + \frac{4|g_{\text{m}}|^2}{\gamma_{\text{m}} + \Gamma_{\text{cool}}}}. \quad (5.2.7)$$

We see that n_{res} has the same structure as that of $n_{\text{LC}}^{(\text{ss})}$, as pointed out in Section 5.1.2: A weighted average of weighted averages (this is true for general detunings δ , see Eq. (5.2.5)). In fact, the only difference between the two (in addition to labelling, $\gamma_{\text{LC}} \leftrightarrow \gamma_{\text{link}}$) is the disappearance of γ_{LC} ($\rightarrow 0$) from the innermost average as we go from Eq. (5.2.6) to (5.2.7). Thus, judging from Eq. (5.2.7) (or Eq. (5.2.5)) for n_{res} , there exists a regime, $\frac{4|g_{\text{m}}|^2}{\gamma_{\text{m}} + \Gamma_{\text{cool}}} \gg \gamma_{\text{link}}$, where the target does not “see” the reservoir of the link. This is an important indication that destructive interference takes place, suppressing heating of the target by the link reservoir. It may be seen as Electromagnetically Induced Transparency (EIT) where two paths to the link interfere destructively, rendering it (at least partially) transparent. This observation suggests that we may perform efficient cooling using the ‘indirect’ scheme, as we shall indeed see below.

It must be added to the above, however, that $\frac{4|g_{\text{m}}|^2}{\gamma_{\text{m}} + \Gamma_{\text{cool}}} \rightarrow \infty$ entails $\gamma_{\text{res}} \rightarrow 0$ showing that n_{res} and γ_{res} must in general be optimized simultaneously; this analysis will be carried out later in this chapter.

Finally, it is interesting to note that, by comparing Eqs. (4.2.15) and (5.2.4), we may obtain $n_{\text{LC}}^{(\text{ss})}$ (with ‘LC’ \rightarrow ‘link’) as the inverse Fourier transform of $n_{\text{res}}(\omega_t)$, Eq. (5.2.5), evaluated at $t = 0$ (and multiplied by $\gamma_{\text{res}}/g_t^2$). This may be interpreted as the target only seeing a particular spectral component of the link occupancy.

5.2.1 Strong coupling regime of the cooling system

We would like to verify that the reservoir description contains the physics that we would expect. For sufficiently strong coupling between LC and membrane, we would expect hybridization of these degrees of freedom to occur. In this regime the more natural way of thinking about the LC and the membrane is in terms of their (collective) normal modes, which will be split in energy. If we take the bare, rotating frame frequencies of target system, link and mechanical mode to be on resonance, then for sufficiently strong normal mode splitting, we will expect the target system to be effectively decoupled from the link-mechanical system. Indeed, we recognize these features by considering the plots of n_{res} and γ_{res} presented in Fig. 5.2.3.

It must be noted that as we move into the strong coupling regime, the splitting of the energy levels will bring the counter-rotating terms, that we have neglected in making the Rotating Wave Approximation (RWA), closer to resonance. Thus, our theory is only valid as long as $|g_{\text{m}}| \ll \omega_{\text{m}}$. It is not necessary to make the

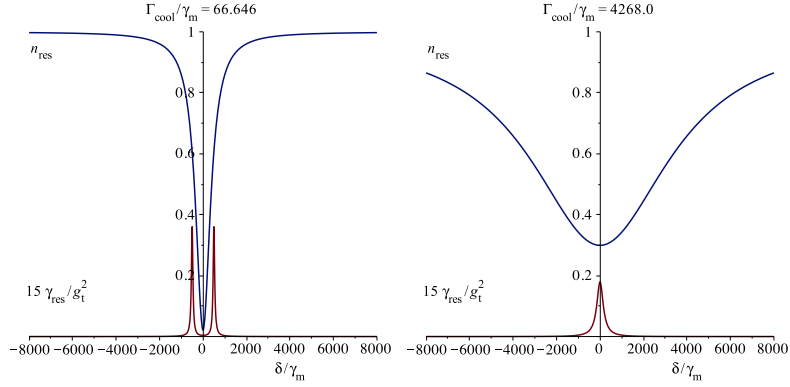


Figure 5.2.3: Illustrative plots of γ_{res} and n_{res} as functions of target detuning δ from the common bare frequency of link and mechanical DoF (i.e., setting $\Delta = -\omega_m$) for $C_m = 10^4$. (Note the exaggeration of γ_{res} by a factor of 15.) The first plot exhibits hybridization of link and mechanical DoF, while the second falls outside the strong coupling regime due to the larger induced rate Γ_{cool} on the mechanical DoF.

RWA in setting up the structured reservoir formalism for our cooling system. In fact the required Fourier space correlation functions can be deduced from the calculation given in Ref. [18].² However, working within the RWA leads to substantially simpler equations. All results obtained are thus subject to the condition that the RWA must be valid for the chosen parameters.

5.3 Harmonic oscillator analysis

A particular benefit of analysing the indirect cooling of a harmonic oscillator degree of freedom is that this particular case is exactly solvable; the exact solution can be obtained by means of the procedures given in section 4.2. This allows for a comparison between the structured reservoir result and the exact solution. From this comparison the stability of the structured reservoir description can be gauged: How far can we deviate from the validity conditions before the effective description breaks down.

The full set of equations of motion for the cooling system connected to a harmonic oscillator target is (in a rotating frame w.r.t. the target frequency)

$$\begin{aligned}
 \dot{\hat{a}} &= -\left[\frac{1}{2}(\gamma_m + \Gamma_{\text{cool}}) + i\delta\right] \hat{a} - \sqrt{\gamma_m} \hat{a}_{\text{in},m} - \sqrt{\Gamma_{\text{cool}}} \hat{a}_{\text{in},\text{cool}} - ig_m \hat{b} \\
 \dot{\hat{b}} &= -\left[\frac{1}{2}\gamma_{\text{link}} + i\tilde{\Delta}\right] \hat{b} - \sqrt{\gamma_{\text{link}}} \hat{b}_{\text{in},\text{link}} - ig_m^* \hat{a} - ig_t^* \hat{c}, \\
 \dot{\hat{c}} &= -\frac{1}{2}\gamma_t \hat{c} - \sqrt{\gamma_t} \hat{c}_{\text{in},t}(t) - ig_t \hat{b},
 \end{aligned} \tag{5.3.1}$$

where \hat{c} is the annihilation operator of the target oscillator.

²Essentially the information is contained in Eqs. (13,14) subject to suitable relabeling.

The first analysis of this particular instance of the indirect cooling scheme will be carried out in the following section using the structured reservoir description of the cooling system arrived at in Section 5.2. Next, in Section 5.3.2, we will solve the full set of equations (5.3.1) exactly.

5.3.1 Structured reservoir treatment

Making the weak coupling/narrow width assumption required by the structured reservoir formalism, $\gamma_t, |g_t| \ll (\gamma_m + \Gamma_{\text{cool}}), \gamma_{\text{link}}$, we may effectively replace Eqs. (5.3.1) by a single Heisenberg-Langevin equation for the target oscillator:

$$\dot{\hat{c}}(t) = -\frac{1}{2}[\gamma_t + \gamma_{\text{res}}]\hat{c}(t) - \sqrt{\gamma_t}\hat{c}_{\text{in},t}(t) - \sqrt{\gamma_{\text{res}}}\hat{F}_{\text{res}}(t), \quad (5.3.2)$$

where $\langle \hat{c}_{\text{in},t}^\dagger(t)\hat{c}_{\text{in},t}(t') \rangle = n_{\text{in},t}\delta(t-t')$ while γ_{res} and the proportionality constant of $\langle \hat{F}_{\text{res}}^\dagger(t)\hat{F}_{\text{res}}(t') \rangle = n_{\text{res}}\delta(t-t')$ are given by Eqs. (5.2.3) and (5.2.5). The steady state occupancy of an oscillator described by such an equation has already been derived in Eq. (5.1.2):

$$n_{\text{HO}}^{(\text{ss})} = \langle \hat{c}^\dagger(t)\hat{c}(t) \rangle_{\text{ss}} = \frac{\gamma_t n_{\text{in},t} + \gamma_{\text{res}} n_{\text{res}}}{\gamma_t + \gamma_{\text{res}}}, \quad (5.3.3)$$

a weighted average of the two reservoir occupancies. The rest of the analysis is concerned with optimizing this expression.

5.3.1.1 General considerations regarding optimization

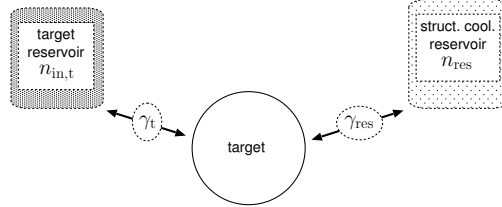


Figure 5.3.1: A cooling target subjected to the influence of two reservoirs: A 'local' thermal reservoir and a structured reservoir (the effective description of the 'indirect' cooling scheme).

We will now consider how to adjust the parameters of the setup in order to cool the target as much as possible. The scenario is depicted in Fig. 5.3.1, a stripped-down version of Fig. 5.2.1. First we must establish which parameters are available for tuning. The target reservoir accounts for environmental influences that we cannot control except by lowering the ambient temperature by means of precooling, thereby lowering $n_{\text{in},t}$. This is technically demanding in practice and hence an option we prefer to avoid. However, in the optimization analysis below we will make a simplifying assumption that renders the effect of manipulating $n_{\text{in},t}$ trivial. Turning to the interaction with the structured cooling reservoir, characterized by the quantities $\gamma_{\text{res}}, n_{\text{res}}$, we start out by making

the following general observations: Given that $n_{\text{res}} < n_{\text{in,t}}$ (as is required for cooling to be possible) it is clear from Eq. (5.3.3) that we would want γ_{res} to be as large as possible in order for the cooling reservoir to dominate the thermal one. Furthermore, we want the effective “temperature” n_{res} of the cooling reservoir to be as low as possible. In short: We want to couple as strongly as possible to a cooling reservoir which is as cold as possible. Unfortunately, these are conflicting requirements as has already been indicated above; as a consequence we must perform simultaneous optimization of the two quantities $\gamma_{\text{res}}, n_{\text{res}}$.

In view of Chapter 2, parameters which we reasonably can assume some control over include $|g_{\text{m}}|$, the link-mechanics coupling strength, and Γ_{cool} , the effective mechanical cooling rate induced by the cavity-assisted cooling mechanism (the driving force behind our scheme). Moreover, the detunings $\delta = \omega_{\text{m}} - \omega_{\text{t}}, \tilde{\Delta} = -(\Delta + \omega_{\text{t}})$ are assumed tunable. In the same vein as for γ_{t} , we assume the thermal reservoir rates $\gamma_{\text{link}}, \gamma_{\text{m}}$ to be given quantities. Finally, it is clear from the expressions for $\gamma_{\text{res}}, n_{\text{res}}$ and the above considerations that we would like $|g_{\text{t}}|$ to be as large as possible, at least to the extent that the structured reservoir description remains valid.

To allow for a relatively simple optimization below, we will assume the occupancy of the assisting cavity reservoir to be essentially zero $n_{\text{cool}} \approx 0$ and all remaining thermal reservoirs to share a common mean occupancy $n_{\text{th}} \equiv n_{\text{in,t}} = n_{\text{link}} = n_{\text{m}}$. The former assumption is an accurate description in the case of an optical cavity assisting the mechanical cooling (in the absence of drive fluctuations), while the latter is true if target, link and mechanical modes are on resonance without the aid of drive fields. Even though these conditions are not fulfilled in general, it is a decent starting point for assessing the potential of the scheme. In view of these simplifying assumptions, we restate Eqs. (5.2.3), (5.2.5), and (5.3.3) as:

$$\frac{n_{\text{HO}}^{(\text{ss})}}{n_{\text{th}}} = \frac{1 + \frac{\gamma_{\text{res}}}{\gamma_{\text{t}}} \frac{n_{\text{res}}}{n_{\text{th}}}}{1 + \frac{\gamma_{\text{res}}}{\gamma_{\text{t}}}} \quad (5.3.4)$$

$$\frac{\gamma_{\text{res}}}{\gamma_{\text{t}}} = \frac{C_{\text{t}}}{4} \frac{1 + \frac{1}{4} C_{\text{m}} \frac{\gamma_{\text{m}}(\gamma_{\text{m}} + \Gamma_{\text{cool}})}{\frac{1}{4}(\gamma_{\text{m}} + \Gamma_{\text{cool}})^2 + \delta^2}}{\frac{1}{4} \left(1 + \frac{1}{4} C_{\text{m}} \frac{\gamma_{\text{m}}(\gamma_{\text{m}} + \Gamma_{\text{cool}})}{\frac{1}{4}(\gamma_{\text{m}} + \Gamma_{\text{cool}})^2 + \delta^2} \right)^2 + d(\delta, \tilde{\Delta})^2} \quad (5.3.5)$$

$$\frac{n_{\text{res}}}{n_{\text{th}}} = \frac{1 + \frac{1}{4} C_{\text{m}} \frac{\gamma_{\text{m}}(\gamma_{\text{m}} + \Gamma_{\text{cool}})}{\frac{1}{4}(\gamma_{\text{m}} + \Gamma_{\text{cool}})^2 + \delta^2} \left(\frac{\gamma_{\text{m}}}{\gamma_{\text{m}} + \Gamma_{\text{cool}}} \right)}{1 + \frac{1}{4} C_{\text{m}} \frac{\gamma_{\text{m}}(\gamma_{\text{m}} + \Gamma_{\text{cool}})}{\frac{1}{4}(\gamma_{\text{m}} + \Gamma_{\text{cool}})^2 + \delta^2}} \quad (5.3.6)$$

where $d(\delta, \tilde{\Delta}) \equiv \tilde{\Delta} - |g_{\text{m}}|^2 \frac{\delta}{\frac{1}{4}(\gamma_{\text{m}} + \Gamma_{\text{cool}})^2 + \delta^2}$ and we have introduced the (unloaded) *cooperativities* of the target-link and link-mechanics couplings, respectively:

$$C_{\text{t}} \equiv \frac{4|g_{\text{t}}|^2}{\gamma_{\text{t}}\gamma_{\text{link}}} \quad \text{and} \quad C_{\text{m}} \equiv \frac{4|g_{\text{m}}|^2}{\gamma_{\text{m}}\gamma_{\text{link}}}.$$

It follows from the remarks made above that we will want the target cooperativity C_{t} as large as possible while C_{m} is considered a tunable parameter to be optimized.

In summary, the parameter set over which we will optimize $n_{\text{HO}}^{(\text{ss})}/n_{\text{th}}$ is $\{C_{\text{m}}, \Gamma_{\text{cool}}, \delta, \tilde{\Delta}\}$. Even though it is reasonable to consider these parameters tunable, in practice

they will only be so to a certain extent, i.e., within some given range determined by the experimental setup. While the detunings $\delta, \tilde{\Delta}$ will be taken to be unrestricted throughout, we will in Section 5.3.1.5 discuss how upper bounds $C_m^{(\max)}, \Gamma_{\text{cool}}^{(\max)}$ on the range of practically available values of C_m and Γ_{cool} affect the optimization. To keep things separate, we perform the optimization refraining from interpreting the physics of the results until Section 5.3.1.6.

Candidates for minima of the function $(n_{\text{HO}}^{(\text{ss})}/n_{\text{th}})(C_m, \Gamma_{\text{cool}}, \delta, \tilde{\Delta})$ are given as the simultaneous solutions to the equations $\nabla(n_{\text{HO}}^{(\text{ss})}/n_{\text{th}}) = \vec{0}$. As shown in Appendix A.2, it is permissible to perform the optimization by: 1) Finding the minimum of $n_{\text{HO}}^{(\text{ss})}/n_{\text{th}}$ w.r.t. to one parameter as a function of the remaining ones, 2) evaluate $n_{\text{HO}}^{(\text{ss})}/n_{\text{th}}$ at this function, 3) proceed by minimizing w.r.t. the next parameter and so on. This is the strategy we shall follow below.

5.3.1.2 Optimal detunings $\delta, \tilde{\Delta}$: Identifying weak coupling vs. hybridized regimes

We start the optimization by determining the optimal values of the detunings $\delta, \tilde{\Delta}$. First off, given tunability of $\tilde{\Delta}$ we may always pick the value of this parameter so that the function $d(\delta, \tilde{\Delta} = \tilde{\Delta}_{(\text{opt})})$ vanishes:

$$\tilde{\Delta}_{(\text{opt})} \equiv |g_m|^2 \frac{\delta}{\frac{1}{4}(\gamma_m + \Gamma_{\text{cool}})^2 + \delta^2}.$$

This is indeed the optimal value of $\tilde{\Delta}$ because this parameter only enters through $d(\delta, \tilde{\Delta})$ in $\gamma_{\text{res}}/\gamma_t$, hence we can maximize the latter individually w.r.t. $\tilde{\Delta}$ without the risk of increasing $n_{\text{res}}/n_{\text{th}}$. Obviously this maximum occurs for $d(\delta, \tilde{\Delta}_{(\text{opt})}) = 0$ and inserting this value into Eq. (5.3.5) results in

$$\left. \frac{\gamma_{\text{res}}}{\gamma_t} \right|_{d(\delta, \tilde{\Delta})=0} = \frac{C_t}{1 + \frac{1}{4}C_m \frac{\gamma_m(\gamma_m + \Gamma_{\text{cool}})}{\frac{1}{4}(\gamma_m + \Gamma_{\text{cool}})^2 + \delta^2}}. \quad (5.3.7)$$

Henceforth, we will implicitly fix $\tilde{\Delta} = \tilde{\Delta}_{(\text{opt})}$ unless otherwise noted. On the basis of Eqs. (5.3.6) and (5.3.7) we may then minimize $n_{\text{HO}}^{(\text{ss})}/n_{\text{th}}$, Eq. (5.3.4), w.r.t. the remaining detuning δ that now only enters as δ^2 :

$$\left[\frac{\partial}{\partial(\delta^2)} \frac{n_{\text{HO}}^{(\text{ss})}}{n_{\text{th}}} \right]_{\delta^2=\delta_{(\text{opt})}^2} = 0 \Rightarrow \delta_{(\text{opt})}^2 = \gamma_m^2 \left(1 + \frac{\Gamma_{\text{cool}}}{\gamma_m} \right) \left[\frac{C_m}{\sqrt{1+C_t}} - \left(1 + \frac{\Gamma_{\text{cool}}}{\gamma_m} \right) \right], \quad (5.3.8)$$

from which it can be seen that when the bracketed term of Eq. (5.3.8) is positive, the equation yields a non-zero $|\delta_{(\text{opt})}|$; in case the bracketed term is negative, there is no optimum on the interior of the interval $\delta^2 \in [0; \infty[$ in which case the minimum of $n_{\text{HO}}^{(\text{ss})}/n_{\text{th}}$ can be seen to occur for $\delta_{(\text{opt})} = 0$. Hence, in terms of the Heaviside step function $H[x]$,

$$\delta_{(\text{opt})}^2 = H \left[\frac{C_m}{\sqrt{1+C_t}} - \left(1 + \frac{\Gamma_{\text{cool}}}{\gamma_m} \right) \right] \gamma_m^2 \left(1 + \frac{\Gamma_{\text{cool}}}{\gamma_m} \right) \left[\frac{C_m}{\sqrt{1+C_t}} - \left(1 + \frac{\Gamma_{\text{cool}}}{\gamma_m} \right) \right] \quad (5.3.9)$$

The condition for a non-zero $\delta_{(\text{opt})}$ is equivalent to

$$\frac{C_m}{\sqrt{1+C_t}} > \left(1 + \frac{\Gamma_{\text{cool}}}{\gamma_m}\right) \Leftrightarrow \frac{4|g_m|^2}{\gamma_{\text{link}}(\gamma_m + \Gamma_{\text{cool}})} > \sqrt{1+C_t},$$

a strong coupling criterion for the cooling system (link and mechanical mode) entailing hybridization between these two degrees of freedom, see Fig. 5.2.3. Based on these findings we go on to analyze the weak and strong coupling regimes, $\delta_{(\text{opt})} = 0$ and $|\delta_{(\text{opt})}| > 0$, separately, with the intention of eventually combining the two to find the global optimum.

5.3.1.3 Optimization analysis for the weak coupling regime, $\delta_{(\text{opt})} = 0$

Note that $\delta = 0$ entails $\tilde{\Delta}_{(\text{opt})} = 0$, so that all three subsystems - target, link and mechanical modes - are indeed resonant. By setting $\delta = 0$ in Eqs. (5.3.6) and (5.3.7), these expressions simplify to

$$\begin{aligned} \left. \frac{\gamma_{\text{res}}}{\gamma_t} \right|_{\delta=0} &= \frac{C_t}{1 + C_m \frac{\gamma_m}{\gamma_m + \Gamma_{\text{cool}}}} \\ \left. \frac{n_{\text{res}}}{n_{\text{th}}} \right|_{\delta=0} &= \frac{1 + C_m \frac{\gamma_m}{\gamma_m + \Gamma_{\text{cool}}} \left(\frac{\gamma_m}{\gamma_m + \Gamma_{\text{cool}}} \right)}{1 + C_m \frac{\gamma_m}{\gamma_m + \Gamma_{\text{cool}}}}. \end{aligned} \quad (5.3.10)$$

Optimal Γ_{cool} for fixed C_m Minimizing $n_{\text{HO}}^{(\text{ss})}/n_{\text{th}}$, Eq. (5.3.4), with respect to Γ_{cool} for fixed C_m and $\delta = 0$ we obtain

$$\left. \frac{d}{d\Gamma_{\text{cool}}} \left(\left. \frac{n_{\text{HO}}^{(\text{ss})}}{n_{\text{th}}} \right|_{\delta=0} \right) \right|_{\Gamma_{\text{cool}}=\Gamma_{\text{cool}}^{(\text{opt})}} = 0 \Rightarrow \frac{\Gamma_{\text{cool}}^{(\text{opt})}}{\gamma_m} = \sqrt{\frac{(1+C_m)(1+C_t+C_m)}{1+C_t}} \quad (5.3.11)$$

as the only solution; since $(n_{\text{HO}}^{(\text{ss})}/n_{\text{th}})|_{\delta=0} = 1$ at both boundaries of $\Gamma_{\text{cool}} \in [0; \infty[$, $\Gamma_{\text{cool}}^{(\text{opt})}/\gamma_m$ must be a minimum point (since we cannot heat the target). Importantly, by rewriting this expression as

$$\frac{\Gamma_{\text{cool}}^{(\text{opt})}}{\gamma_m} = \frac{1+C_m}{\sqrt{1+C_t}} \sqrt{1 + \frac{C_t}{1+C_m}} > \frac{C_m}{\sqrt{1+C_t}} - 1,$$

we see from what was gathered in Section 5.3.1.2 that the quantity $\Gamma_{\text{cool}}^{(\text{opt})}$, Eq. (5.3.11), lies *within* the weak coupling regime for which $\delta = 0$ and $\tilde{\Delta} = 0$ are indeed optimal. Evaluating $(n_{\text{HO}}^{(\text{ss})}/n_{\text{th}})|_{\delta=0}$, Eq. (5.3.4), at $\Gamma_{\text{cool}}^{(\text{opt})}$ we find the minimal steady state occupancy of the target relative to that of the ‘‘intrinsic’’ thermal reservoirs as a function of C_m

$$\left. \frac{n_{\text{HO}}^{(\text{ss})}}{n_{\text{th}}} \right|_{\delta=0, \Gamma_{\text{cool}}=\Gamma_{\text{cool}}^{(\text{opt})}} = \frac{2}{1 + \sqrt{\frac{(1+C_t)(1+C_m)}{1+C_t+C_m}}}. \quad (5.3.12)$$

The minimum in the weak coupling regime is achieved by taking $C_m \rightarrow \infty$, which means that also $\Gamma_{\text{cool}}^{(\text{opt})} \rightarrow \infty$: $(n_{\text{HO}}^{(\text{ss})}/n_{\text{th}}) \rightarrow 2(1 + \sqrt{1+C_t})^{-1}$. As this set of parameters is unreachable in practice, we will in a Section 5.3.1.5 optimize subject to restricted parameter ranges as promised earlier. In preparation for this, it is necessary to instead fix Γ_{cool} and optimize w.r.t. C_m .

Optimal C_m for fixed Γ_{cool} Thus, on the other hand minimizing $n_{\text{HO}}^{(\text{ss})}/n_{\text{th}}$ with respect to C_m for fixed Γ_{cool} and $\delta = 0$ we find

$$\left. \frac{d}{dC_m} \left(\frac{n_{\text{HO}}^{(\text{ss})}}{n_{\text{th}}} \right) \right|_{\delta=0} \Bigg|_{C_m=C_m^{(\text{opt})}} = 0 \Rightarrow C_m^{(\text{opt})} = \sqrt{1 + C_t} \left(1 + \frac{\Gamma_{\text{cool}}}{\gamma_m} \right), \quad (5.3.13)$$

as the only solution. It lies exactly on the boundary between the weak coupling and hybridized regimes; to be clear, the (one-sided) derivative vanishes at this point, but we cannot conclude at this point that $C_m = C_m^{(\text{opt})}$ is a minimum. If C_m is increased beyond the value given by Eq. (5.3.13) while keeping Γ_{cool} fixed, then no longer is $\delta_{(\text{opt})} = 0$ and hence Eqs. (5.3.10) would fail to be the relevant expressions to consider for these sets of values $(C_m, \Gamma_{\text{cool}})$ according to Section 5.3.1.2. To find the global optimum we must therefore analyse the hybridized regime.

5.3.1.4 Optimization analysis for the hybridized regime, $\delta_{(\text{opt})}^2 > 0$

We now consider the strong coupling/hybridized regime identified in Section 5.3.1.2, i.e., the part of parameter space $(C_m, \Gamma_{\text{cool}})$ where $\frac{C_m}{\sqrt{1+C_t}} > \left(1 + \frac{\Gamma_{\text{cool}}}{\gamma_m} \right)$, δ and $\tilde{\Delta}$ being fixed at their optimal values (as functions of the former two). To this end, we evaluate Eqs. (5.3.6) and (5.3.7) at $\delta = \delta_{(\text{opt})}(C_m, \Gamma_{\text{cool}}) \neq 0$ as given by Eq. (5.3.8) and insert them into $n_{\text{HO}}^{(\text{ss})}/n_{\text{th}}$, Eq. (5.3.4), thereby arriving at the strong coupling occupancy

$$\left. \frac{n_{\text{HO}}^{(\text{ss})}}{n_{\text{th}}} \right|_{\delta^2=\delta_{(\text{opt})}^2>0} = \frac{2 + \frac{C_t}{1+\sqrt{1+C_t}} \frac{1}{1+\frac{\Gamma_{\text{cool}}}{\gamma_m}}}{1 + \sqrt{1 + C_t}}, \quad (5.3.14)$$

valid for $\frac{\Gamma_{\text{cool}}}{\gamma_m} \leq \frac{C_m}{\sqrt{1+C_t}} - 1$. Notably, Eq. (5.3.14) is independent of C_m . Taken together with what was found in the second half of Section 5.3.1.3 regarding the weak coupling regime, where $\left. (n_{\text{HO}}^{(\text{ss})}/n_{\text{th}}) \right|_{\delta=\delta_{(\text{opt})}=0}$ was sought minimized w.r.t. C_m , this shows that the minimum of $n_{\text{HO}}^{(\text{ss})}/n_{\text{th}}$ w.r.t. C_m for fixed Γ_{cool} is achieved for any $C_m \in [\sqrt{1+C_t}(1 + \Gamma_{\text{cool}}/\gamma_m); \infty[$, that is, any value C_m which puts $(C_m, \Gamma_{\text{cool}})$ in the strong coupling regime. Put differently, as we approach the strong coupling regime by increasing C_m (for fixed Γ_{cool}) the slope of $\left. (n_{\text{HO}}^{(\text{ss})}/n_{\text{th}}) \right|_{\delta=\delta_{(\text{opt})}}$ along the C_m -axis approaches zero until, crossing the boundary, it settles at exactly zero in the strong coupling regime (a plot illustrating this is provided in Fig. 5.3.2).

Finally, we minimize $\left. (n_{\text{HO}}^{(\text{ss})}/n_{\text{th}}) \right|_{\delta^2=\delta_{(\text{opt})}^2>0}$, Eq. (5.3.14), with respect to Γ_{cool} (for fixed C_m , entering the upper bound of the domain): The fact that the slope w.r.t. to Γ_{cool} is negative on the entire strong coupling domain implies that no candidates for a minimum is to be found here. This allows us to conclude that for fixed C_m the *global* minimum of $n_{\text{HO}}^{(\text{ss})}/n_{\text{th}}$ occurs at $\Gamma_{\text{cool}} = \Gamma_{\text{cool}}^{(\text{opt})}$ given by Eq. (5.3.11), the value indentified within the weak coupling regime (thus, $\delta_{(\text{opt})} = \tilde{\Delta}_{(\text{opt})} = 0$).

5.3.1.5 Optimization given restricted parameter ranges

In reality, the parameters $C_m, \Gamma_{\text{cool}}$ will be restricted to certain finite ranges $C_m \in [0; C_m^{(\text{max})}]$, $\Gamma_{\text{cool}} \in [0; \Gamma_{\text{cool}}^{(\text{max})}]$. Therefore, we would like to be able to assess the achievable degree of cooling in an implementation with a given set of parameters $\{C_t^{(\text{max})}, C_m^{(\text{max})}, \Gamma_{\text{cool}}^{(\text{max})}\}$; recall that, as argued early on, it is always advantageous to have the highest possible coupling to the target system so that $C_t^{(\text{opt})} = C_t^{(\text{max})}$, independent of the other parameters (therefore this has simply been denoted C_t in the above calculation).

In the course of the analysis given in the previous sections we have found that the only minimum of the function $(n_{\text{HO}}^{(\text{ss})}/n_{\text{th}}) \Big|_{\delta^2 = \delta_{(\text{opt})}^2}$ on the domain $(C_m, \Gamma_{\text{cool}}) \in \mathbb{R}_+^2$ is an asymptotic one as both parameters approach infinity (in certain ways). Thus, the global minimum value in the presence of finite ranges must occur somewhere on the boundary³ $\{(C_m^{(\text{max})}, \Gamma_{\text{cool}})\}_{\Gamma_{\text{cool}} \in [0; \Gamma_{\text{cool}}^{(\text{max})}] \cup \{(C_m, \Gamma_{\text{cool}}^{(\text{max})})\}_{C_m \in [0; C_m^{(\text{max})}]}$. Any pair of parameters $\{C_m^{(\text{max})}, \Gamma_{\text{cool}}^{(\text{max})}\}$ falls within one of the following three distinct cases as we will establish shortly: (C_m, C_t) -limited, $(\Gamma_{\text{cool}}, C_t)$ -limited or a third, intermediate regime. These are illustrated in Fig. 5.3.2.

(C_m, C_t) -limited regime

This is characterized by the following relationship between the upper bounds

$$\frac{\Gamma_{\text{cool}}^{(\text{max})}}{\gamma_m} \geq \sqrt{\frac{(1 + C_m^{(\text{max})})(1 + C_t^{(\text{max})} + C_m^{(\text{max})})}{1 + C_t^{(\text{max})}}}.$$

In this case, for any fixed $C_m \in [0; C_m^{(\text{max})}]$ the corresponding $\Gamma_{\text{cool}}^{(\text{opt})}$ given by Eq. (5.3.11) will not exceed $\Gamma_{\text{cool}}^{(\text{max})}$; thus, we can consider Γ_{cool} unrestricted and optimize Eq. (5.3.12) on the interval $C_m \in [0; C_m^{(\text{max})}]$. The minimum occurs for $C_m = C_m^{(\text{max})}$ yielding the following global minimum occupancy on the space of available parameter values

$$\frac{n_{\text{HO}}^{(\text{ss})}}{n_{\text{th}}} \Big|_{\text{opt.}} = \frac{2}{1 + \sqrt{\frac{(1 + C_t^{(\text{max})})(1 + C_m^{(\text{max})})}{1 + C_t^{(\text{max})} + C_m^{(\text{max})}}}}. \quad (5.3.15)$$

$(\Gamma_{\text{cool}}, C_t)$ -limited regime

This second regime occurs when the upper bounds satisfy

$$\frac{\Gamma_{\text{cool}}^{(\text{max})}}{\gamma_m} \leq \frac{C_m^{(\text{max})}}{\sqrt{1 + C_t^{(\text{max})}}} - 1.$$

³Precluding boundary segments along which either C_m or Γ_{cool} are zero.

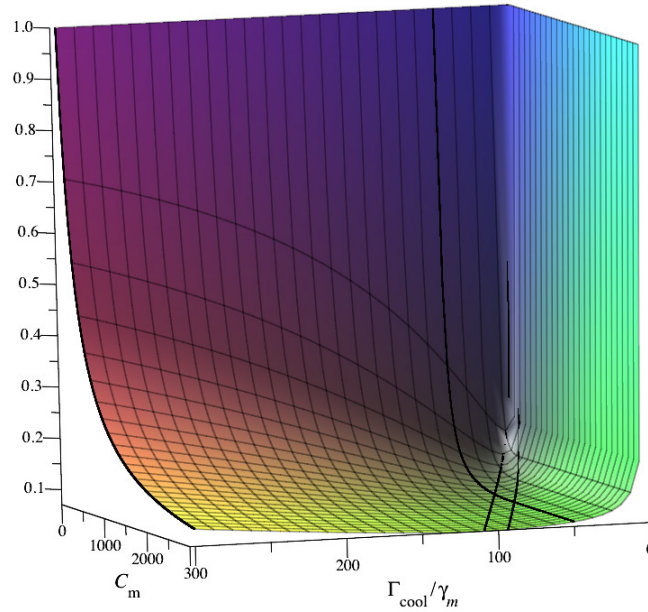


Figure 5.3.2: Plot of minimal occupancy as function of $C_m, \tilde{\Gamma}_{\text{cool}}$ for fixed $C_t = 1000$. Two black “diagonal” lines are shown in the plot, the rightmost of which is the hybridization boundary. We visualize the three parameter regimes by truncating the $\tilde{\Gamma}_{\text{cool}}$ -axis at different $\tilde{\Gamma}_{\text{cool}}^{(\text{max})}$ (black lines perpendicular to that axis): The leftmost cut, $\tilde{\Gamma}_{\text{cool}}^{(\text{max})} = 300$, puts us in the (C_m, C_t) -limited regime with the optimum occurring at the leftmost diagonal line at $C_m = C_m^{(\text{opt})}$. Next, the rightmost cut, $\tilde{\Gamma}_{\text{cool}}^{(\text{max})} = 50$, brings us into the $(\Gamma_{\text{cool}}, C_t)$ -limited regime with the optimum value being achieved for any point along the cut at or above the hybridization threshold (rightmost diagonal line). Finally, if the “corner” of the domain of available values $(C_m^{(\text{opt})}, \Gamma_{\text{cool}}^{(\text{max})})$ lie between the two diagonal lines, then we are in the intermediate regime for which the optimum is obtained at the corner.

Here, the roles are reversed so that for any fixed $\Gamma_{\text{cool}} \in [0; \Gamma_{\text{cool}}^{(\text{max})}]$, $C_m^{(\text{opt})}$ given by Eq. (5.3.13) does not exceed $C_m^{(\text{max})}$; hence C_m can be considered unrestricted and, recalling that $C_m^{(\text{opt})}$ traces out the strong coupling boundary, we are prompted to optimize Eq. (5.3.14) on the entire interval $\Gamma_{\text{cool}} \in [0; \Gamma_{\text{cool}}^{(\text{max})}]$ resulting in $\Gamma_{\text{cool}} = \Gamma_{\text{cool}}^{(\text{max})}$ and the global minimum occupancy of

$$\left. \frac{n_{\text{HO}}^{(\text{ss})}}{n_{\text{th}}} \right|_{\text{opt.}} = \frac{2 + \frac{C_t^{(\text{max})}}{1 + \sqrt{1 + C_t^{(\text{max})}}} \frac{1}{1 + \frac{\Gamma_{\text{cool}}^{(\text{max})}}{\gamma_m}}}{1 + \sqrt{1 + C_t^{(\text{max})}}}. \quad (5.3.16)$$

Note that for given $\Gamma_{\text{cool}}^{(\text{max})}$ (within the $(\Gamma_{\text{cool}}, C_t)$ -limited regime) this occupancy may be achieved for any $C_m \in [C_m^{(\text{opt})}; C_m^{(\text{max})}]$ as the minimum occupancy is independent of C_m in the strong coupling regime, $C_m \geq C_m^{(\text{opt})}$; however, the

required detunings $\delta_{(\text{opt})}$, $\tilde{\Delta}_{(\text{opt})}$ will start to deviate from zero as we move into the interior of the hybridized regime.

Intermediate regime

Finally a third regime arises when $\Gamma_{\text{cool}}^{(\text{max})}/\gamma_{\text{m}}$ is in the remaining, intermediate interval:

$$\frac{C_{\text{m}}^{(\text{max})}}{\sqrt{1+C_{\text{t}}^{(\text{max})}}} - 1 < \frac{\Gamma_{\text{cool}}^{(\text{max})}}{\gamma_{\text{m}}} < \sqrt{\frac{(1+C_{\text{m}}^{(\text{max})})(1+C_{\text{t}}^{(\text{max})}+C_{\text{m}}^{(\text{max})})}{1+C_{\text{t}}^{(\text{max})}}}$$

Considering first the boundary segment $\{(C_{\text{m}}, \Gamma_{\text{cool}}^{(\text{max})})\}_{C_{\text{m}} \in [0; C_{\text{m}}^{(\text{max})}]}$ of fixed $\Gamma_{\text{cool}} = \Gamma_{\text{cool}}^{(\text{max})}$, we note that $\left. \frac{\partial}{\partial C_{\text{m}}} (n_{\text{HO}}^{(\text{ss})}/n_{\text{th}}) \right|_{\delta^2 = \delta_{(\text{opt})}^2}$ on this interval is negative. This can be seen from the fact that the only extremum, a minimum, on the larger segment $\{(C_{\text{m}}, \Gamma_{\text{cool}}^{(\text{max})})\}_{C_{\text{m}} \in [0; \infty[}$ occurs at $C_{\text{m}} = \sqrt{1+C_{\text{t}}^{(\text{max})}}(1+\Gamma_{\text{cool}}^{(\text{max})}/\gamma_{\text{m}}) > C_{\text{m}}^{(\text{max})}$ (the inequality follows from the definition of the intermediate regime); thus, the function must decrease monotonously on the segment under consideration. From this it follows that the only minimum candidate on this segment is $(C_{\text{m}}^{(\text{max})}, \Gamma_{\text{cool}}^{(\text{max})})$.

Completely parallel arguments apply to the other boundary segment, $\{(C_{\text{m}}^{(\text{max})}, \Gamma_{\text{cool}})\}_{\Gamma_{\text{cool}} \in [0; \Gamma_{\text{cool}}^{(\text{max})}]}$. The only minimum on the supersegment $\{(C_{\text{m}}^{(\text{max})}, \Gamma_{\text{cool}})\}_{\Gamma_{\text{cool}} \in [0; \infty[}$ occurs at

$$\frac{\Gamma_{\text{cool}}}{\gamma_{\text{m}}} = \sqrt{\frac{(1+C_{\text{m}}^{(\text{max})})(1+C_{\text{t}}^{(\text{max})}+C_{\text{m}}^{(\text{max})})}{1+C_{\text{t}}^{(\text{max})}}} > \frac{\Gamma_{\text{cool}}^{(\text{max})}}{\gamma_{\text{m}}},$$

therefore the minimum candidate must be located at the upper endpoint $(C_{\text{m}}^{(\text{max})}, \Gamma_{\text{cool}}^{(\text{max})})$, coinciding with the candidate of the first segment.

Based on this we conclude that in the intermediate regime the optimal choice is $(C_{\text{m}}^{(\text{max})}, \Gamma_{\text{cool}}^{(\text{max})})$. We note that it follows from the definition of the intermediate regime that the parameter pair $(C_{\text{m}}^{(\text{max})}, \Gamma_{\text{cool}}^{(\text{max})})$ lies within the weak coupling regime for which $\delta_{(\text{opt})} = \tilde{\Delta}_{(\text{opt})} = 0$. Hence, we may obtain the minimum occupancy by evaluating γ_{res} and n_{res} , Eqs. (5.3.10), at $(C_{\text{m}}^{(\text{max})}, \Gamma_{\text{cool}}^{(\text{max})})$ and combine these quantities in the usual combination, Eq. (5.3.4). The resulting expression for the optimal steady state occupancy depends on all three maximal values, $(C_{\text{t}}^{(\text{max})}, C_{\text{m}}^{(\text{max})}, \Gamma_{\text{cool}}^{(\text{max})})$, and hence neither is specifically limiting the cooling performance. For the same reason, it is hard to rewrite the result in a particularly revealing form, but we state it here for later reference (to shorten the notation we have introduced the dimensionless quantity $\tilde{\Gamma}_{\text{cool}}^{(\text{max})} \equiv \Gamma_{\text{cool}}^{(\text{max})}/\gamma_{\text{m}}$):

$$\left. \frac{n_{\text{HO}}^{(\text{ss})}}{n_{\text{th}}} \right|_{\text{opt.}} = \frac{(1+\tilde{\Gamma}_{\text{cool}}^{(\text{max})}+C_{\text{m}}^{(\text{max})})^2 + C_{\text{t}}^{(\text{max})}[(1+\tilde{\Gamma}_{\text{cool}}^{(\text{max})})^2 + C_{\text{m}}^{(\text{max})}]}{(1+\tilde{\Gamma}_{\text{cool}}^{(\text{max})}+C_{\text{m}}^{(\text{max})})^2 + C_{\text{t}}^{(\text{max})}(1+\tilde{\Gamma}_{\text{cool}}^{(\text{max})}+C_{\text{m}}^{(\text{max})})(1+\tilde{\Gamma}_{\text{cool}}^{(\text{max})})}. \quad (5.3.17)$$

5.3.1.6 Bottleneck interpretation of the results

Moving on to interpreting the above results physically, we remark that it is meaningful to think of the cooling scenario in terms of bottlenecks. It is obvious from a physical standpoint that setting either of $\{C_t, C_m, \Gamma_{\text{cool}}\}$ equal to zero will break the cooling chain connecting target with the cooling source. However, apart from such extreme cases perhaps, it is not immediately obvious which are the relevant bottlenecks to consider (judging from the equations of motion, for instance). But now that we have solved the problem fully (within the limits of the approximations employed), we are in a position to identify the relevant combinations of parameters which can reasonable be interpreted as constituting bottlenecks in the cooling performance.

Only three different quantities appear in the final expressions given in the previous section: $\{C_t^{(\text{max})}, C_m^{(\text{max})}, \tilde{\Gamma}_{\text{cool}}^{(\text{max})} \equiv \Gamma_{\text{cool}}^{(\text{max})}/\gamma_m\}$, all of them dimensionless. In the three regimes indentified there, distinguished by different relationships among the three parameters, either of $\{C_m^{(\text{max})}, \tilde{\Gamma}_{\text{cool}}^{(\text{max})}\}$ may drop out of the formula for the steady state occupancy of the target; these are the (C_m, C_t) - and $(\Gamma_{\text{cool}}, C_t)$ -limited regimes, respectively. The reason that no regime arises where $C_t^{(\text{max})}$ drops out of the expression for the final occupancy is that the theory was derived specifically in the weak target coupling limit. Because of this, the strong coupling effects present in the theory that lead to saturation for C_m are absent for the target-link coupling quantified by C_t . We will now provide a physical interpretation of the results in the three parameter regimes identified above.

(C_m, C_t) -limited regime

$$\frac{\Gamma_{\text{cool}}^{(\text{max})}}{\gamma_m} \geq \sqrt{\frac{(1 + C_m^{(\text{max})})(1 + C_t^{(\text{max})} + C_m^{(\text{max})})}{1 + C_t^{(\text{max})}}}$$

In practical terms, this is the regime where we have good control over the cavity-assisted cooling of the mechanical degree of freedom to the extent that we are able to tune the cooling rate Γ_{cool} to the optimal value of

$$\frac{\Gamma_{\text{cool}}^{(\text{opt})}}{\gamma_m} = \sqrt{\frac{(1 + C_m^{(\text{max})})(1 + C_t^{(\text{max})} + C_m^{(\text{max})})}{1 + C_t^{(\text{max})}}}$$

resulting in the target occupancy given by Eq. (5.3.15). We may say that this is the regime where there is no bottleneck related to the cavity-assisted cooling. It remains to be characterized in what way the two limiting parameters (C_m, C_t) give rise to bottlenecks. For significant cooling we must have $C_t^{(\text{max})}, C_m^{(\text{max})} \gg 1$ and under these conditions we may approximate the target occupancy, Eq. (5.3.15), in terms of the *reduced cooperativity* $C_{\text{red}}^{(\text{max})-1} \equiv C_t^{(\text{max})-1} + C_m^{(\text{max})-1}$, as

$$\left. \frac{n_{\text{HO}}^{(\text{ss})}}{n_{\text{th}}} \right|_{\text{opt.}} = \frac{2}{1 + \sqrt{\frac{(1+C_t^{(\text{max})})(1+C_m^{(\text{max})})}{1+C_t^{(\text{max})}+C_m^{(\text{max})}}} \approx \frac{2}{1 + \sqrt{C_{\text{red}}^{(\text{max})}}} \approx \frac{2}{\sqrt{C_{\text{red}}^{(\text{max})}}}. \quad (5.3.18)$$

An analogy from the realm of electric circuits is the reduced electric conductance of two resistive elements connected in series. Conductance may be defined as inverse resistance and the former is the more relevant notion for purposes of analogy to the cooperativities, since larger conductance implies larger current in parallel to larger cooperativity leading to increased cooling. This physical scenario has the same topology as our indirect cooling scheme and we may parallel the flow of electrical current to the extraction of heat from the target.

Inherent in the reciprocal addition is the feature that if one of the constituents is significantly larger than the other, then it effectively vanishes from the reciprocal sum, leaving the reduced quantity equal to the smaller of the constituents. In the circuit scenario this corresponds to replacing one of the two resistors by a conductor. We may thus tap into our intuition about this situation in order to understand the cooling scheme in the regime where we are not limited by the cavity-assisted cooling mechanism.

If the individual cooperativities are comparable, $C_t^{(\max)} \sim C_m^{(\max)}$, they both contribute significantly to $C_{\text{red}}^{(\max)}$ that quantifies the width of the bottleneck which is hence a joint bottleneck of the two parameters. On the other hand, if they are not of comparable magnitude then $C_{\text{red}}^{(\max)} \approx \min[C_t^{(\max)}, C_m^{(\max)}]$, in analogy to what was described above, and hence either $C_t^{(\max)}$ or $C_m^{(\max)}$ is the bottleneck. Considering the latter case in the context of Eq. (5.3.18), we see that if the individual cooperativities are very different, $C_t^{(\max)} \gg\gg C_m^{(\max)}$, then the first expression of the equation is approximately

$$\left. \frac{n_{\text{HO}}^{(\text{ss})}}{n_{\text{th}}} \right|_{\text{opt.}} \approx \frac{2}{1 + \sqrt{1 + \min[C_t^{(\max)}, C_m^{(\max)}]}} \approx \frac{2}{\sqrt{\min[C_t^{(\max)}, C_m^{(\max)}]}}, \quad (5.3.19)$$

where in the latter expression we have again taken the limit of significant cooling, $C_t^{(\max)}, C_m^{(\max)} \gg 1$. Note that the reduced cooperativity will always obey $C_{\text{red}}^{(\max)} \leq C_t^{(\max)}, C_m^{(\max)}$.

It is now time to compare the optimum in Eq. (5.3.19) of the 'indirect' scheme to that of the 'direct' scheme considered for the LC circuit mode in Section 5.1.2. In the 'indirect' scheme the optimum is $\max\{\sqrt{\gamma_t \gamma_{\text{link}}}/|g_t|; \sqrt{\gamma_m \gamma_{\text{link}}}/|g_m|\}$ whereas in Eq. (5.1.8) for the 'direct' cooling we found the optimum $\gamma_{\text{LC}}/|g_m|$ expressed as fractions of the thermal occupancy. Since $\gamma_t \ll \gamma_{\text{link}}$ (and typically also $\gamma_m \ll \gamma_{\text{link}}$), this is a very positive result as it shows that 'indirect' cooling via a rapidly decaying link, for instance an LC circuit mode $\gamma_{\text{link}} = \gamma_{\text{LC}}$, may be performed much more efficiently than 'direct' cooling of the link itself. The result shows that weak coupling $|g_t|$ may be compensated for by a long lifetime $1/\gamma_t$. Returning to the fridge analogy suggested previously in this chapter, we can in fact cool the food even in absence of significant cooling of the air in the fridge. We illustrate this unusual situation by showing simultaneous plots of the target and link steady state occupancies for the resonant case, see Fig. 5.3.3. In the limit where the structured reservoir description is valid, the occupancy of the link system is simply that given by Eq. 5.1.4, that is, the occupancy of the link in absence of a target, $|g_t| = 0$.

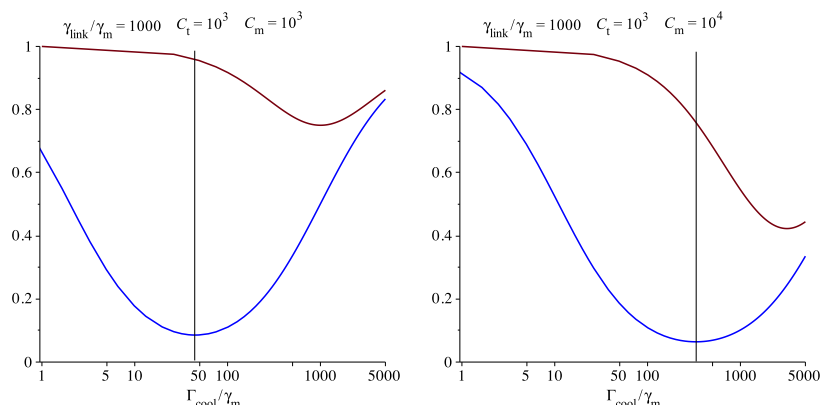


Figure 5.3.3: Plots of target and link occupancies as a function of $\Gamma_{\text{cool}}/\gamma_m$ for the on-resonant case with $C_t = 10^3$, $(\gamma_{\text{link}}/\gamma_m) = 10^3$. We see that the minimum occupancy for the target in general occurs for a value of $\Gamma_{\text{cool}}/\gamma_m$ for which little link cooling is achieved (see black lines).

$(\Gamma_{\text{cool}}, C_t)$ -limited regime

$$\frac{\Gamma_{\text{cool}}^{(\max)}}{\gamma_m} \leq \frac{C_m^{(\max)}}{\sqrt{1 + C_t^{(\max)}}} - 1$$

This corresponds to the situation where we are able to achieve strong coupling between the mechanical mode and the link mode for any value of Γ_{cool} available to us. To get an understanding for this regime, we consider the formula (5.3.16) for the minimal occupancy in the significant cooling limit $C_t^{(\max)} \gg 1$, $(\Gamma_{\text{cool}}^{(\max)})/\gamma_m \gg 1$

$$\left. \frac{n_{\text{HO}}^{(\text{ss})}}{n_{\text{th}}} \right|_{\text{opt.}} = \frac{2 + \frac{C_t^{(\max)}}{1 + \sqrt{1 + C_t^{(\max)}}} \frac{1}{1 + \frac{\Gamma_{\text{cool}}^{(\max)}}{\gamma_m}}}{1 + \sqrt{1 + C_t^{(\max)}}} \approx \frac{2 + \sqrt{C_t^{(\max)}} \left(\frac{\Gamma_{\text{cool}}^{(\max)}}{\gamma_m} \right)^{-1}}{\sqrt{C_t^{(\max)}}} = \frac{2}{\sqrt{C_t^{(\max)}}} + \frac{\gamma_m}{\Gamma_{\text{cool}}^{(\max)}}.$$

Hence, we see that we will be limited by the smaller of the quantities $(\sqrt{C_t^{(\max)}}/2)$, $(\Gamma_{\text{cool}}^{(\max)})/\gamma_m$. This is very much compatible with the picture we arrived at in the (C_m, C_t) -limited regime above, see Eq. (5.3.19). In fact, by examining the defining conditions of the (C_m, C_t) - and $(\Gamma_{\text{cool}}, C_t)$ -limited regimes, it can be verified that we can consistently combine the two in writing

$$\left. \frac{n_{\text{HO}}^{(\text{ss})}}{n_{\text{th}}} \right|_{\text{opt.}} \approx \max \left[\frac{2}{\sqrt{C_t^{(\max)}}}, \frac{2}{\sqrt{C_m^{(\max)}}}, \frac{\gamma_m}{\Gamma_{\text{cool}}^{(\max)}} \right], \quad (5.3.20)$$

valid in the significant cooling limit $C_t^{(\max)}, C_m^{(\max)}, (\Gamma_{\text{cool}}^{(\max)})/\gamma_m \gg 1$ when one of the arguments in Eq. (5.3.20) is significantly larger than the two others. This simple expression captures the essence of the bottlenecks that limit the performance of the 'indirect' cooling scheme. We must, however, check that this picture is consistent with the third, intermediate regime.

Intermediate regime

To see if Eq. (5.3.20) is compatible with this regime, we examine the expression for the occupancy, Eq. (5.3.17), in the cases $C_m^{(\max)} \gg C_t^{(\max)}$ and $C_m^{(\max)} \ll C_t^{(\max)}$ below.

If $C_m^{(\max)} \ll C_t^{(\max)}$, it follows from the intermediate regime condition that $(\Gamma_{\text{cool}}^{(\max)}/\gamma_m) \lesssim \sqrt{C_m^{(\max)}}$, from which we can simplify Eq. (5.3.17) to read

$$\left. \frac{n_{\text{HO}}^{(\text{ss})}}{n_{\text{th}}}\right|_{\text{opt.}} \lesssim \frac{C_m^{(\max)} + 2C_t^{(\max)}}{C_m^{(\max)} + C_t^{(\max)} \frac{\Gamma_{\text{cool}}^{(\max)}}{\gamma_m}} \approx 2 \frac{\gamma_m}{\Gamma_{\text{cool}}^{(\max)}},$$

which does not modify the picture above considerably. In the other limit, $C_m^{(\max)} \gg C_t^{(\max)}$, the intermediate regime interval essentially shrinks to a point $(\Gamma_{\text{cool}}^{(\max)}/\gamma_m) \approx C_m^{(\max)}/\sqrt{C_t^{(\max)}}$ in which case the two other regimes apply.

5.3.2 Exact solution

The entire structured reservoir analysis above relies on the assumptions $\gamma_t, |g_t| \ll (\gamma_m + \Gamma_{\text{cool}}), \gamma_{\text{link}}$ to be valid. But it is not clear exactly how large $\gamma_t, |g_t|$ are allowed to be before the structured reservoir picture breaks down and the results obtained are no longer accurate. To explore this matter, we will now obtain the exact steady state occupancy of the target oscillator by solving the full set of equations of motion (5.3.1) analytically; this can be achieved using either of the methods developed in Section 4.2. Here we will employ the time-domain procedure presented in Section 4.2.1, where the main burden of the calculation is to solve the Lyapunov equation, equivalent to a set of linear equations.

We note that, working within the Rotating Wave Approximation, the drift matrix M does not couple annihilation and creation operators, in which case we only have to solve N^2 real coupled equations, as opposed to $(2N)^2$, to obtain the matrix Γ (where N is the number of oscillators). These are the equations contained in the upper left $N \times N$ block⁴ of the Lyapunov equation (4.2.10). In our case this means that we have to solve $3^2 = 9$ coupled linear equations.⁵

One of the outcomes of the optimization analysis presented as part of the structured reservoir treatment of the problem was that it is never necessary to use parameter sets lying in the interior of the hybridized regime (for the link-mechanical subsystem) to achieve the minimal target occupancy. Therefore, to avoid dealing with unnecessarily large expressions, we derive the exact solution for the resonant case only (that is, with all bare detunings equal to zero $\delta = \tilde{\Delta} = 0$).

The exact formula can be written in a form suggestive of the structured reservoir result Eq. (5.3.4), from which exact analogies of the reservoir decay rate $\gamma_{\text{res}}^{(\text{ex})}$ and occupancy $n_{\text{res}}^{(\text{ex})}$ can be extracted. We emphasize that the identification of such quantities in the exact result is to a large extent artificial – strictly speaking,

⁴Half of the off-diagonal equations are redundant due to the symmetry of the Lyapunov equation as noted elsewhere.

⁵This set of equations was solved analytically using Maple. The resulting formula required considerable rewriting in order to arrive at the form presented below.

the reservoir interpretation only makes sense in the appropriate parameter regime – but, it makes it easier to verify the structured reservoir result.

The exact result is

$$n_{\text{HO}}^{(\text{ss,ex})} = \frac{n_{\text{in,t}} + \frac{\gamma_{\text{res}}^{(\text{ex})}}{\gamma_t} n_{\text{res}}^{(\text{ex})}}{1 + \frac{\gamma_{\text{res}}^{(\text{ex})}}{\gamma_t}}, \quad (5.3.21)$$

where

$$\begin{aligned} \frac{\gamma_{\text{res}}^{(\text{ex})}}{\gamma_t} &= \frac{C_t}{1 + C_m \frac{\gamma_m}{\gamma_m + \Gamma_{\text{cool}}}} \frac{1}{1 + \frac{4|g_m|^2}{(\gamma_m + \Gamma_{\text{cool}} + \gamma_t)(\gamma_{\text{link}} + \gamma_t)}} \\ &\quad \times \left[1 + \frac{\gamma_{\text{link}} \gamma_t + 4|g_t|^2}{(\gamma_m + \Gamma_{\text{cool}} + \gamma_{\text{link}})(\gamma_m + \Gamma_{\text{cool}} + \gamma_t)} \right. \\ &\quad \left. + \frac{4|g_m|^2}{(\gamma_m + \Gamma_{\text{cool}} + \gamma_t)(\gamma_{\text{link}} + \gamma_t)} \left(1 + \frac{(\gamma_{\text{link}} + \gamma_t) \gamma_t}{(\gamma_m + \Gamma_{\text{cool}})(\gamma_m + \Gamma_{\text{cool}} + \gamma_{\text{link}})} \right) \right] \end{aligned}$$

and $n_{\text{res}}^{(\text{ex})} = \frac{N}{D}$ where

$$\begin{aligned} N &= (\gamma_t n_{\text{in,t}} + \gamma_{\text{link}} n_{\text{link}}) \left(1 + \frac{4|g_t|^2}{(\gamma_m + \Gamma_{\text{cool}} + \gamma_{\text{link}})(\gamma_m + \Gamma_{\text{cool}} + \gamma_t)} \right) \\ &\quad + \frac{1}{(\gamma_m + \Gamma_{\text{cool}} + \gamma_{\text{link}})(\gamma_m + \Gamma_{\text{cool}} + \gamma_t)} \left(\gamma_t n_{\text{in,t}} \gamma_{\text{link}} (\gamma_{\text{link}} + \gamma_t) + 4|g_m|^2 \right) \\ &\quad \times \left[\frac{\gamma_t}{\gamma_m + \Gamma_{\text{cool}}} (\gamma_t n_{\text{in,t}} + \gamma_{\text{link}} n_{\text{link}}) - \gamma_t n_{\text{in,t}} + (\gamma_m + \Gamma_{\text{cool}} + \gamma_{\text{link}} + \gamma_t) \frac{\gamma_m n_m + \Gamma_{\text{cool}} n_{\text{cool}}}{\gamma_m + \Gamma_{\text{cool}}} \right] \end{aligned}$$

and D follows from N by setting *all* reservoir occupancies equal to one, $n_i = 1$,

$$\begin{aligned} D &= \gamma_t + \gamma_{\text{link}} + \frac{1}{(\gamma_m + \Gamma_{\text{cool}} + \gamma_{\text{link}})(\gamma_m + \Gamma_{\text{cool}} + \gamma_t)} \\ &\quad \times \left[(\gamma_{\text{link}} + \gamma_t)(\gamma_{\text{link}} \gamma_t + 4|g_t|^2) + 4|g_m|^2 \left(\gamma_m + \Gamma_{\text{cool}} + \gamma_{\text{link}} + \frac{(\gamma_{\text{link}} + \gamma_t) \gamma_t}{\gamma_m + \Gamma_{\text{cool}}} \right) \right]. \end{aligned}$$

5.3.3 Comparison of reservoir result to exact solution

To begin with, we must of course verify that the exact solution reduces to the structured reservoir result in the appropriate limit,

$$\gamma_{\text{res}}^{(\text{ex})} \rightarrow \gamma_{\text{res}}, \quad n_{\text{res}}^{(\text{ex})} \rightarrow n_{\text{res}} \quad \text{for } \gamma_t, |g_t| \ll \gamma_m + \Gamma_{\text{cool}}, \gamma_{\text{link}};$$

this is indeed the case.⁶ The transition corresponds to taking $\gamma_t, |g_t| \rightarrow 0$ in a way so that C_t is kept finite. In the structured reservoir calculation the

⁶Subject to the additional criterion $|g_t| \ll |g_m| \sqrt{1 + \frac{\gamma_m + \Gamma_{\text{cool}}}{\gamma_{\text{link}}}}$: In considering how the smallness conditions affect the denominator D of $n_{\text{res}}^{(\text{ex})}$, we are prompted to compare $|g_t|^2$ to $|g_m|^2 (1 + \frac{\gamma_m + \Gamma_{\text{cool}}}{\gamma_{\text{link}}})$. It does not follow from the stated conditions that we may neglect the former term. However, it contributes positively to D leading to a smaller $n_{\text{res}}^{(\text{ex})}$; hence, by neglecting this term anyway we would not risk overestimating the performance predicted by the structured reservoir result. Realistically, the term is not likely to be significant since if $|g_t| \sim |g_m| \sqrt{1 + \frac{\gamma_m + \Gamma_{\text{cool}}}{\gamma_{\text{link}}}}$ the requirements of the structured reservoir theory would imply $|g_m| \sqrt{1 + \frac{\gamma_m + \Gamma_{\text{cool}}}{\gamma_{\text{link}}}} \ll \gamma_m + \Gamma_{\text{cool}}, \gamma_{\text{link}}$.

quantities $\gamma_t, |g_t|$ enter only through C_t , hence this theory predicts a constant minimum occupancy along a path in parameter space for which C_t is constant. In the following we will use this property to see how the exact theory deviates from this.

5.3.3.1 Stability of reservoir description

Plots of exact vs. structured reservoir result for the target occupancy as functions of γ_t for fixed C_t and evaluated at the optimum $\tilde{\Gamma}_{\text{cool}} = \tilde{\Gamma}_{\text{cool}}^{(\text{opt})}$ (for fixed C_m) as predicted by the structured reservoir theory are shown in Fig. 5.3.4. Hence, the values plotted for the exact theory will in general be less than optimal as the exact theory will have corrections to $\tilde{\Gamma}_{\text{cool}}^{(\text{opt})}$ of the structured reservoir theory. The reason for not minimizing the exact occupancies is to have a plot that indicates the magnitude of the error associated with trusting the structured reservoir theory. In the case of a harmonic oscillator target, the structured reservoir theory is not necessary for optimizing the parameters, which can be done numerically from the exact solution. However, for any other target system for which the problem lacks an exact solution, Fig. 5.3.4 is useful as an indication of the (mathematical) stability of the structured reservoir theory. The plots show significant deviations from the reservoir prediction as γ_t approaches γ_m if C_t is of the same order of magnitude as C_m . Since this implies $|g_t| \sim |g_m|$, the breakdown exhibited in these plots was to be expected.

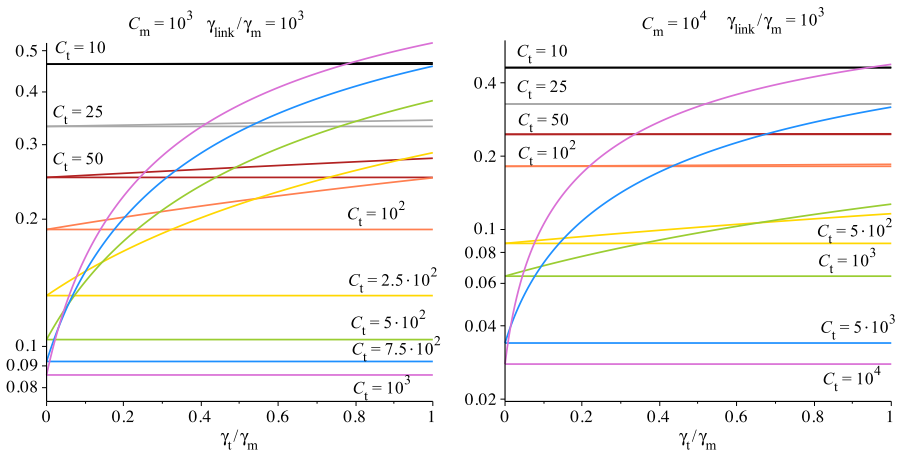


Figure 5.3.4: Structured reservoir vs. exact results for the target occupancy as functions of γ_t for various fixed C_t both evaluated at $\tilde{\Gamma}_{\text{cool}} = \tilde{\Gamma}_{\text{cool}}^{(\text{opt})}$ (fixed C_m) of the structured reservoir theory. The former theory yields constant functions since it only depends on γ_t through C_t .

To complement Fig. 5.3.4 we now consider plots of *optimized* exact minimal occupancies. The minimization of $n^{(\text{ss,ex})}/n_{\text{th}}$ is performed by locating optimal values of C_t and $\tilde{\Gamma}_{\text{cool}}$ graphically for fixed C_m . The target occupancy is plotted alongside that of the 'link' oscillator, also calculated in the exact theory (as the structured reservoir description breaks down, the 'link' will be appreciably influenced by the target).

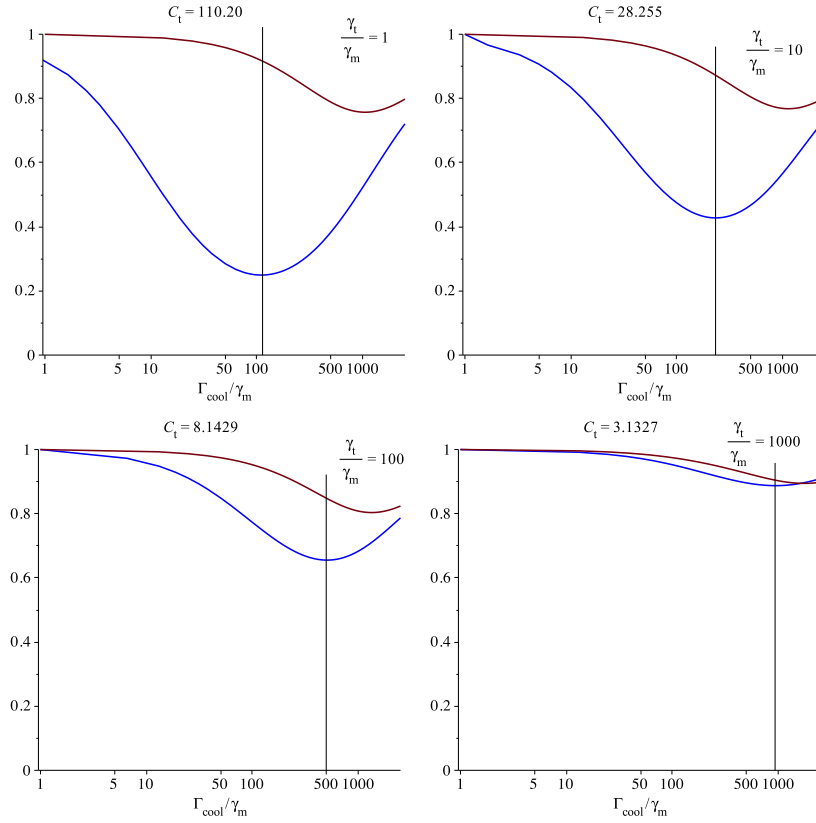


Figure 5.3.5: Minimized, exact target occupancy (blue curves) plotted alongside the simultaneous exact link occupancy (red curves) as functions of $\tilde{\Gamma}_{\text{cool}}$ for various (γ_t/γ_m) . Optimized w.r.t. C_t for fixed $C_m = 1000$, $(\gamma_{\text{link}}/\gamma_m) = 1000$; the optimal values of $\tilde{\Gamma}_{\text{cool}}$ for the target are marked by black lines.

The optimal values of $\tilde{\Gamma}_{\text{cool}}$ that can be read off from the plots in Fig. 5.3.5 all exceed the corresponding optimum $\tilde{\Gamma}_{\text{cool}}^{(\text{opt})}$ in the reservoir theory for the (C_t, C_m) -limited regime, Eq. (5.3.11). Thus, these optima lie in the unhybridized parameter domain for the cooling system.⁷ The optimal value of C_t is seen to decrease with increasing (γ_t/γ_m) , meaning that the optimal $|g_t|^2$ does not increase in proportion with this quantity.⁸ The plots show clearly that the EIT-like effect of cooling through a “hot” link persists all the way up to $\gamma_t \sim \gamma_{\text{link}}$. Hence, this effect is *not* limited to an extreme and perhaps unrealistic regime $\gamma_t \ll \gamma_{\text{link}}$, $(\gamma_m + \Gamma_{\text{cool}})$; on the contrary, it should manifest itself in a wide interval of γ_t -values, although certainly for strong cooling $\gamma_t \ll \gamma_{\text{link}}$, $(\gamma_m + \Gamma_{\text{cool}})$ is required.

⁷The cooling system is unhybridized according to the criterion identified within the structured reservoir theory in Section 5.3.1.2. Going outside the parameter regime where this theory is valid can only push the hybridization boundary towards higher $|g_m|$ since in general the target system will induce additional broadening of the link.

⁸The ratio of optimal target coupling strengths $|g_t^{(\text{II})}|/|g_t^{(\text{I})}|$ between successive pairs of the plots are approximately $\{1.6, 1.7, 2.0\}$.

5.4 Implementations

Much of the discussion in this chapter have been phrased somewhat abstractly in terms of the 'target', 'link' and 'mechanical' subsystems, although a few examples have been provided along the way. The intention behind this approach is to emphasize the generality of the scheme and thereby encourage imaginative thinking regarding possible applications. The structured reservoir theory for the cooling system is limited to 'link' and 'mechanical' modes describable as bosonic harmonic oscillators, but this is not a severe limitation since it accomodates a wide range of implementations.

In this section we will mention a few possible implementations of the abstract 'indirect' cooling scheme proposed in this thesis. They will only be considered rather superficially and a more thorough evaluation should be carried out in the near future.

5.4.1 Nuclear spin cooling

One could imagine having the nuclear spins of an ensemble of atoms as the target subsystem to be cooled, i.e., polarized. This could have possible applications to Nuclear Magnetic Resonance Imaging (NMRI) in which nuclear spin polarization and the ensuing relaxation are key ingredients. By introducing a prepolarized substance into the patient, for instance optically pumped ^3He , the NMRI resolution may be improved [16]. The 'indirect' cooling scheme could be imagined as an alternative method for prepolarizing the nuclear spins.

For this purpose the 'link' system could be an electrical LC circuit, since by placing the ensemble of atoms in the inductor their nuclear spins would interact with the circuit mode via the induced magnetic field. The setup is imagined to be realized at room temperature for which cooling of the mechanical mode is preferably performed opto-mechanically due to the low reservoir occupancy at optical frequencies.

A general analysis of spin ensemble cooling would be quite complicated because we would have to take into account the collective states of the spins. If a number of spins form a collective state of length $\hbar\sqrt{i(i+1)}$, we are prevented from polarizing this subset of spins below the bottom rung of ladder, $m_i = -i$, the minimum value of the magnetic quantum number. However, if the coherence between these spins are destroyed, we may cool them further. In the terminology of spin ensembles, the time-scale over which the phase coherence between spins decohere is called the T_2 time. Hence, if T_2 is short compared to other time-scales in the system, the limiting effect just described effectively vanishes.

Another important time-scale for the spin ensemble, to which T_2 must be compared, is T_1 , the thermal equilibration time of the polarization of the ensemble along the external magnetic field axis. To achieve significant polarization our cooling mechanism should in the first place be able to outperform the thermalization implied by T_1 ; in the terms of the cooling derivations above, this simply corresponds to $\gamma_{\text{res}} > \gamma_{\text{t}}$, the induced cooling rate must overwhelm the intrinsic decay rate.

To avoid the complications of dealing with the dark states that arise from a finite T_2 time, we assume T_2 to be much shorter than all other time-scales

of the problem. In this short T_2 regime, we are essentially cooling the spins individually since the life-time of their collective states is negligible. Hence we may mathematically consider the equations of motion for a single spin subject to our cooling scheme. Solving these we can calculate the expectation value of the polarization of that single spin; due to the aforementioned assumption, this will equal the polarization of the entire ensemble.

5.4.1.1 Structured reservoir result for a single spin

We apply the structured reservoir formalism derived in Section 4.3, valid under the conditions $\gamma_t, |g_t| \ll \gamma_{\text{link}}, (\gamma_m + \Gamma_{\text{cool}})$ in the resonant case that we will consider here. The polarization of the spin will be determined as a compromise between the thermalization with the surroundings, quantified by $\gamma_t = 1/[2n(\omega_{\text{link}})T_1]$ (see below), and the influence from our cooling system. Since T_1 times can be very long, even up to the order of hours, these long-lived spins fit the requirements of the structured reservoir cooling theory very well.

The effective Heisenberg-Langevin equations for the operators $\hat{\sigma}_z = |\uparrow\rangle\langle\uparrow| - |\downarrow\rangle\langle\downarrow|$, $\hat{\sigma}^+ = |\uparrow\rangle\langle\downarrow|$ and $\hat{\sigma}^- = |\downarrow\rangle\langle\uparrow|$ are (in a suitable rotating frame) [25]

$$\begin{aligned}\dot{\hat{\sigma}}^- &= -\frac{1}{2}(\gamma_t + \gamma_{\text{res}})\hat{\sigma}^- - \hat{\sigma}_z(\sqrt{\gamma_t}\hat{f}_{\text{in},t} + \sqrt{\gamma_{\text{res}}}\hat{F}_{\text{res}}) \\ \dot{\hat{\sigma}}_z &= -(\gamma_t + \gamma_{\text{res}})(\mathbf{1} + \hat{\sigma}_z) + [\hat{\sigma}^+(\sqrt{4\gamma_t}\hat{f}_{\text{in},t} + \sqrt{4\gamma_{\text{res}}}\hat{F}_{\text{res}}) + \text{H.c.}].\end{aligned}$$

Cooling of a two-level target is an example of a scenario where no exact solution exists. It is the products of operators on the right-hand side that prevents an exact solution. However, by formal integration and back-substitution an iterative series expansion can be obtained. To lowest order and in the Markov approximation we may derive the following expectation value [3]⁹

$$\langle\dot{\hat{\sigma}}_z(t)\rangle = -(\gamma_t + \gamma_{\text{res}})\left\{2\frac{\gamma_t n_{\text{in},t} + \gamma_{\text{res}} n_{\text{res}}}{\gamma_t + \gamma_{\text{res}}} + 1\right\} \langle\hat{\sigma}_z(t)\rangle + 1\},$$

from which the steady state polarization follows by setting the left-hand side equal to zero:

$$\langle\hat{\sigma}_z\rangle_{\text{ss}} = -\left[2\frac{\gamma_t n_{\text{in},t} + \gamma_{\text{res}} n_{\text{res}}}{\gamma_t + \gamma_{\text{res}}} + 1\right]^{-1}. \quad (5.4.1)$$

We see that it is exactly the same weighted average of reservoir occupancies that determine the steady state as for the harmonic oscillator target. In the regime of weak polarization, we may approximate Eq. (5.4.1) as

$$\langle\hat{\sigma}_z\rangle_{\text{ss}} \approx -\left[2\frac{\gamma_t n_{\text{in},t} + \gamma_{\text{res}} n_{\text{res}}}{\gamma_t + \gamma_{\text{res}}}\right]^{-1}.$$

In this regime, the improvement factor in the polarization as compared to the thermal polarization is

$$\frac{\langle\hat{\sigma}_z\rangle_{\text{ss}}}{\langle\hat{\sigma}_z\rangle_{\text{th}}} = \left[\frac{1 + \frac{\gamma_{\text{res}}}{\gamma_t} \frac{n_{\text{res}}}{n_{\text{in},t}}}{1 + \frac{\gamma_{\text{res}}}{\gamma_t}}\right]^{-1}, \quad (5.4.2)$$

⁹In this reference the derivation is carried out for coupling to a single reservoir, but it may easily be generalized to the situation of two uncorrelated reservoirs. This quickest way to do this is to combine the two reservoirs as $\sqrt{\gamma_{\text{res}} + \gamma_t}\hat{F} \equiv \sqrt{\gamma_{\text{res}}}\hat{F}_{\text{res}} + \sqrt{\gamma_t}\hat{f}_{\text{in},t}$ from which it follows that the occupancy related to \hat{F} must be $\bar{n} = \frac{\gamma_t n_{\text{in},t} + \gamma_{\text{res}} n_{\text{res}}}{\gamma_t + \gamma_{\text{res}}}$.

which is the inverse of Eq. (5.3.4), the expression encountered in the treatment of the harmonic oscillator. Thus, if we again assume all intrinsic reservoirs to have the same mean occupancy, the entire optimization analysis of Section 5.3.1 carries over to the single spin case.

5.4.1.2 Nuclear spin coupling strength

To assess the feasibility of this scheme, we must therefore estimate the achievable target cooperativity¹⁰ $C_t = |g_t|^2/(\gamma_t \gamma_{\text{link}})$ for the LC to nuclear spin connection. This requires us to calculate the coupling constant $|g_t|$ of a single nuclear spin to the magnetic field of the inductor in the circuit. To this end, we need the zero-point magnetic field B_0 that appears in the quantized expression for the magnetic field energy

$$U_B = V_m \frac{B_0^2}{2\mu_0} \left(\hat{b}^\dagger \hat{b} + \frac{1}{2} \right),$$

where V_m is the mode volume and μ_0 the vacuum permeability. Comparing this to the form $\hbar\omega(\hat{b}^\dagger \hat{b} + \frac{1}{2})$ which also includes the energy stored in the electric field we can deduce

$$B_0 = \sqrt{\frac{\hbar\omega\mu_0}{V_m}} = 5 \cdot 10^{-14} \text{T} \cdot \sqrt{\frac{\omega}{2\pi(3 \cdot 10^6 \text{Hz})}} \sqrt{\frac{10^{-6} \text{m}^3}{V_m}},$$

where ω is the circuit frequency. Assuming the quantization axis of the spin to be along the z -axis while the field of the inductor points in the x -direction, the interaction Hamiltonian in the Rotating Wave Approximation reads $\hat{H}_{\text{int}}/\hbar = \frac{g_t}{2}(\hat{\sigma}^+ \hat{b} + \hat{b}^\dagger \hat{\sigma}^-)$. The single-spin coupling constant is

$$g_t = \frac{g_n \mu_N B_0}{\sqrt{2}\hbar},$$

where the gyromagnetic ratio of a nucleus $g_n \mu_N/\hbar$ typically has a magnitude in the range $2\pi(1 \dots 40) \cdot 10^6 \frac{\text{Hz}}{\text{T}}$. Taking $g_n \mu_N/\hbar = 2\pi(4 \cdot 10^7 \frac{\text{Hz}}{\text{T}})$ and $\omega = 2\pi(3 \cdot 10^6 \text{Hz})$, we find for different mode volumes V_m :

$$\begin{aligned} g_t &= 2\pi \cdot (1.41 \cdot 10^{-6} \text{Hz}), [V_m = 1 \text{cm}^3 = 10^{-6} \text{m}^3] \\ &= 2\pi \cdot (4.46 \cdot 10^{-5} \text{Hz}), [V_m = 1 \text{mm}^3 = 10^{-9} \text{m}^3] \\ &= 2\pi \cdot (1.41 \cdot 10^{-3} \text{Hz}), [V_m = (100 \mu\text{m})^3 = 10^{-12} \text{m}^3] \\ &= 2\pi \cdot (4.46 \cdot 10^{-2} \text{Hz}), [V_m = (10 \mu\text{m})^3 = 10^{-15} \text{m}^3]. \end{aligned}$$

The intrinsic target decay rate γ_t is related to the equilibration time T_1 of the polarization by $T_1^{-1} = 2n(\omega_{\text{link}})\gamma_t$ as can be seen by considering rate equations (in the high-temperature limit); here we have assumed that the Lamor frequency has been tuned into resonance with the link. Assuming $T_1 = 10\text{s}$, $\gamma_{\text{link}} = 2\pi(10\text{Hz})$ and $\omega_{\text{link}} = 2\pi \cdot 6\text{MHz}$ and use the mode volume $V_m = (100 \mu\text{m})^3$ we arrive at the target-link cooperativity

$$C_t = \frac{|g_t|^2}{\gamma_t \gamma_{\text{link}}} \approx 9,$$

¹⁰The coupling constant is defined differently here relative to the structured reservoir description, therefore a factor of 2 has been absorbed into g_t .

where $n(\omega_{\text{link}}) \approx k_{\text{B}}T/(\hbar\omega_{\text{link}})$. Assuming that we are $(C_{\text{m}}, C_{\text{t}})$ -limited with $C_{\text{m}} \gg C_{\text{t}}$, we find from Eq. (5.3.19) that

$$\frac{1 + \frac{\gamma_{\text{res}}}{\gamma_{\text{t}}} \frac{n_{\text{res}}}{n_{\text{in,t}}}}{1 + \frac{\gamma_{\text{res}}}{\gamma_{\text{t}}}} \approx \frac{2}{1 + \sqrt{1 + C_{\text{t}}}} \approx 2^{-1};$$

comparing with Eq. (5.4.2) we see that this means an enhancement of the thermal polarization by a factor of 2: $\langle \hat{\sigma}_z \rangle_{\text{ss}} = 2 \times \langle \hat{\sigma}_z \rangle_{\text{th}}$. But this is a very small improvement since the absolute thermal polarization is usually on the order of $\sim 10^{-6}$. Judging from this result, spin cooling does not seem like a feasible application of the 'indirect' cooling scheme. Even going to the extremely small mode volume $V_{\text{m}} = (10\mu\text{m})^3$ would only improve the thermal polarization by a factor of 50.

5.4.2 Indirect mechanical cooling

Another idea for an implementation of the cooling scheme would be to cool a second 'target' mechanical mode via a 'link' LC in turn coupled to the usual directly laser cooled mechanical mode. If the two mechanical modes live in similar structures (two identical membranes, for instance), it is reasonable to expect $\gamma_{\text{t}} \sim \gamma_{\text{m}}$. Perhaps a more likely scenario is the cooling of a mechanical mode of a somewhat different object not amenable to cavity-assisted cooling.

It is not clear if this is compatible with the requirements of the structured reservoir theory, but since the target mode is describable as a harmonic oscillator, we may turn to the exact solution available to us in this case. In fact, relevant plots for this situation were already presented in Fig. 5.3.5 for C_{m} . Assuming that we can realize any value of Γ_{cool} we would like, the plot for $\gamma_{\text{t}}/\gamma_{\text{m}} = 1$ shows that the occupancy of the target mechanical mode may be reduced to 1/4 of the thermal occupancy for the stated parameters, $C_{\text{m}} = 1000$, $(\gamma_{\text{link}}/\gamma_{\text{m}}) = 1000$.

5.4.3 Indirect cooling of LC circuit with high Q-factor

In the setup just sketched in the previous section, the 'target' mechanical mode could be replaced with a second LC circuit of relatively high quality factor, Q . This could be useful due to the following: The 'link' circuit must have a small capacitance to enable significant electromechanical coupling to, for instance, a thin membrane as the interaction relies on relative capacitance changes. If one wants to avoid an AC bias field, the 'link' must be tuned into resonance with the laser cooled mechanical mode by picking a sufficiently large inductance L to balance the small C (recall that $\omega_{\text{LC}} = (LC)^{-1/2}$). The large L is likely to entail a small Q -value, i.e., a large γ_{link} . However, the 'target' LC circuit does not have to conform to the mechanical coupling and may therefore be designed to have a relatively high Q -value, that is, relatively small γ_{t} .

Chapter 6

Conclusions and perspectives

6.1 Electromechanical coupling calculations

6.1.1 Conclusions

We have developed a Hamiltonian framework for characterizing capacitive electromechanical coupling scenarios in terms of coupling strength, induced mechanical frequency shift and equilibrium configuration in the presence of a bias voltage. The formulas derived for these quantities are phrased in terms of a unit cell capacitance function that in general must be determined numerically for the particular physical setup under consideration. The procedure takes into account the mode shapes involved but assumes approximate symmetries that makes it computationally manageable.

The procedure was then applied to the specific setup which prompted its development: A vibrating membrane capacitively coupled to an interdigitated capacitor and compared with available measurement data from ongoing, preliminary experiments. The level of agreement in this comparison suggests that the framework could be a valuable tool in the design of electromechanical interfaces.

6.1.2 Perspectives

Regarding the future of this framework, two aspects are relevant:

Firstly, it will be interesting to compare to new measurement results as they become available from the membrane group at QUANTOP. Data from experiments with membranes of various different material compositions will allow for a better assessment of the modeling. As the experiment matures, it is expected that successful coupling constant measurements can be performed, which would allow for a more detailed comparison between experiment and calculation. Moreover, it should be investigated to what extent the framework is applicable to other existing setups.

Secondly, the capabilities of the framework should be exploited fully. The calculation reported here, in application to the experiment, considered only lowest order contributions. By implementing the algorithm for determining the

static deflection of the membrane, more accurate calculations become possible. Furthermore, the corrections that arise from adiabatically eliminating the fast circuit modes should also be calculated for the membrane-IDC experiment. In addition to the quantities mentioned above, the framework may also be used to calculate the coupling between distinct mechanical modes induced by the electromechanical interaction (as indicated during the derivation). However, for consistency these supposedly small corrections should be compared to estimates of the error introduced by the approximate symmetry assumptions (that make the unit cell segmentation approach mathematically possible).

Theoretically, it would be gratifying to carry out a more rigorous quantization of the circuit-mechanics system in the spirit of Ref. [15], in which the cavity opto-mechanical case is treated.

6.2 Extending cavity-mechanical cooling

6.2.1 Conclusions

We have proposed a scheme for extending cavity-mechanical single-mode cooling to a long-lived target system via a rapidly decaying link degree of freedom. Using an effective, structured reservoir theory, the performance of the scheme was fully optimized and a simple physical picture in terms of bottlenecks was given. Our results lead to the surprising conclusion that cooling of the target system may occur even if the link mode is not cooled significantly. This is contrary to our intuition from bulk cooling and provides a new avenue for thinking about single-mode cooling in terms of interference effects akin to Electromagnetically Induced Transparency.

To supplement the above, a partial analysis regarding the validity regime of the structured reservoir theory was given based on the exact harmonic oscillator solution. While it remains to formulate a succinct statement characterizing the deviations from the structured reservoir result, the qualitative effect of cooling via a hot link was seen to persist for a significant range of parameters.

Finally, a few ideas for implementations of the cooling scheme were briefly discussed.

6.2.2 Perspectives

Since cooling techniques play an omnipresent role in physics, the results obtained here could turn out to be of wide interest. However further investigation is called for, both theoretically as well as regarding the assesment of potential applications.

To begin with, it would be useful to finish the partial mathematical stability analysis given in this thesis by extracting a compact statement about the regime of validity for the structured reservoir description. Having a better understanding of the boundaries of this regime would make it easier to determine which physical systems are realistic cooling targets within the scheme.

The optimization analysis in the structured reservoir limit could be generalized by allowing the thermal reservoirs to have distinct mean occupancies $n_{\text{th}1} \neq$

$n_{\text{th}2}$. This could be relevant even for resonant operation if an AC drive is involved in achieving the resonance condition .

It would also be relevant to perform a more general derivation where we consider the cavity-mechanical cooling mechanism on equal footing with the other modes of the system rather than as a Markovian reservoir. Note that the induced mechanical cooling rate Γ_{cool} enter all final formulas in the combination $\Gamma_{\text{cool}}/\gamma_{\text{m}}$. Based on the induced rate expressions that have appeared in course of the derivation, it is tempting to speculate that in switching to the more general theory, the following replacement will occur

$$\frac{\Gamma_{\text{cool}}}{\gamma_{\text{m}}} \rightarrow \frac{4|g_{\text{cool}}|^2}{\gamma_{\text{m}}\kappa} \equiv C_{\text{cool}},$$

where κ is the linewidth of the cavity assisting in the cooling of the mechanical degree of freedom and g_{cool} is the coupling constant involved in this interaction. Another generalization of the derivation that could be relevant at some point is to refrain from making the Rotaing Wave Approximation in the coupling between the link and mechanical modes.

Apart from these theoretical consideration, an important task is to assess various potential implementations of the cooling scheme more thoroughly. Finally, it should be noted that the scheme might even be based on a cooling mechanism different from that of cavity-assisted sideband cooling. For instance, an optically pumped spin-ensemble might replace the cavity-cooled membrane as the source of cooling.

Bibliography

- [1] Ian Johnston Rhind Aitchison and Anthony J. G. Hey. *Gauge Theories in Particle Physics*. Graduate Student Series in Physics. Institute of Physics Publishing, 2nd edition edition, 1989.
- [2] M. Aspelmeyer, S. Gröblacher, K. Hammerer, and N. Kiesel. Quantum optomechanics—throwing a glance. *J. Opt. Soc. Am. B*, 27(6):A189–A197, Jun 2010.
- [3] Stephen M. Barnett and Paul M. Radmore. *Methods in Theoretical Quantum Optics*. Oxford University Press, 2003.
- [4] R. H. Bartels and G. W. Stewart. Solution of the matrix equation $ax + xb = c$. *Comm. of the ACM*, 15(9):820–826, 1972.
- [5] Edmund X. DeJesus and Charles Kaufman. Routh-hurwitz criterion in the examination of eigenvalues of a system of nonlinear ordinary differential equations. *Phys. Rev. A*, 35:5288–5290, Jun 1987.
- [6] Michel H. Devoret. Quantum fluctuations in electrical circuits. In S. Reynaud, E. Giacobino, and J. Zinn-Justin, editors, *Quantum Fluctuations, Les Houches, Session LXIII, 1995*. Elsevier Science B.V., 1997.
- [7] J. M. Dobrindt, I. Wilson-Rae, and T. J. Kippenberg. Parametric normal-mode splitting in cavity optomechanics. *Phys. Rev. Lett.*, 101:263602, Dec 2008.
- [8] Jürgen Eschner, Giovanna Morigi, Ferdinand Schmidt-Kaler, and Rainer Blatt. Laser cooling of trapped ions. *J. Opt. Soc. Am. B*, 20(5):1003–1015, May 2003.
- [9] Crispin W. Gardiner and Peter Zoller. *Quantum Noise*, volume 56 of *Springer series in synergetics*. Springer, second enlarged edition edition, 2000.
- [10] David Jeffery Griffiths. *Introduction to electrodynamics*. Prentice Hall, 3rd edition, 1999.
- [11] Sebastian Hofer. Theory of generation and verification of opto-mechanical correlations (diplomarbeit). Master’s thesis, Leopold-Franzens-Universität Innsbruck, 2009.

- [12] A M Jayich, J C Sankey, B M Zwickl, C Yang, J D Thompson, S M Girvin, A A Clerk, F Marquardt, and J G E Harris. Dispersive optomechanics: a membrane inside a cavity. *New Journal of Physics*, 10:095008, 2008.
- [13] M. J. Kastoryano, F. Reiter, and A. S. Sørensen. Dissipative preparation of entanglement in optical cavities. *Phys. Rev. Lett.*, 106:090502, Feb 2011.
- [14] T. J. Kippenberg and K. J. Vahala. Cavity optomechanics: Back-action at the mesoscale. *Science*, 321(5893):1172–1176, 2008.
- [15] C. K. Law. Interaction between a moving mirror and radiation pressure: A hamiltonian formulation. *Phys. Rev. A*, 51:2537–2541, Mar 1995.
- [16] Michele Leduc and Pierre Jean Nacher. Polarized helium to image the lung. *AIP Conference Proceedings*, 770(1):381–389, 2005.
- [17] A. Mari and J. Eisert. Cooling by heating: Very hot thermal light can significantly cool quantum systems. *Phys. Rev. Lett.*, 108:120602, Mar 2012.
- [18] Florian Marquardt, Joe P. Chen, A. A. Clerk, and S. M. Girvin. Quantum theory of cavity-assisted sideband cooling of mechanical motion. *Phys. Rev. Lett.*, 99:093902, Aug 2007.
- [19] Florian Marquardt and Steven M. Girvin. Optomechanics. *Physics*, 2:40, May 2009.
- [20] A. D. O’Connell, M. Hofheinz, M. Ansmann, Radoslaw C. Bialczak, M. Lenander, Erik Lucero, M. Neeley, D. Sank, H. Wang, M. Weides, J. Wenner, John M. Martinis, and A. N. Cleland. Quantum ground state and single-phonon control of a mechanical resonator. *Nature*, 464(7289):697–703, 04 2010.
- [21] Fernando Pastawski, Lucas Clemente, and Juan Ignacio Cirac. Quantum memories based on engineered dissipation. *Phys. Rev. A*, 83:012304, 2011.
- [22] C. A. Regal and K. W. Lehnert. From cavity electromechanics to cavity optomechanics. *Journal of Physics: Conference Series*, 264:012025, 2011.
- [23] A. Schliesser, R. Riviere, G. Anetsberger, O. Arcizet, and T. J. Kippenberg. Resolved-sideband cooling of a micromechanical oscillator. *Nat Phys*, 4(5):415–419, 05 2008.
- [24] Silvan Schmid, Christofer Hierold, and Anja Boisen. Modeling the kelvin polarization force actuation of micro- and nanomechanical systems. *Journal of Applied Physics*, 107(5):054510, 2010.
- [25] K. Stannigel, P. Rabl, A. S. Sørensen, M. D. Lukin, and P. Zoller. Optomechanical transducers for quantum-information processing. *Phys. Rev. A*, 84:042341, 2011.
- [26] K. Stannigel, P. Rabl, A. S. Sørensen, P. Zoller, and M. D. Lukin. Optomechanical transducers for long-distance quantum communication. *Phys. Rev. Lett.*, 105:220501, Nov 2010.

- [27] J. M. Taylor, A. S. Sørensen, C. M. Marcus, and E. S. Polzik. Laser cooling and optical detection of excitations in a lc electrical circuit. *Phys. Rev. Lett.*, 107:273601, 2011.
- [28] L. Tian and Hailin Wang. Optical wavelength conversion of quantum states with optomechanics. *Phys. Rev. A*, 82:053806, Nov 2010.
- [29] Eduard Ventsel and Theodor Krauthammer. *Thin Plates and Shells: Theory, Analysis, and Applications*. Marcel Dekker, Inc., New York, New York, 2001.
- [30] D. J. Wilson, C. A. Regal, S. B. Papp, and H. J. Kimble. Cavity optomechanics with stoichiometric sin films. *Phys. Rev. Lett.*, 103:207204, Nov 2009.
- [31] I Wilson-Rae, N Nooshi, J Dobrindt, T J Kippenberg, and W Zwerger. Cavity-assisted backaction cooling of mechanical resonators. *New Journal of Physics*, 10:095007, 2008.
- [32] I. Wilson-Rae, N. Nooshi, W. Zwerger, and T. J. Kippenberg. Theory of ground state cooling of a mechanical oscillator using dynamical backaction. *Phys. Rev. Lett.*, 99:093901, Aug 2007.

Appendix A

Mathematical derivations

A.1 Inversion of the kinetic energy matrix

The matrix $\underline{\underline{M}} \in \mathbb{R}^{N \times N}$ was defined in Eq. (3.1.13) as

$$\begin{aligned} (\underline{\underline{M}})_{i,j} &\equiv \delta_{i,j}L_i + L_0, \quad i, j \in \{1, \dots, N\} \\ &= \begin{pmatrix} L_1 + L_0 & L_0 & \cdots & L_0 \\ L_0 & L_2 + L_0 & \cdots & L_0 \\ \vdots & \vdots & \ddots & \vdots \\ L_0 & L_0 & \cdots & L_N + L_0 \end{pmatrix} \end{aligned}$$

To be able to argue more clearly below we introduce the $\mathbb{R}^{n \times n}$ matrix-valued function of the ordered set $\{l_1, l_2, \dots, l_n\}$ and l_0

$$\underline{\underline{\mathcal{M}}}(\{l_1, l_2, \dots, l_n\}; l_0) = \text{diag}(\{l_1, l_2, \dots, l_n\}) + \underline{\underline{l_0}}^{(n)},$$

where $\text{diag}(\{\dots\})$ produces a diagonal matrix with elements given by the ordered set in the argument and $\underline{\underline{l_0}}^{(n)}$ is the $\mathbb{R}^{n \times n}$ matrix with all entries equal to l_0 . In this notation, $\underline{\underline{M}} = \underline{\underline{\mathcal{M}}}(\{L_1, L_2, \dots, L_N\}; L_0)$.

The matrix may be inverted by using Kramer's rule, $\underline{\underline{M}}^{-1} = \frac{1}{\det(\underline{\underline{M}})} \text{Adj}(\underline{\underline{M}})$, in terms of the adjugate matrix. The entries of the latter are given by $[\text{Adj}(\underline{\underline{M}})]_{i,j} = (-1)^{i+j} M_{j,i}$ where $M_{j,i}$ is the determinant of the matrix obtained by removing the j 'th row and the i 'th column of $\underline{\underline{M}}$.

It will prove useful to determine $\det(\underline{\underline{M}})$ first. Taking note of the fact that adding a multiple of one row to another does not change the determinant, we now transform $\underline{\underline{M}}$ into a lower triangular matrix by such operations. First we subtract the first row, R_1 , from the remaining rows, then we add $-\sum_{i=2}^N R_i \frac{L_0}{L_i}$

to the first row, assuming all L_i to be non-zero:

$$\begin{aligned} \begin{pmatrix} L_1 + L_0 & L_0 & \cdots & L_0 \\ L_0 & L_2 + L_0 & \cdots & L_0 \\ \vdots & \vdots & \ddots & \vdots \\ L_0 & L_0 & \cdots & L_N + L_0 \end{pmatrix} &\rightarrow \begin{pmatrix} L_1 + L_0 & L_0 & \cdots & L_0 \\ -L_1 & L_2 & \cdots & 0 \\ \vdots & \vdots & \ddots & \vdots \\ -L_1 & 0 & \cdots & L_N \end{pmatrix} \\ &\rightarrow \begin{pmatrix} L_1(1 + \sum_{i=1}^N \frac{L_0}{L_i}) & 0 & \cdots & 0 \\ -L_1 & L_2 & \cdots & 0 \\ \vdots & \vdots & \ddots & \vdots \\ -L_1 & 0 & \cdots & L_N \end{pmatrix}. \end{aligned}$$

The determinant of a triangular matrix is the product of its diagonal elements, it thus follows from the above that

$$\det(\underline{\underline{M}}) = \left(\prod_{i=1}^N L_i \right) \left(1 + \sum_{i=1}^N \frac{L_0}{L_i} \right) = \left(\prod_{i=0}^N L_i \right) \left(\sum_{i=0}^N \frac{1}{L_i} \right). \quad (\text{A.1.1})$$

It is clear that this expression for $\det(\underline{\underline{M}})$ may be used to evaluate the determinant of any matrix of the form $\underline{\underline{M}}$ (although care must be exerted in the case of arguments equal to zero, $l_i = 0$).

Let us first consider the diagonal elements of the adjugate matrix, $[\text{Adj}(\underline{\underline{M}})]_{j,j} = (-1)^{2j} M_{j,j}$. Removing the j 'th row and column from $\underline{\underline{M}}$ merely produces the $\mathbb{R}^{(N-1) \times (N-1)}$ matrix $\underline{\underline{M}}(\{L_1, \dots, L_N\} \setminus \{L_j\}; L_0)$, i.e., a matrix of the same structure as $\underline{\underline{M}}$ but with no L_j appearing, therefore we can use Eq. (A.1.1) to determine $M_{j,j}$ and thus

$$\begin{aligned} [\text{Adj}(\underline{\underline{M}})]_{j,j} &= \left(\prod_{\substack{i=0 \\ i \neq j}}^N L_i \right) \left(\sum_{\substack{i=0 \\ i \neq j}}^N \frac{1}{L_i} \right) = \frac{1}{L_j} \left(\prod_{i=0}^N L_i \right) \left(\left[\sum_{i=0}^N \frac{1}{L_i} \right] - \frac{1}{L_j} \right) \Rightarrow \\ [\underline{\underline{M}}^{-1}]_{j,j} &= \frac{1}{L_j} - \frac{1}{L_j^2} \left[\sum_{i=0}^N \frac{1}{L_i} \right]^{-1} \end{aligned} \quad (\text{A.1.2})$$

Now for the off-diagonal elements of $[\text{Adj}(\underline{\underline{M}})]_{i,j} = (-1)^{i+j} M_{j,i}$. Contrary to the diagonal elements $[\text{Adj}(\underline{\underline{M}})]_{j,j} = M_{j,j}$ which were easily seen to be determinants of matrices of the form $\underline{\underline{M}}$, this is not immediately obvious in the off-diagonal case, $M_{j,i}$. However, given the matrix resulting from removing the j 'th row and the i 'th column of $\underline{\underline{M}}$, we may perform row or column swaps and thereby transform the matrix into a form compatible with $\underline{\underline{M}}$. Since $\underline{\underline{M}}$ is symmetric, we may for definiteness restrict our attention to the case $j > i$. Removing the j 'th row and the i 'th column of $\underline{\underline{M}}$ results in the matrix $\underline{\underline{M}}(\{L_1, \dots, L_j \rightsquigarrow 0, \dots, L_N\} \setminus \{L_i\}; L_0)$ (where L_j is replaced by 0, $L_j \rightsquigarrow 0$) *except* that the rows containing the entries $L_k + L_0$ for $i < k < j$ are displaced one step below the diagonal; thus it takes $j - i - 1$ row swaps to attain the aforementioned $\underline{\underline{M}}$ matrix. Eq. (A.1.1) was derived under the assumption that all L_l were non-zero, but since the determinant is a continuous function of any L_l it contains

we may take the formal limit $L_j \rightarrow 0$ to obtain

$$\begin{aligned} \det[\underline{M}(\{L_1, \dots, L_j \rightsquigarrow 0, \dots, L_N\} \setminus \{L_i\}; L_0)] &= \lim_{L_j \rightarrow 0} \left(\prod_{\substack{l=0 \\ l \neq i}}^N L_l \right) \left(\sum_{\substack{l=0 \\ l \neq i}}^N \frac{1}{L_l} \right) \\ &= \left(\prod_{\substack{l=0 \\ l \neq i, j}}^N L_l \right) \lim_{L_j \rightarrow 0} \left(1 + L_j \sum_{\substack{l=0 \\ l \neq i, j}}^N \frac{1}{L_l} \right) = \prod_{\substack{l=0 \\ l \neq i, j}}^N L_l = \frac{1}{L_i L_j} \prod_{l=0}^N L_l. \end{aligned}$$

Therefore, accounting for the $j - i - 1$ row swaps, we have for the off-diagonal elements

$$\begin{aligned} [\text{Adj}(\underline{M})]_{i,j} &= (-1)^{i+j} M_{j,i} = (-1)^{i+j} (-1)^{j-i-1} \frac{1}{L_i L_j} \prod_{l=0}^N L_l = -\frac{1}{L_i L_j} \prod_{l=0}^N L_l \Rightarrow \\ (\underline{M}^{-1})_{i,j} &= -\frac{1}{L_i L_j} \left[\sum_{l=0}^N \frac{1}{L_l} \right]^{-1}, \end{aligned} \quad (\text{A.1.3})$$

since $(-1)^{i+j} (-1)^{j-i-1} = (-1)^{2j-1} = -1$. Combining the respective expressions for the diagonal and off-diagonal elements, Eqs. (A.1.2) and (A.1.3), we arrive at the inverse of \underline{M} ,

$$(\underline{M}^{-1})_{i,j} = \delta_{i,j} \frac{1}{L_i} - \frac{1}{L_i L_j} \left[\sum_{k=0}^N \frac{1}{L_k} \right]^{-1},$$

as can be verified by inspection.

A.2 Step-wise optimization

Here, it is shown how the solution of the equations

$$\nabla f(C_m, \Gamma_{\text{cool}}, \delta) = \vec{0} \quad (\text{A.2.1})$$

may be performed in a step-wise manner (writing $f \equiv \frac{n_{\text{HO}}^{(\text{ss})}}{n_{\text{th}}}$ and leaving out $\tilde{\Delta}$ as optimization w.r.t. this parameter turns out to be trivial). We start by optimizing w.r.t. δ by solving

$$\left. \frac{\partial f}{\partial \delta} \right|_{\delta=\delta_{\text{opt}}} = 0 \Rightarrow \delta_{\text{opt}} = \delta_{\text{opt}}(C_m, \Gamma_{\text{cool}}), \quad (\text{A.2.2})$$

assuming the function δ_{opt} to be single-valued.¹ Based on this, we substitute the function δ_{opt} into f which leads us to define the function $\tilde{f} = f(C_m, \Gamma_{\text{cool}}, \delta_{\text{opt}})$. The main point of this section is that in order to proceed towards the solution

¹In our specific optimization we just need to decide on an arbitrary sign for δ_{opt} to achieve this, only δ^2 enters the equations after the elimination of $\tilde{\Delta}$.

of Eq. (A.2.1), we may take the *total* derivative of \tilde{f} w.r.t. one of the remaining parameters, for instance,

$$\frac{d\tilde{f}}{d\Gamma_{\text{cool}}} = \frac{\partial\tilde{f}}{\partial\Gamma_{\text{cool}}} + \frac{\partial\tilde{f}}{\partial\delta_{\text{opt}}} \frac{d\delta_{\text{opt}}}{d\Gamma_{\text{cool}}}, \quad (\text{A.2.3})$$

since, by construction $\frac{\partial\tilde{f}}{\partial\delta_{\text{opt}}} = \frac{\partial f}{\partial\delta} \Big|_{\delta=\delta_{\text{opt}}} = 0$ from Eq. (A.2.2), this reduces to

$$\frac{d\tilde{f}}{d\Gamma_{\text{cool}}} = \frac{\partial\tilde{f}}{\partial\Gamma_{\text{cool}}},$$

and we may thus optimize by solving

$$\left. \frac{d\tilde{f}}{d\Gamma_{\text{cool}}} \right|_{\Gamma_{\text{cool}}=\Gamma_{\text{cool}}^{(\text{opt})}} = 0 \Rightarrow \Gamma_{\text{cool}}^{(\text{opt})} = \Gamma_{\text{cool}}^{(\text{opt})}(C_{\text{m}}),$$

again assuming that we obtain a single-valued function $\Gamma_{\text{cool}}^{(\text{opt})}(C_{\text{m}})$. Proceeding in the same way, we define $\tilde{\tilde{f}} = \tilde{f} \Big|_{\Gamma_{\text{cool}}=\Gamma_{\text{cool}}^{(\text{opt})}} = f(C_{\text{m}}, \Gamma_{\text{cool}}^{(\text{opt})}, \delta_{\text{opt}})$ and find

$$\frac{d\tilde{\tilde{f}}}{dC_{\text{m}}} = \frac{\partial\tilde{\tilde{f}}}{\partial C_{\text{m}}} + \frac{\partial\tilde{\tilde{f}}}{\partial\Gamma_{\text{cool}}^{(\text{opt})}} \frac{d\Gamma_{\text{cool}}^{(\text{opt})}}{dC_{\text{m}}} + \frac{\partial\tilde{\tilde{f}}}{\partial\delta_{\text{opt}}} \frac{d\delta_{\text{opt}}}{dC_{\text{m}}},$$

from which the last two terms on the right-hand side are seen to vanish due to $\frac{\partial\tilde{\tilde{f}}}{\partial\Gamma_{\text{cool}}^{(\text{opt})}} = \frac{\partial\tilde{f}}{\partial\Gamma_{\text{cool}}} \Big|_{\Gamma_{\text{cool}}=\Gamma_{\text{cool}}^{(\text{opt})}} = 0$ and $\frac{\partial\tilde{\tilde{f}}}{\partial\delta_{\text{opt}}} = \frac{\partial\tilde{f}}{\partial\delta_{\text{opt}}} \Big|_{\Gamma_{\text{cool}}=\Gamma_{\text{cool}}^{(\text{opt})}} = 0$ as follows from the above. Therefore, we may finally solve

$$\left. \frac{d\tilde{\tilde{f}}}{dC_{\text{m}}} \right|_{C_{\text{m}}=C_{\text{m}}^{(\text{opt})}} = 0$$

to determine $C_{\text{m}}^{(\text{opt})}$. The set $\{C_{\text{m}}^{(\text{opt})}; \Gamma_{\text{cool}}^{(\text{opt})}(C_{\text{m}}^{(\text{opt})}); \delta_{\text{opt}}(C_{\text{m}}^{(\text{opt})}, \Gamma_{\text{cool}}^{(\text{opt})}(C_{\text{m}}^{(\text{opt})}))\}$ is indeed the desired solution to Eqs. (A.2.1) as

$$\begin{aligned} 0 &= \left. \frac{d\tilde{\tilde{f}}}{dC_{\text{m}}} \right|_{C_{\text{m}}=C_{\text{m}}^{(\text{opt})}} = \left. \frac{\partial\tilde{\tilde{f}}}{\partial C_{\text{m}}} \right|_{C_{\text{m}}=C_{\text{m}}^{(\text{opt})}} \\ &= \left. \frac{\partial f}{\partial C_{\text{m}}} \right|_{C_{\text{m}}=C_{\text{m}}^{(\text{opt})}, \Gamma_{\text{cool}}=\Gamma_{\text{cool}}^{(\text{opt})}(C_{\text{m}}^{(\text{opt})}), \delta=\delta_{\text{opt}}(C_{\text{m}}^{(\text{opt})}, \Gamma_{\text{cool}}^{(\text{opt})}(C_{\text{m}}^{(\text{opt})}))} \end{aligned}$$

and two similar expressions show each of the component equations to be fulfilled.

Appendix B

Source code

MATLAB script for calculating the dimensionless capacitance \tilde{C}_{cell} for the unit cell of the IDC-membrane geometry depicted in Fig. 3.1.5. Note that the script uses as its characteristic length $L_p = 2\Delta x$ the center-to-center distance between neighboring fingers of the same polarity.

```
function f=C_IDC_sub(x,h,epsilonMem,r,t,epsilonSub,n)
% Note: All lengths are in units of the center-to-center
%       distance between two positive fingers.
% epsilonMem > 1 is the rel. dielectric constant of the membrane,
% if epsilonMem == -1 then the membrane is a perfect conductor.
% epsilonSub is the dielectric constant of the substrate
% x is the distance between top of electrodes and the membrane
% h is the thickness of membrane
% r is the width of each finger
% t is the thickness of each finger
% n is meshlevel. Indicates how fine the mesh should be.

%Set up geometry
if epsilonMem == -1 % dielectric membrane
gd=[3.0000    3.0000    3.0000    3.0000    3.0000;...
    4.0000    4.0000    4.0000    4.0000    4.0000;...
   -0.5000   -0.5000    0.0-r/2  -0.5000   -0.5000;...
    0.0000   -0.5+r/2  0.0000    0.0000    0.0000;...
    0.0000   -0.5+r/2  0.0000    0.0000    0.0000;...
   -0.5000   -0.5000    0.0-r/2  -0.5000   -0.5000;...
   -1.0000         0         0      x+t     -1.0000;...
   -1.0000         0         0      x+t     -1.0000;...
    1.0000     t         t      x+t+h         0;...
    1.0000     t         t      x+t+h         0];

else % conducting membrane
gd=[3.0000    3.0000    3.0000    3.0000;...
    4.0000    4.0000    4.0000    4.0000;...
   -0.5000   -0.5000    0.0-r/2  -0.5000;...
    0.0000   -0.5+r/2  0.0000    0.0000;...
```

```

0.0000    -0.5+r/2    0.0000    0.0000;...
-0.5000    -0.5000    0.0-r/2    -0.5000;...
-1.0000         0         0         -1.0000;...
-1.0000         0         0         -1.0000;...
x+t         t         t         0;...
x+t         t         t         0];
end

sf='R1-R2-R3';

if epsilonmem ~=-1 % dielectric membrane
    ns =[82    82    82    82    82;...
        49    50    51    52    53];

else % conducting membrane
    ns =[82    82    82    82    ;...
        49    50    51    52    ];
end

%decompose into minimal
geom g=decsf(gd,sf,ns);

%boundary condition matrix
if epsilonmem ~=-1 % dielectric membrane
b=
[1  1  1  0  0  1  1  1  1  1  1  1  1  0  1  1  1  1  1;...
 0  1  1  1  1  1  1  0  0  0  0  0  0  1  1  1  0  0  0;...
 1  1  1  1  1  1  1  1  1  1  1  1  1  1  1  1  1  1  1;...
 1  1  1  1  1  1  1  1  1  1  1  1  1  1  1  1  1  1  1;...
48 1  1  1  1  1  1  1 48 48 48 48 48 1  1  1 48 48 48 48;...
48 1  1  1  1  1  1  1 48 48 48 48 48 1  1  1 48 48 48 48;...
48 48 48 48 48 48 48 48 48 48 48 48 48 48 48 48 48 48 48;...
48 48 48 48 48 48 48 48 48 48 48 48 48 48 48 48 48 48 48;...
49 49 49 49 49 49 49 49 49 49 49 49 49 49 49 49 49 49 49;...
48 48 49 48 48 48 49 48 48 48 48 48 48 48 49 48 48 48 48];

else % perf. conductor
    b = zeros(12,13,'double');
    b(1:12,1) = [1, 1, 1, 1, 1, 1, 3, '0', '0', '1', '0.5'];
    b(1:10,2) = [1, 1, 1, 1, 1, 1, '0', '0', '1', '0'];
    b(1:10,3) = [1, 1, 1, 1, 1, 1, '0', '0', '1', '1'];
    b(1:10,4) = [1, 1, 1, 1, 1, 1, '0', '0', '1', '0'];
    b(1:10,5) = [1, 1, 1, 1, 1, 1, '0', '0', '1', '1'];
    b(1:6,6) = [1, 0, 1, 1, '0', '0'];
    b(1:6,7) = [1, 0, 1, 1, '0', '0'];
    b(1:6,8) = [1, 0, 1, 1, '0', '0'];
    b(1:10,9) = [1, 1, 1, 1, 1, 1, '0', '0', '1', '0'];
    b(1,10) = [0];
    b(1:10,11) = [1, 1, 1, 1, 1, 1, '0', '0', '1', '1'];
    b(1:6,12) = [1, 0, 1, 1, '0', '0'];

```

```

        b(1:6,13) = [1, 0, 1, 1, '0', '0'];
    end

    %set up mesh
    [p,e,t]=initmesh(g);
    %refine mesh n-1 times
    for l=1:(n-1)
        [p,e,t]=refinemesh(g,p,e,t);
    end

    %dielectric constant
    %Fourth component of t gives the region number of each triangle
    if epsilonmem ~= -1
        % dielectric membrane, regions 1&2: free space,
        % region 3: substrate, region 4: membrane
        epsilonarr = (t(4,:)==4)*epsilonmem+(t(4,:)==3)*epsilonub...
            +1.0*((t(4,:)==1)+(t(4,:)==2));
    else
        % conducting membrane, region 1: free space, region 2: substrate
        epsilonarr = (t(4,:)==2)*epsilonub + 1.0*(t(4,:)==1);
    end

    %solve equation to find potential
    u=assempe(b,p,e,t,epsilonarr,0,0);

    %Fields
    [Ex,Ey]=pdegrad(p,t,u);
    Dx=Ex.*epsilonarr;
    Dy=Ey.*epsilonarr;
    %energy and capacitance
    [ar,~,~,~]=pdetrng(p,t);
    energy=sum(ar.*(Ex.*Dx+Ey.*Dy))/2;

    %with unit voltage, the capacitance is just this
    % number times epsilon_0 times perperdicular length
    capacitance=2*energy;
    f=capacitance;

```